Università degli Studi di Torino

Dipartimento di Biotecnologie e Scienze per la Vita

Dottorato di ricerca in Medicina Molecolare

XXIX ciclo

“ p140Cap as a “suppressor” of breast cancer features: from the primary tumour to the metastasis through the cancer microenvironment ”

Tutor **Candidato**

Prof.ssa Paola Defilippi **Vincenzo Salemme**

ABSTRACT

Increasing data indicate the key role of the tumour microenvironment in cancer progression, metastasis formation and treatment sensitivity, where the tumour stroma and the immune infiltrate strongly influence tumour features. Our recent studies indicate that the adaptor protein p140Cap is highly expressed in about 50% of ERBB2-amplified breast cancer patients. Its expression correlates with increased patient survival and decreased probability to develop metastasis. Causally, p140Cap negatively regulates breast tumour properties both *in vitro* and in the NeuT preclinical mouse model and counteracts metastasis formation. Moreover, we observed that p140Cap expression affects tumour immune infiltrate composition in a syngeneic ERBB2+ breast cancer model, by reducing level of G-CSF mRNA and protein, both in tumour cells and in *in vivo* tumours. Accordingly, *in vivo*, we observed a reduced mobilization of G-CSF-dependent myeloid-derived suppressor cells (MDSCs-$CD11b^{+}Ly6G^{+}Ly6C^{lo}$) from bone marrow and a decreased level of MDSCs infiltration in tumours, blood and spleen of mice orthotopically injected with p140Cap tumour cells, compared to controls. The poor immune suppressive microenvironment associated to p140Cap-expression, was also confirmed by an increase in$CD8^{+}$ T lymphocytes, in M1 macrophages and in Natural Killer lymphocytes, together with a decrease in M2 macrophages and FoxP3 regulatory T cells. Interestingly, p140Cap significantly reduces the fraction of cancer stem cells, their ability to generate mammosphere and their *in vivo* tumour initiation features, by modulating their proliferative potential, identified as Sca1/Ki67 double positive cells. Overall, these data indicate that p140Cap may affect the cancer stem cell compartment, impairing enhanced G-CSF production and limiting ERBB2 tumour aggressiveness by creating a tumour microenvironment unfavorable to tumour progression.

INTRODUCTION

Breast cancer (BC) is one of the most common cancers with greater than 1,300,000 cases and 450,000 deaths each year worldwide[1,2]. Clinically, breast cancer is classified into three basic therapeutic groups: the estrogen receptor (ER)-positive group, the ERBB2 (also called HER2)-positive group, and the triple-negative breast cancers (TNBCs, also called basal-like), lacking expression of ER, progesterone receptor (PR) and ERBB2[2].

The ERBB2 oncogene (the human V-Erb-B2 Avian Erythroblastic Leukemia Viral Oncogene Homolog 2) is a tyrosine kinase receptor, which belongs to the ERBB family. ERBB2 gene amplification and receptor over-expression are causally linked to oncogenesis in ~20% of breast cancers and define a molecular breast cancer subtype characterized by an adverse clinical outcome[3,4,5]. ERBB2 amplified tumours are a biologically non-homogeneous subgroup of breast cancers[6]. Indeed, although the ERBB2 gene is located in the most highly rearranged segment in chromosome 17 (17q12-q21)[7], the amplification of the surrounding genomic region is a highly variable process that leads to a complex pattern of amplicons. The genes included in the amplicons may significantly contribute to ERBB2 tumour progression and treatment efficacy[7,8,9,10,11].

ERBB2 tyrosine kinase activation at the plasma membrane triggers key signaling pathways that direct general tumorigenicity, including escape from apoptosis, increased cell proliferation and migration, and epithelial to mesenchymal transition (EMT)[12,13].

p140Cap is a multisite docking protein, highly expressed in brain, testis and epithelial-rich tissues such as lung and mammary gland, characterized by conserved sequence motifs that can associate with multiple effectors[14,15].

We have previously described the p140Cap adaptor protein as a molecule that interferes with adhesion properties and growth factor-dependent signaling, thus affecting tumour features in breast cancer cells[15,16,17,18]. Recent reports have underlined that p140Cap regulates proliferation and migration in colon, lung, gastric, cutaneous squamous carcinoma and osteosarcoma cancer cells[18,19,20,21,22,23].

Indeed, in a cohort of breast cancer patients, p140Cap expression was linked to a less aggressive breast cancer disease[24], leading to the hypothesis that in these tumours p140Cap may counteract tumour fitness. However, it was not possible to assess the relevance of p140Cap expression for

patient survival in that cohort[24], thus leaving open the question of the relevance of p140Cap to breast cancer prognosis.

In our recent work[25], we set out to tackle the relevance of p140Cap in human breast cancer by analyzing a large consecutive cohort of patients with invasive breast cancer and we demonstrated a strong association between p140Cap and improved survival of ERBB2 patients.

We analyzed p140Cap expression, by immunohistochemistry (IHC), on a consecutive cohort of 622 invasive breast cancers available in a tissue microarray. Data for p140Cap expression were available for 515 out of 622 samples (Fig. 1A; Table 1). Positive p140Cap status (IHC score $\geq$1) was associated with good prognosis markers, such as negative lymph node status (P=0.014, where P=Pearson χ2-test), ER and progesterone receptor (PgR)-positive status (P=0.0002 and P=0.0049, respectively), small tumour size (pT1 versus pT2–pT4, P<0.0001), low grade (P<0.0001), low proliferative status (Ki67, P=0.0013), and ERBB2-positive status (P=0.0344). Positive p140Cap status was also associated to breast cancer molecular subtypes, being expressed in >85% of Luminal A tumours, 77% of Luminal B, and only 56% of triple-negative tumours (Table 1).

In univariate analysis, a positive p140Cap status was associated with a lower risk of developing distant metastasis, and of death from breast cancer in the entire breast cancer cohort (Fig. 1B). However, a more in-depth analysis revealed that the prognostic effect of p140Cap in the consecutive cohort of breast cancer patients was to be ascribed to its performance in the subgroup of ERBB2-amplified breast cancers (Fig. 1C), in which a high p140Cap status predicts a significantly lower probability of developing a distant event (left panel), and a clear difference in survival (right panel). By contrast, no significative differences could be observed in patients not harboring ERBB2 amplification (Fig. 1D).

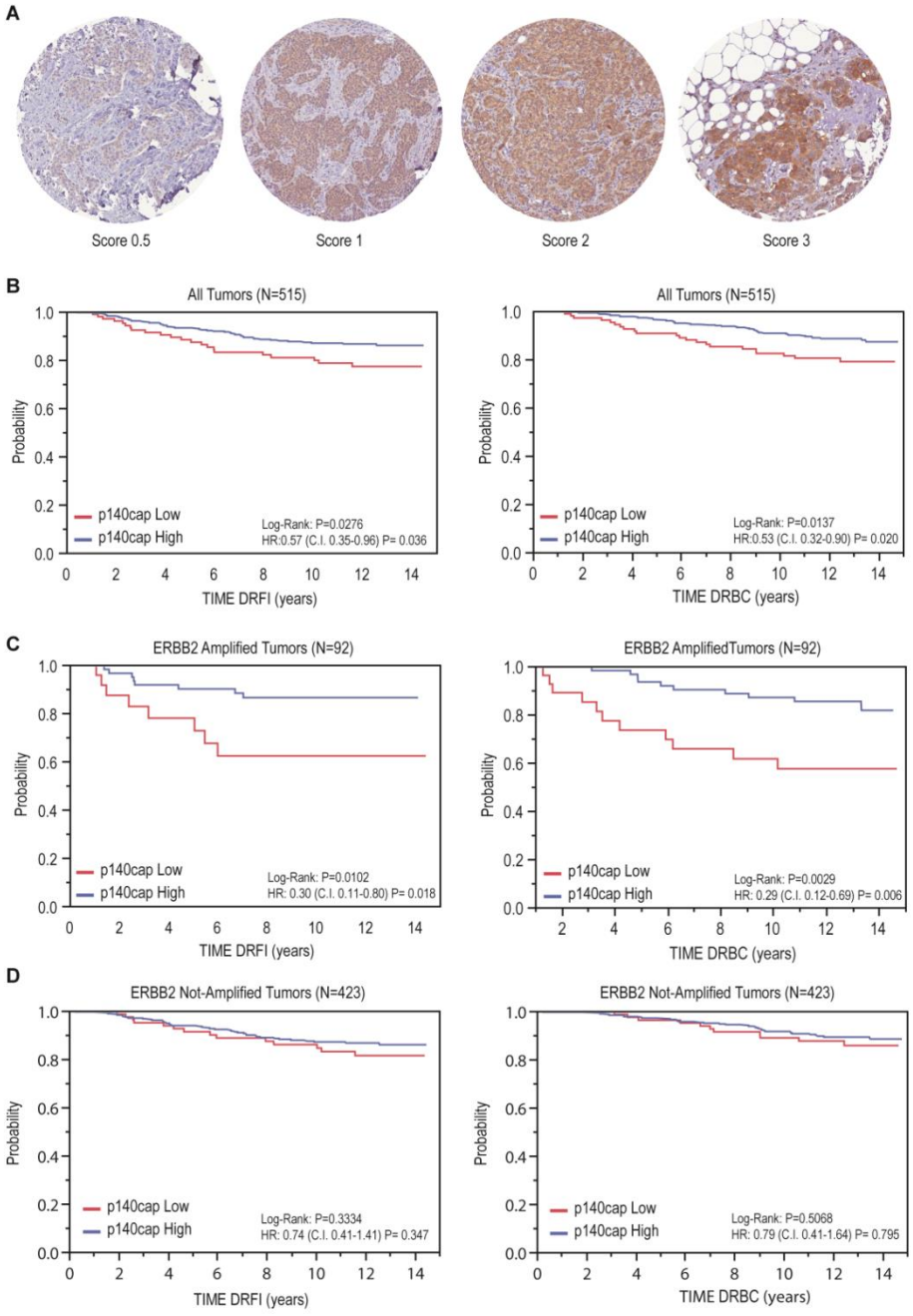

Figure 1. Prognostic Relevance of p140Cap expression in breast tumours. **(A)** p140Cap expression was measured by IHC on tissue microarray (TMA) samples. For the purpose of correlation with clinical and pathological parameters, tumours were classified based on the intensity of p140Cap staining as 0.5-3: p140Cap-Low (IHC score < 1) and p140Cap-High (IHC score ≥1). Images are representative of p140Cap expression scoring according to intensity staining in TMA. In tumour tissues, the IHC signals were associated with the tumour cell component and not with the adjacent or infiltrating stroma. **(B)** p140Cap expression in the whole cohort**:** Distant Recurrence Free Interval (DRFI)[26] (left panel: Hazard Ratio: 0.57, P= 0.036); and Death Related to Breast Cancer (DRBC) (right panel: Hazard Ratio: 0.53, P= 0.020). **(C)** p140Cap expression in ERBB2 positive patients**:** DRFI (left panel: Hazard Ratio: 0.30, P= 0.018); and DRBC (right panel: Hazard Ratio: 0.29, P= 0.006). **(D)** p140Cap expression in ERBB2 negative patients**:** DRFI (left panel: Hazard Ratio: 0.74, P= 0.347); and DRBC (right panel: Hazard Ratio: 0.41, P= 0.795).

		p140cap LOW (<1)	p140cap HIGH (≥1)	Pearson χ2 P-Value
All Patient		114 (22.1%)	401 (77.9%)	
Nodal Status	Negative	46 (17.56 %)	216 (82.44 %)	**0.0146**
	Positive	**65 (26.53 %)**	180 (73.47 %)	
Subtype	Luminal A	22 (13.02 %)	147 (62.86 %)	**0.0004**
	Luminal B	58 (23.20 %)	192 (76.80 %)	
	Luminal B Her2 Positive	9 (27.27 %)	24 (72.73 %)	
	HER2 Positive	13 (37.14 %)	22 (62.86 %)	
	Triple Negative	12 (42.86 %)	16 (57.14 %)	
ER	Positive	88 (19.56 %)	362 (80.44 %)	**0.0002**
	Negative	**26 (40 %)**	39 (60 %)	
PgR	Positive	77 (19.35 %)	321 (80.65 %)	**0.0049**
	Negative	**37 (31.62 %)**	80 (68.38 %)	
pT	pT1	45 (12.86 %)	305 (87.14 %)	**<0.0001**
	pT2/pT3/pT4	**69 (41.82 %)**	96 (58.18 %)	
Grade	G1	11 (8.73 %)	115 (91.27 %)	**<0.0001**
	G2	53 (22.84 %)	179 (77.16 %)	
	G3	**49 (32.67 %)**	101 (67.33%)	
Ki-67	LOW	24 (13.87 %)	149 (86.13 %)	**0.0013**
	HIGH	**90 (26.32 %)**	252 (73.68 %)	
ERBB2 Status	Negative	92 (20.58 %)	355 (79.42 %)	**0.0294**
	Positive	**22 (32.35 %)**	46 (67.65 %)	
Age	<35	5 (25 %)	15 (75 %)	0.3094
	35-65	83 (20.65 %)	319 (79.35 %)	
	>65	26 (27.96 %)	67 (72.04 %)	

ER: estrogen receptor; PgR: progesterone receptor; pT: primary tumour size; Ki67: marker of proliferation grade.

Table 1. Correlation of p140Cap expression with clinic-pathological characteristics of Breast Cancer Patients. Analysis of p140Cap expression was performed on the Invasive Breast Cancer Consecutive Cohort (N = 622*) operated in the European Institute of Oncology, Milano, Italy, in the year 2000. Expression was measured by IHC on TMA. p140Cap high expression was defined 22 when tumours display an expression score ≥1. p-values (Pearson) were measured by Chi Square test. Note that the number of scored cases is lower than the total number of cases since: i) in some cases, individual cores detached from the slides during the manipulations; ii) clinical information was not available for all patients. In tumour tissues the IHC signals were associated with the tumour cell component and not with the adjacent or infiltrating stroma. *Only for 515 of 622 samples expression data for p140Cap was available.

The relationship with ERBB2 could be explained by the fact that p140Cap is encoded by the SRCIN1 gene, located at Chromosome 17q12, one million base pair centromeric to the ERBB2 gene. However, the co-amplification of SRCIN1 gene in the context of the ERBB2-related disease has not yet been deeply investigated.

To assess how frequently the SRCIN1 gene may be included in the ERBB2 amplicon, BAC array Comparative Genomic Hybridization (aCGH) was performed. The analysis of 200 ERBB2-amplified tumours from a large Swedish Cohort[8], showed that the SRCIN1 gene is altered in 70% of cases, with 123 cases (61.5% of the total) showing a copy number (CN) gain for SRCIN1 (Fig. 2A). Moreover, mRNA expression and SRCIN1 gene CN from 50 of the 200 ERBB2 amplified tumours were significantly correlated, giving a Pearson correlation of 0.77 (Fig. 2B). Further, we analyzed by FISH a consecutive series of 77 breast cancer patients at diagnosis with a mix of probes for SRCIN1and the centromeric region (CEP17) of chromosome 17. While in 43 ERBB2-negative breast cancers SRCIN1 CN was never altered, in ERBB2-amplified tumours[27], 56% of the specimens were amplified for SRCIN1 (Fig. 2C). These data indicate that alterations at the level of the SRCIN locus are strictly linked to chromosomal rearrangements that result in ERBB2 amplification. Altogether, these results show that the SRCIN1 gene is frequently, but not obligatorily, co-amplified with ERBB2 in breast cancers, arguing for a potential role of SRCIN1 as a determinant of the clinical heterogeneity of ERBB2 tumours. These observations also provided us with the testable hypothesis that the presence of SRCIN1 may attenuate the intrinsic biological aggressiveness of breast tumours with ERBB2 alterations.

In conclusion:

- p140Cap expression associates with reduced risk of metastasis (and death from cancer), in the ERBB2-amplified subgroup of breast cancer patients, arguing for a possible role of p140Cap in counteracting the migratory and/or metastatic ability of ERBB2-amplified tumour cells;

- the SRCIN1 gene is frequently, but not obligatorily, co-amplified with ERBB2 in breast cancers, arguing for a potential role of SRCIN1 as a determinant of the clinical heterogeneity of ERBB2 tumours.

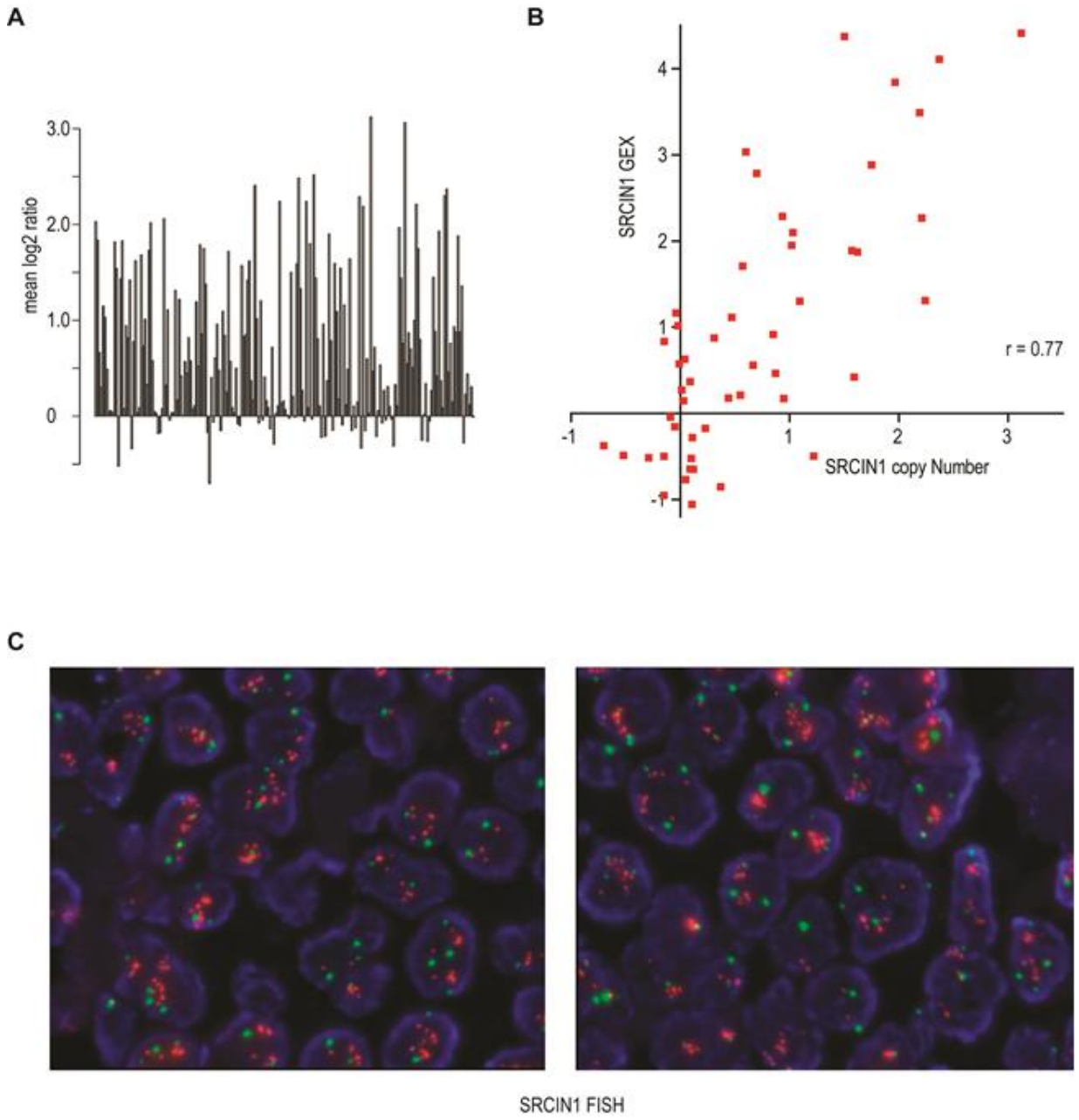

Figure 2. SRCIN1 gene alterations in human ERBB2 breast cancer samples. (A) SRCIN1 gene copy number across 200 ERBB2 amplified breast cancer samples analyzed by aCGH. Y-axis corresponds to log2 transformed copy number, where values >0 correspond to increased copy numbers, and values <0 to copy number loss. Bars represent individual samples. **(B)** Correlation of SRCIN1 gene expression (GEX) (y-axis) and SRCIN1 gene copy number (x-axis) for 50 ERBB2 amplified cases from ref.[6]. To assess whether this increase in SRCIN1 gene copy number results in increased mRNA expression, gene expression data were compared with aCGH $\log_2$ ratios using the Pearson correlation as described in[28]. Pearson's coefficient of correlation is 0.77. **(C)** p140Cap FISH of breast cancer tissues. Representative images of two cases of ERBB2 amplified tissues, labeled with a mix of two probes SRCIN1/CEP1; Red (SRCIN1) and green (CEP17) spots were automatically acquired at 175 X, using Metafer, by a MetaSystem scanning station. Panel a: 95% SRCIN1 amplification; average SRCIN1/nuclei=11.7; panel b: 90% SRCIN1 amplification; average SRCIN1/nuclei= 13,4.

AIMS

The data shown above also provided us with the testable hypothesis that the presence of SRCIN1/p140Cap is causal in attenuating the intrinsic biological aggressiveness of breast tumours with ERBB2 alterations. To test this hypothesis, we moved to the well-established preclinical mouse model of ERBB2 breast cancer, the NeuT mice.

In this context, we investigated whether and how:

1) p140Cap limits *in vivo* tumorigenicity of NeuT spontaneous tumours;

2) p140Cap limits *in vivo* metastasis onset of NeuT-derived orthotopic syngeneic tumours;

3) p140Cap impacts on the microenvironment of NeuT-derived orthotopic syngeneic tumours.

RESULTS

1) p140Cap limits *in vivo* tumorigenicity of NeuT spontaneous tumours

Characterization of the MMTV-p140Cap-NeuT breast cancer mouse model

To better understand the role of p140Cap in breast cancer, we generated a transgenic (Tg) mouse model in which p140Cap expression is driven under the control of the MMTV promoter (MMTV-p140Cap; Fig. 3A), to cross them with a well-characterized model of ERBB2-dependent breast carcinogenesis, the Tg MMTV-NeuT mouse model[29,30]. We selected two MMTV-p140Cap lines with a strong expression and a clear epithelial localization of p140Cap in the mammary gland (Fig. 3B, C). We also analyzed p140Cap expression in different tissues (Fig. 3D) showing that our transgene of interest is expressed in mammary glands, parotid glands, lungs, and, at a minor extent, in brain. Moreover, p140Cap expression in Tg mice does not impair mammary gland development and differentiation (Fig. 3E). We did not observe any differences in TEB number, ductal elongation and ductal network area during mammary gland growth and development in virgin mice and any significant trend to lobular increase during pregnancy and lactation, but a small impairment in post weaning lobular involution in Tg mice.

The MMTV-p140Cap transgenic mice was then crossed with both FVB-MMTV-NeuT[31] and BALB/c-MMTV-NeuT[29,30] mice, which display different tumour onset times, to generate p140Cap-NeuT mice. p140Cap expression in tumours derived from these mice was confirmed by Western blot analysis (Fig. 4A). When compared to either FVB-NeuT or BALB/c-NeuT mice, the corresponding p140-NeuT mice showed a significant delay in the appearance of the first tumour (Fig. 4B, Fisher's exact test, Two sided, P=0.0022; P=0.0056) associated with a significant decrease in the total tumour burden (Fig. 4C, unpaired t-test: ***P<0.001, *P<0.05). Histological analyses showed morphological differences in the appearance of the two types of tumors (Fig. 4D). NeuT tumours were composed of large solid nodules, separated by delicate bundles of stromal tissue, with necrosis often evident in the centre of the largest nodules (Fig. 4D, panels a,b). Tumours developed in p140-NeuT mice consisted of smaller nodules and sheets of cells separated by more abundant stroma, with cancer cells extending into the stroma in nest-like formations showing distinctive holes between the cancer cells (Fig. 4D, panels c,d).

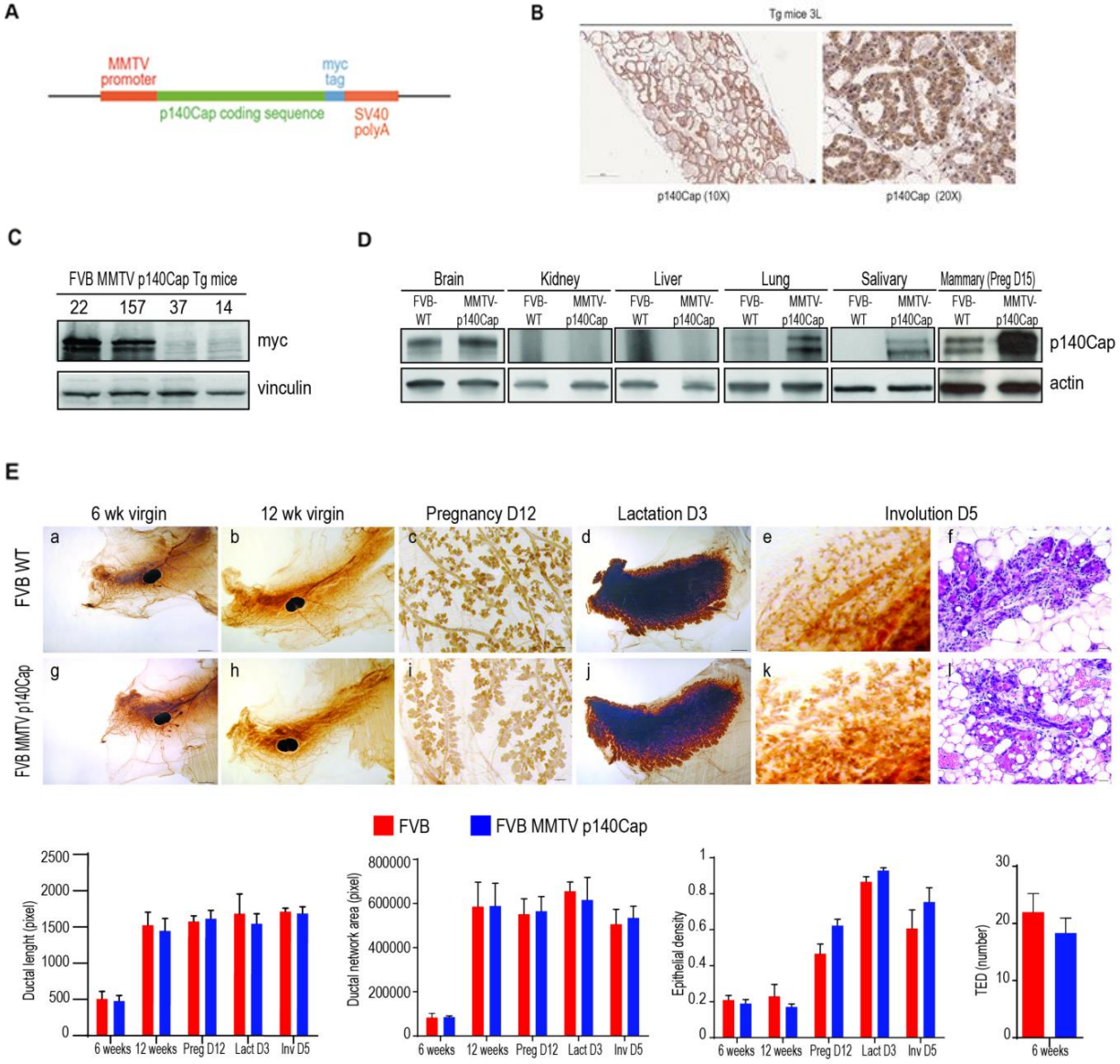

Figure 3. Characterization of MMTV-p140Cap transgenic mice. (A) Expression cassette used for the generation of MMTV-p140Cap transgenic mice. The Myc epitope is inserted at the carboxyterminal region of the protein. **(B)** p140Cap expression in MMTV-p140Cap transgenic mouse lines. Mammary gland tissue protein extracts were prepared at three days lactation from different Tg female mice (22, 157, 37 and 14). **(C)** p140Cap is expressed into the mammary epithelial compartment of the Tg mice. Formalin-fixed paraffin-embedded fourth abdominal mammary glands of Tg mice at 3 days of lactation were analyzed by IHC with anti p140Cap antibodies. **(D)** p140Cap expression in different tissues of the MMTV-p140Cap transgenic mice. Protein extracts from distinct tissues collected from FVB WT or MMTV-p140Cap Tg female at 15 days of pregnancy**. (E)** Mammary glands from WT and MMTV-p140Cap transgenic mice were collected at several stages of physiologic mammary development, namely at 6 weeks (pubertal period) and 12 weeks (mature virgin mammary gland) of age, 12 days of pregnancy, 3 days of lactation and 5 days of post weaning involution. Four parameters were analyzed to compare WT and Tg mammary glands, and reported in histograms (mean ± SEM). Bar: a, b, d, g, h, j 0,2 cm; c, e, i, k 300 µm; f, l 20 µm.

Both tumour types were strongly positive for NeuT (Fig. 4D, panels e–h). A larger percentage of NeuT tumour cells were positive for the proliferation marker PCNA (Fig. 4D, panels i,j), compared to p140-NeuT tumour cells (Fig. 4D, panels k,l). PCNA quantification is shown on the right of Fig. 4D (32±1,560 versus 18,65±2,141). Not significant differences were detectable in activated Caspase 3 staining, in which only a few cells were positive in both tumour types (7,694±2,257 versus 7,381±2,408; Fig. 4D, panels m–p). Activated Caspase 3 quantification is shown on the right of Fig. 3E. Altogether, these results show that p140Cap expression attenuates the phenotype of NeuT tumour *in vivo*, resulting in the development of smaller and lower grade mammary carcinomas.

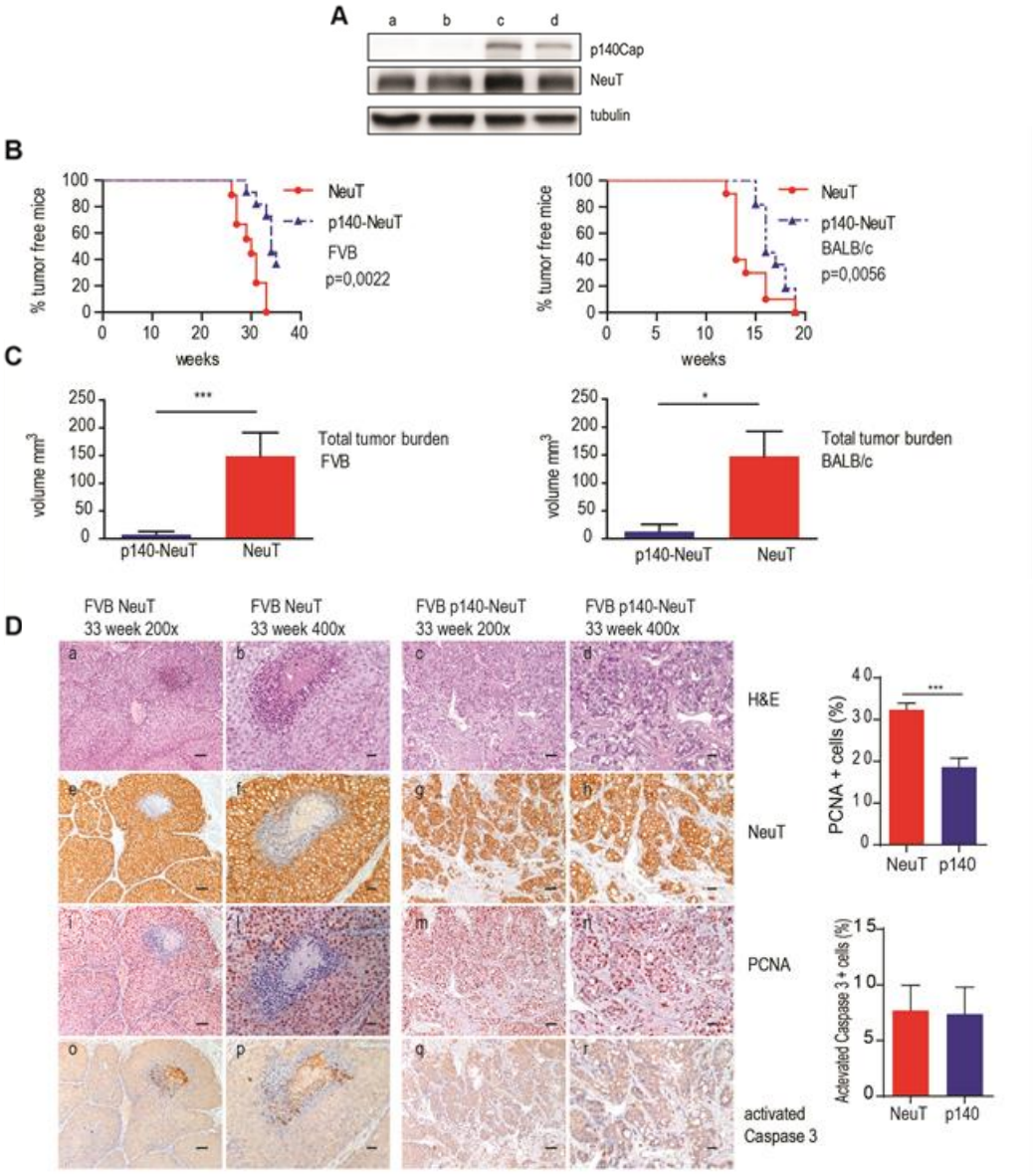

Figure 4. p140Cap expression is causative in limiting tumour growth in NeuT mice. (A) Extracts of tumors derived from NeuT mice (a, b) or p140-NeuT mice (c, d). **(B)** Percentage of tumour free mice in NeuT (red line) and p140Cap-NeuT (blue-dashed line) transgenic animals in both FVB (left) or BALB/c background (right). Twelve mice were

analyzed for each group. Fisher's exact test, Two sided, p= 0,0022; p=0,0056. Error bar: SEM. **(C)** Total tumour burden in NeuT (red) and p140Cap-NeuT (blue) mice in both the FVB (left) or BALB/c backgrounds (right) was measured. Ten mice were analyzed in each group. Unpaired *t*-test: (*p < 0.05; ***p < 0.001). Error bar: SEM. **(D)** Paraffin-embedded sections from three NeuT and three p140Cap-NeuT tumours taken from mice at 33 weeks of age were analyzed for Hematoxylin-Eosin H&E (a-d) and for immunohystochemistry with antibodies to NeuT (e-h), PCNA (i-n) and activated Caspase 3 (o-r). Representative images are shown. Bar first and third columns: 50 microns. Bar second and fourth columns: 20 microns. Histograms on the right show the percentage of PCNA+ (upper panel) and Activated Caspase 3+ (lower panel) cells. Statistical significative differences were evaluated using unpaired *t*-tests (***p < 0.001).

2) p140Cap limits *in vivo* metastasis onset of NeuT-derived orthotopic syngeneic tumours

Characterization of the p140Cap-TuBo syngeneic mouse breast cancer cell model

To further dissect the tumour suppressor role of p140Cap in breast cancer, we took advantage of the NeuT-TuBo cell line, an additional transplantable primary NeuT cell model derived from a tumour arisen in BALB/c-MMTV-NeuT mice[32]. Upon infection with empty or p140Cap retroviruses, we generated NeuT-TuBo (as mock cells), and p140Cap-TuBo cells (Fig. 5A, B). These cells were cloned and selected for the homogenous expression of p140Cap. A pool of 5 clones was used throughout all the experiments.

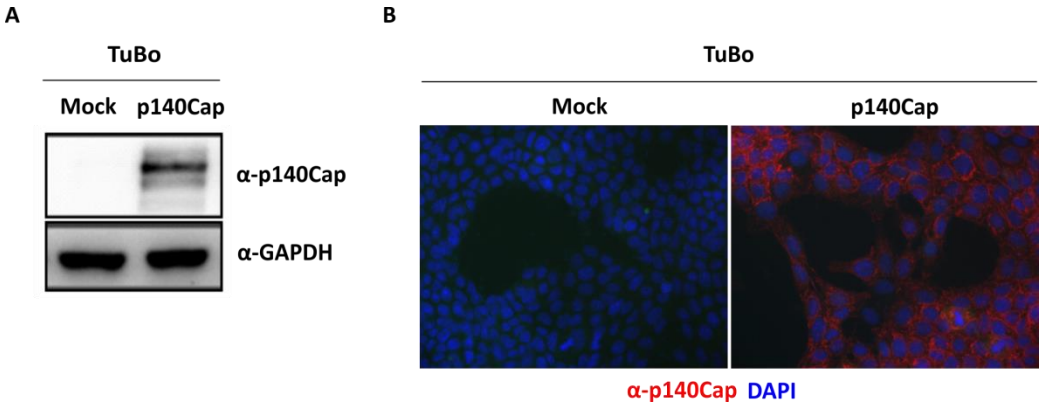

Figure 5. p140Cap expression in TuBo cell line. Mock-TuBo and p140Cap-TuBo cells obtained by stable infection with empty pBABE or pBABE-p140Cap retrovirus. The p140Cap over-expression was checked by western blot analysis **(A)** using antibodies to p140Cap and GAPDH, as loading control, and by immunofluorescence analysis **(B)** using antibodies to p140Cap (red) and DAPI (blue) for nuclei. Representative images are shown.

These cells were characterized *in vitro*, for viability and anchorage-independent growth assay and *in vivo*, for growth, and experimental and spontaneous lung metastasis assay. As expected, p140Cap over-expression caused a significant decrease in cell viability (Fig. 6A) and in the ability to grow in anchorage-independent conditions. In particular p140Cap-TuBo cells formed smaller colonies compared to Mock-TuBo cells (Fig. 6B).

We moved also to an *in vivo* setting, by performing fat pad injection. Effectively, p140Cap-TuBo cells significantly limit tumour cell growth after 26 days upon orthotopic transplantation (Fig. 6C), compared to Mock-TuBo cells.

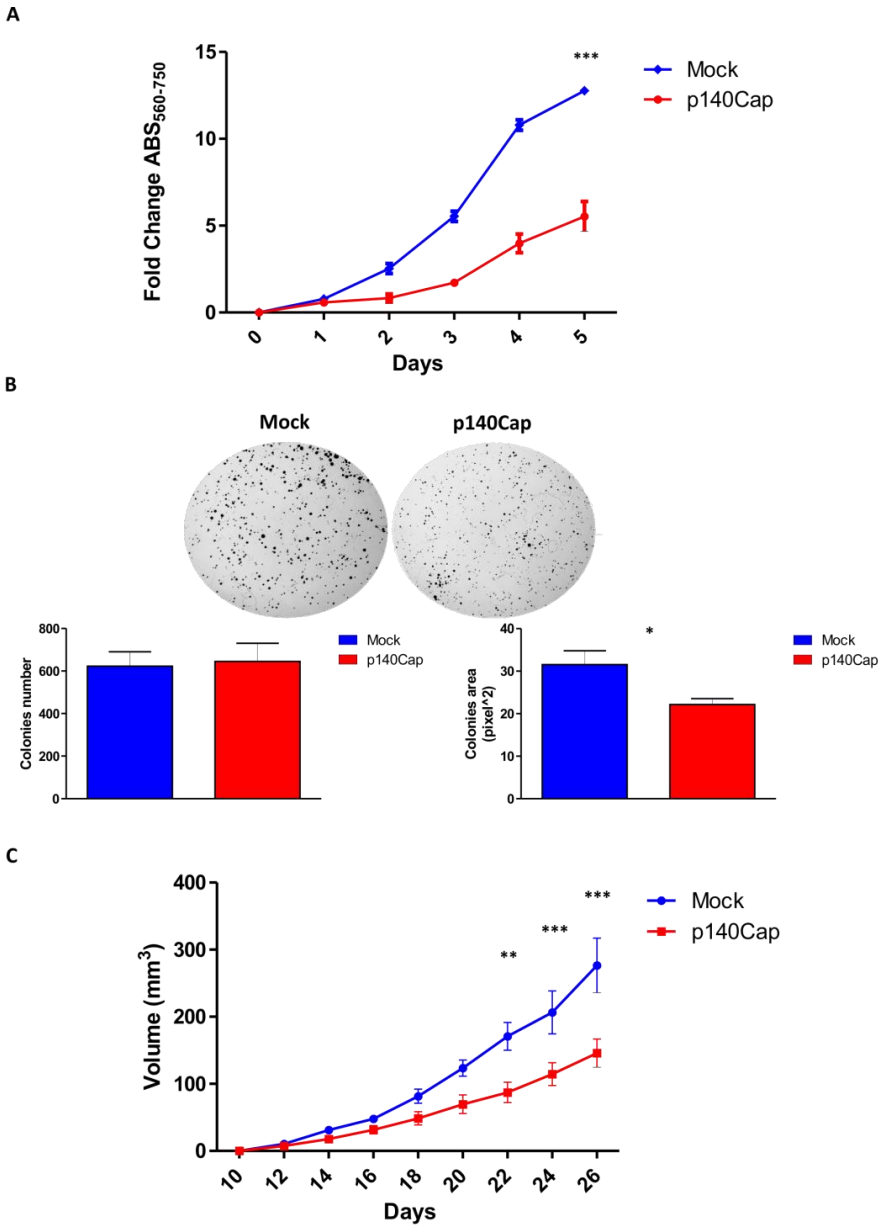

Figure 6. *In vitro* characterization of p140Cap-TuBo cell line. (A) 5x10^3 Mock-TuBo and p140Cap-TuBo cells were plated in 96-wells plate and the cell viability was evaluated by MTT assay. Three independent experiments were

performed. Differences in cell viability were evaluated using two-way ANOVA followed by Bonferroni multiple comparison post hoc tests (***p < 0.001). **(B)** $5x10^4$ Mock-TuBo and p140Cap-TuBo cells were plated in 6-wells plate and ability to growth in soft agar and form colonies was evaluated for 15 days. Two parameters were analysed and reported in histograms (mean ± SEM) to compare Mock and p140Cap-TuBo using unpaired *t*-tests (*p < 0.05). **(C)** 5 x 10^5 Mock-TuBo and p140Cap-TuBo cells were injected in the right fat pads of BALB/c mice. Tumour diameters were measured every two days for 26 days. Three independent experiments were performed using 5 mice per group. Differences in tumour volume were evaluated using two-way ANOVA followed by Bonferroni multiple comparison post hoc tests (***p < 0.001).

Based on the association between p140Cap status and reduced risk of distant metastasis in ERBB2 breast cancer patients, and on the down-regulation of the EMT transcription program, we addressed the putative protective role of p140Cap against the metastatic risk.

By took advantage of the TuBo cell model, in the experimental metastasis assays upon tail vein injection, NeuT-TuBo cells gave rise, after 25 days, to numerous large lung metastasis substituting~80% of lung tissue area. At the same time point, p140Cap-TuBo cells were grown to occupy only ~54% of lung tissue area (Fig. 7A). We also moved to the spontaneous metastasis assay from primary tumours, comparing metastasis formation from tumours of the same size. As shown in figure 7B, tumours originated from p140Cap-TuBo cells gave rise to a significantly reduced number of lung metastasis over tumours grown from NeuT-TuBo cells. Moreover, the immunohistochemical staining with anti NeuT/ERBB2 and anti p140Cap antibodies of lungs with p140Cap-TuBo metastasis showed that while all the metastasis were positive for the NeuT protein, p140Cap strong expression was conserved only in small metastasis (Fig. 7C). Interestingly, larger metastasis expressed only low levels of p140Cap and, accordingly, showed a less nodular histological structure similar to those developed from NeuT-TuBo tumours (Fig. 7D, compare upper and lower panels). Therefore, from these data we can conclude that p140Cap significantly impairs metastasis acting both on tumour cell spreading and on metastatic growth. One mechanism involved is the ability of p140Cap to associate and to down-regulate the Tiam1-Rac1 axis, impairing cell migration and invasion, as described by other members of the Defilippi's lab (for results see[25]).

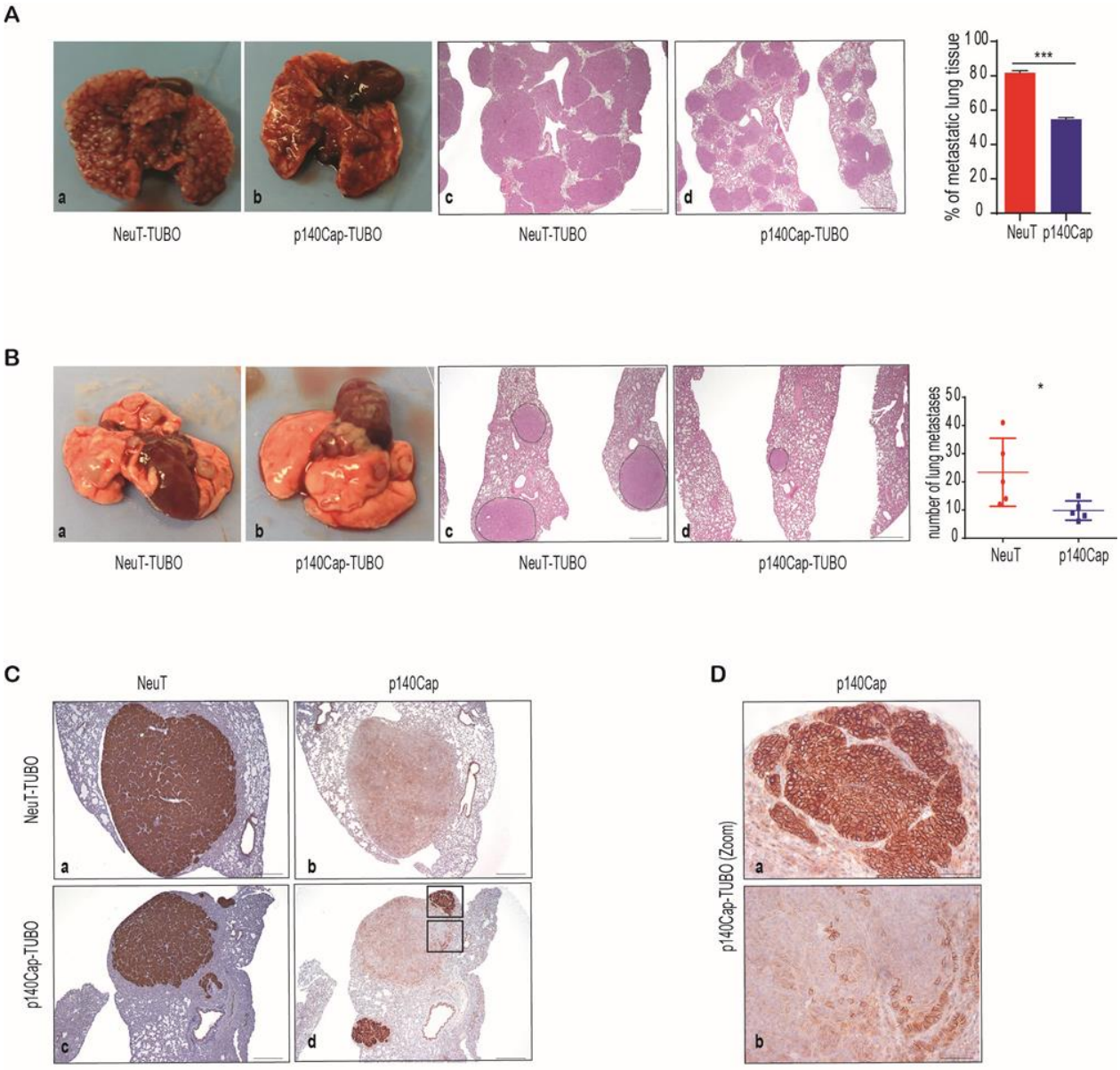

Figure 7. p140Cap impairs spontaneous metastasis. (A, B) Representative gross observation (panel a, b), Hematoxylin&Eosin sections (panel c, d) and quantitative analysis in the experimental lung metastasis assay **(A)** and in the spontaneous lung metastasis assay **(B)**. In **A**, 5 x 10^4 cells were injected into the tail vein of NSG mice. After 4 weeks, the lungs were explanted and analyzed. Two independent experiments were performed using 5 mice per group. The histogram shows the percentage of metastatic lung tissue on total lung area. Statistical significance was evaluated with unpaired *t*-test (***p < 0.001). Error bar: SEM. In B, 10^5 cells were injected in the right fat pads of NSG mice. Tumour volume were measured every week till the tumours reached a 10 mm diameter, when tumours were surgically removed. After 5 weeks, mice were sacrificed and lungs were explanted. The histogram shows the number of lung metastasis. Statistical significance was evaluated with unpaired *t*-test (*p < 0.05). Error bar: SEM. Scale bar A-B: 800 µm. **(C)** NeuT (panel a, c) and p140Cap expression (panel b, d) in spontaneous lung metastasis of mice injected with NeuT-TuBo cells (panel a, b) and mice injected with p140Cap-TuBo cells (panel c, d). Scale bar: 400 µm**. (D)** High magnification fields of rectangular areas in Figure C, panel d. Scale bar: 50 µm.

3) p140Cap impacts on the microenvironment of NeuT-derived orthotopic syngeneic tumours

The field of cancer biology has been long dominated by a cancer cell-centric view, leading to a better characterization of aberrant cancer cell signaling pathways and of cancer cell DNA alteration. Nowadays, it is increasingly evident that not only cancer cells, but also the tissue surrounding these cells, the so called tumour microenvironment (TME), plays an important role in tumour progression, metastasis formation and treatment sensitivity[33,34,35]. The tumour microenvironment includes stromal cells, as well soluble factors and the extracellular matrix (ECM) produced by these cells. Among the stromal cells, endothelial cells (ECs), pericytes, fibroblasts, myofibroblasts, and various bone marrow-derived immune cells are included[36] (Fig. 8).

Some of the principal cell types to arrive in tumours during their development are infiltrating inflammatory cells, bone marrow-derived hematopoietic and endothelial progenitor cells, and carcinoma-associated fibroblasts[37]. Infiltration of tumours by immune cells such as macrophages, lymphocytes, natural killer (NK) cells, and dendritic cells (DCs) is crucial for tumour control[38]. The anticancer immune response generated by these cells is, however, inhibited by the action of immunosuppressive cells, such as myeloid-derived suppressor cell (MDSC) regulatory T cells (Tregs), and type 2-polarized macrophages (M2), which are intrinsically associated with the developing TME. In general, a 'pro-inflammatory' tumour microenvironment and infiltrating CD8-expressing T lymphocytes are associated with improved clinical outcomes in a broad range of tumour types. In contrast, the inhibitory function of MDSCs and Tregs appear to have a major role in disrupting the capacity for the immune control of cancers and are therefore associated with worse outcome.

Cancer-stromal cell interaction further drives tumour cell malignancy. The intercellular communication between cancer cells and tumour microenvironment cells is driven by a complex and dynamic network of chemokines, cytokines, growth factors and extracellular matrix[39,40]. A variety of these cytokines are secreted by cancer cells in the TME and then affect tumour progression. Some of these factors, such as G-CSF, are also able to mobilize immune immature cells directly from the bone marrow to secondary sites, such as the primary tumour.

A better understanding of how the tumour microenvironment affects cancer progression should provide new targets for the isolation and destruction of cancer cells via interference with the

complex crosstalk established between cancer cells, host cells, and their surrounding extracellular matrix.

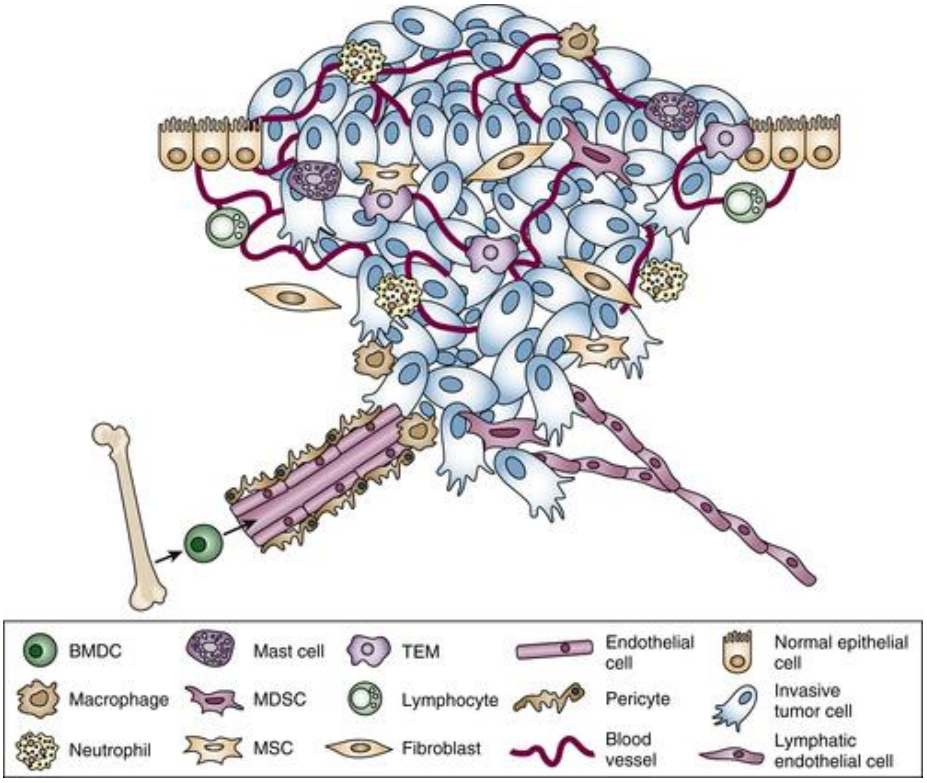

Figure 8. The complexity of the tumour microenvironment. Cells within a tumour are supported by a complex and dynamic microenvironment composed of multiple infiltrating cell types, including endothelial cells, cancer-associated fibroblasts (CAFs), and a variety of bone marrow–derived cells (BMDCs). Major BMDCs within the tumour niche include tumour-associated macrophages (TAMs), myeloid-derived suppressor cells (MDSCs), mesenchymal stem cells (MSCs), and various other cell types from lymphocyte and monocyte lineages[41].

In Breast Cancer, recent evidence has demonstrated that the extent of lymphocyte infiltration in tumour tissue and a class of gene expression signatures have the potential to more precisely define patient's clinical evolution and identify patient subgroups with different sensitivities to standard treatments. The importance of exploring the immune system in both research and clinical settings in defining BC behavior, is proving to be a significant factor[42].

In this part of my work, we asked whether p140Cap could play any role in the composition of breast tumour microenvironment. We already know that, at the best of our knowledge, p140Cap is not expressed in the stromal cells, indicating that all the changes observed in the microenvironment in our experimental systems can be ascribed to cancer cell properties. Taking

advantage of the orthotopic injection of syngenic TuBo cell lines described above[32], we identified an additional anti-tumour property of p140Cap, in its ability to reduce the expression of the Granulocyte-Colony Stimulating Factor (G-CSF), likely due to p140Cap capacity of limiting the breast cancer stem cell compartment. Together, these results describe a new tumour suppressive mechanism by which p140Cap is able to affects BC features, through the negative regulation of pro-tumour microenvironment features.

p140Cap affects breast cancer features through the regulation of the tumour microenvironment composition

p140Cap expression inverse correlates with the immune infiltrate

An important hint highlighting the possible role of p140Cap in regulating the tumour microenvironment composition comes from the bioinformatics approach. The Gene Set Enrichment Analysis (GSEA) of 1095 BC patients from The Cancer Genome Atlas (TCGA) data set has revealed that the expression of the SRCIN1 gene inversely correlates with the immune infiltrate signature (Fig. 9A).

We know that p140Cap expression is limited to the epithelial cancer cells. Therefore, if p140Cap plays any role in regulating tumour immune infiltrate composition, this is likely due to a different capability of the p140Cap expressing breast cancer cells to regulate the secretion of inflammatory soluble factors. In order to identify these factors, we performed a Next Generation Sequence (NGS) RNAseq analysis (Fig. 9B), comparing RNA from Mock-TuBo and p140Cap-TuBo cells. Looking for differentially expressed inflammatory secreted factors, we found a significantly down-regulation of the *Csf*3 gene, as shown in figure 9C and D, from a list of cytokines and factors provided by BIOCARTA.

G-CSF is a well-known cytokine that stimulates the survival, proliferation, differentiation and function of neutrophil precursors and mature neutrophils via the binding to its receptor G-CSFR and plays a key role in neutrophil mobilization from the Bone Marrow (BM)[43,44]. The constitutive expression of G-CSF is found in numerous solid tumours contributing to their growth and progression[45,46].

Therefore, in the NeuT mouse breast cancer model, the RNAseq data, showing a p140Cap-dependent differential expression of the *Csf3* gene, suggest that the presence of p140Cap may affect the composition of the tumour immune microenvironment. Overall, the GSEA and the RNAseq analysis point out that the expression of p140Cap may impact on the breast cancer immune infiltrate, with a putative differential expression of the CSF-3 gene.

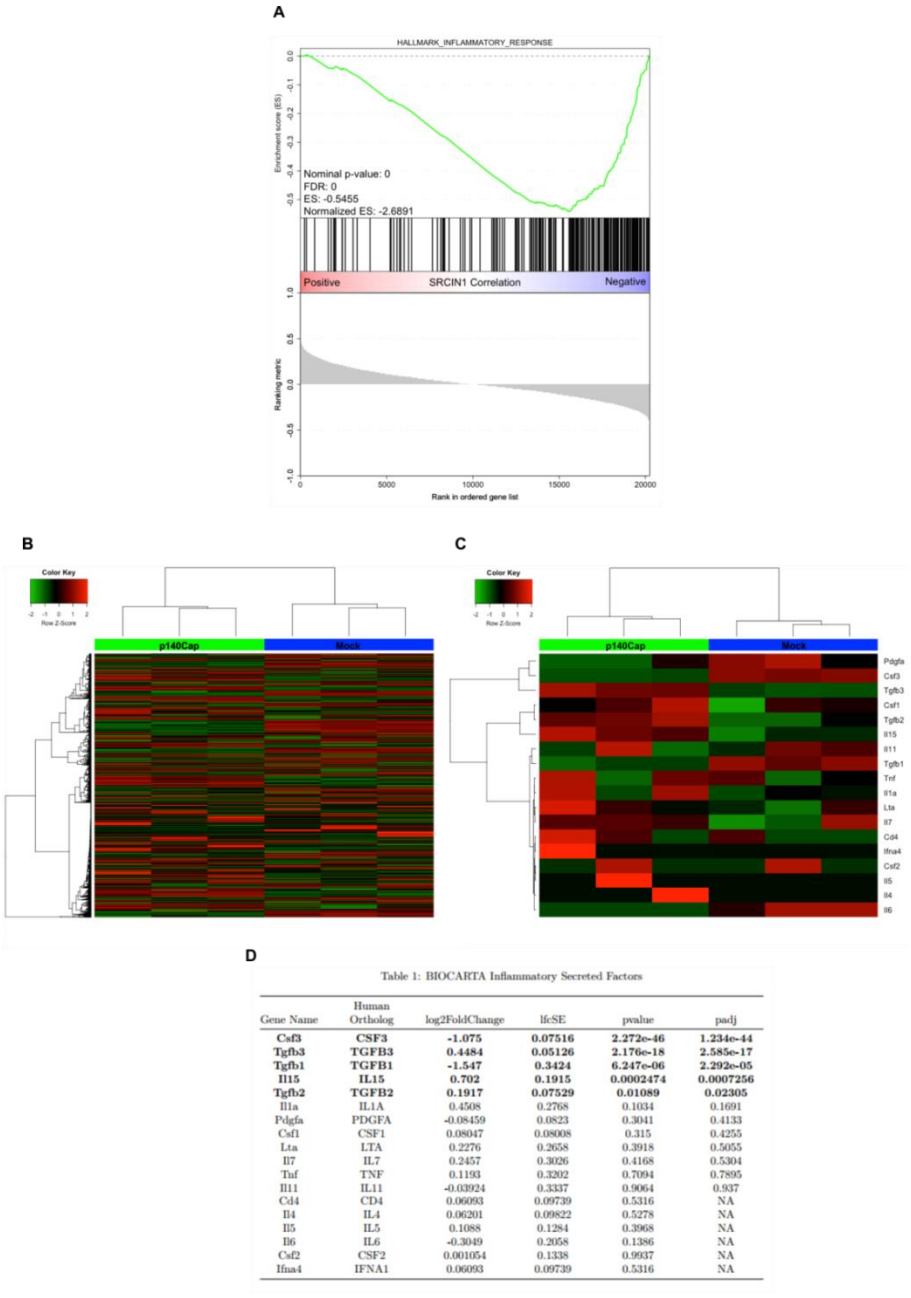

D

Table 1: BIOCARTA Inflammatory Secreted Factors

Gene Name	Human Ortholog	log2FoldChange	lfcSE	pvalue	padj
Csf3	**CSF3**	**-1.075**	**0.07516**	**2.272e-46**	**1.234e-44**
Tgfb3	**TGFB3**	**0.4484**	**0.05126**	**2.176e-18**	**2.585e-17**
Tgfb1	**TGFB1**	**-1.547**	**0.3424**	**6.247e-06**	**2.292e-05**
Il15	**IL15**	**0.702**	**0.1915**	**0.0002474**	**0.0007256**
Tgfb2	**TGFB2**	**0.1917**	**0.07529**	**0.01089**	**0.02305**
Il1a	IL1A	0.4508	0.2768	0.1034	0.1691
Pdgfa	PDGFA	-0.08459	0.0823	0.3041	0.4133
Csf1	CSF1	0.08047	0.08008	0.315	0.4255
Lta	LTA	0.2276	0.2658	0.3918	0.5055
Il7	IL7	0.2457	0.3026	0.4168	0.5304
Tnf	TNF	0.1193	0.3202	0.7094	0.7895
Il11	IL11	-0.03924	0.3337	0.9064	0.937
Cd4	CD4	0.06093	0.09739	0.5316	NA
Il4	IL4	0.06201	0.09822	0.5278	NA
Il5	IL5	0.1088	0.1284	0.3968	NA
Il6	IL6	-0.3049	0.2058	0.1386	NA
Csf2	CSF2	0.001054	0.1338	0.9937	NA
Ifna4	IFNA1	0.06093	0.09739	0.5316	NA

Figure 9. p140Cap expression and immune infiltrate. (A) GSEA plot of Hallmark_Inflammatory_Response gene set from MSigDB~5.0 in 1095 SARCIN1 expressing BC patients from TCGA. The plot shows the distribution of genes in the set that are correlated or not with SRCIN1 expression. **(B)** Heat map illustrating 1700 expressed genes in Mock-TuBo compared with TuBo-p140Cap (n=3). The color scale from green (down-regulated) to red (up-regulated) represents Z scores of log2(FPKM). **(C)** Heat map illustrating a subset of inflammatory secreted factor genes provided

by BIOCARTA in TuBo cells. **(D)** The list of the 18 differentially expressed genes codify for the inflammatory secreted factors provided by BIOCARTA. In bold the statistically significant genes sorted by adjusted p-value.

p140Cap-expressing tumours show decreased G-CSF expression

The *Csf3* RNAseq data were then validated by quantitative RealTime-PCR (qRT-PCR) and Western Blot (WB) analysis on Mock-TuBo and p140Cap-TuBo cells in culture and in tumours generated after orthotopic injection in the fat pad of BALB/c mice. In both p140Cap-TuBo cells and tumours we found a significant reduction of at least 50% in the G-CSF expression level in presence of p140Cap, as shown in figure 10A, B, D and E, compared to the Mock-TuBo model.

These data were further confirmed by an ELISA assay, to assess the level of the G-CSF protein in cell culture supernatants as shown in figure 10C. Consistently, we found that supernatants from p140Cap-TuBo cells contain significantly less G-CSF protein, measured as pg/ml/10^6cells, than Mock-TuBo cells, indicating the existence of a significant inverse correlation between p140Cap expression and levels of secreted G-CSF.

Overall, these data show that, both in breast cancer cells and in tumours, the presence of p140Cap correlates with a reduced G-CSF expression.

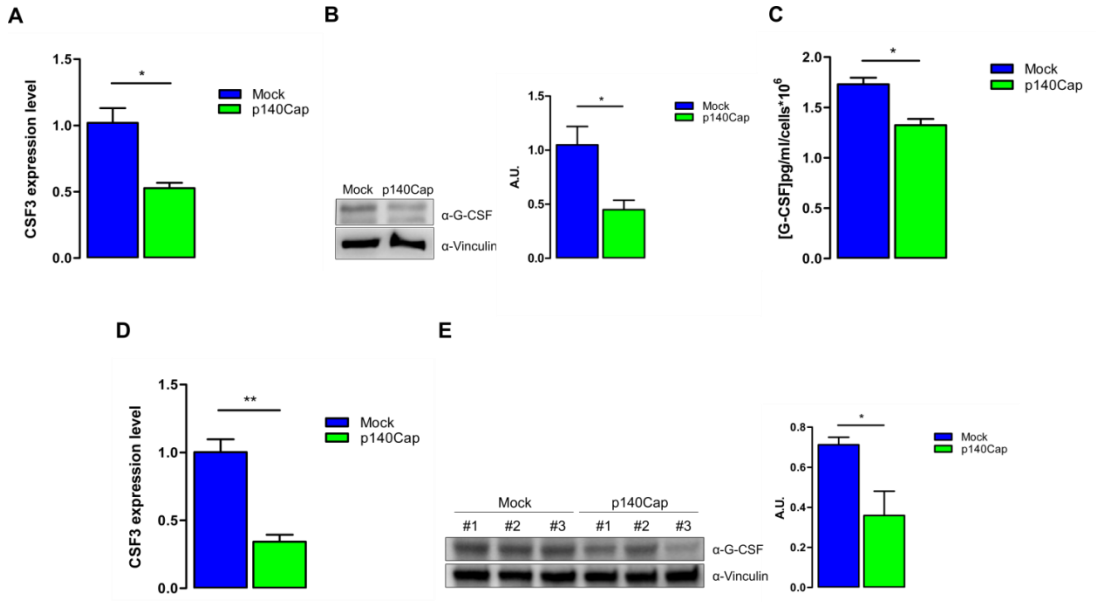

Figure 10. p140Cap reduces G-CSF expression levels. (A, D) qRT-PCR was performed to quantify mRNA expression of *Csf3* expression in Mock and p140Cap TuBo cell lines. RNA was prepared from five biological replicates. qRT–PCR was performed on technical triplicates. Results are expressed in fold change of *Csf*3 gene

expression in p140Cap cells relative to Mock cells. Statistical significative differences were evaluated using unpaired *t*-tests (*P<0.05; **P<0.01). Error bar: s.e.m. **(B, E)** Western blot analysis of G-CSF intracellular protein expression, in cells **(B)** and disaggregated tumours **(E).** Protein extracts from Mock and p140Cap samples were run on 4–15% SDS–PAGE and stained with antibodies to G-CSF. Vinculin was used as an internal standard for protein loading. Histograms show in a.u. the quantification of five independent experiments. Statistical significative differences were evaluated using unpaired *t*-tests (*P<0.05). Error bar: s.e.m. **(C)** ELISA analysis on Mock and p140Cap-expressing cell culture supernatants obtained after three days in culture. The analysis was performed on five independent experiments on technical triplicates. Statistical significative differences were evaluated using unpaired *t*-tests (*P<0.05). Error bar: s.e.m.

p140Cap-expressing tumours show a reduced number of gMDSCs infiltrate

The G-CSF is an important soluble factor responsible for the accumulation into the tumour of a heterogeneous population of myeloid progenitor and precursor cells, responsible of both Granulocyte and Monocyte lineages, namely the Myeloid-Derived Suppressor Cells (MDSCs). These cells are characterized by a strong immune suppressive activity[47,48,49,50].

In physiological conditions these cells, once generated in the bone marrow, completely differentiate into Granulocytes, Macrophages and Dendritic cells. In pathological conditions, such as cancer, factors like the G-CSF, are able to trigger abnormal proliferation of these immature myeloid cells (named IMC), with a partial block of their differentiation. Their abnormal number results in their ability to infiltrate in secondary sites, such as the primary tumours[51].

To assess whether the observed p140Cap-dependent decrease in G-CSF levels may contribute to a differential MDSCs infiltration in tumours, we orthotopically injected Mock-TuBo and p140Cap-TuBo cells in the fat pad of BALB/c mice and we analyzed tumours of the same volume after four weeks of growth. By performing FACS analysis on disaggregated tumours, we quantified both the MDSCs Granulocyte precursors, identified as $CD11b^{+}Ly6G^{+}Ly6C^{lo}$ cell, and the MDSCs Monocytes precursors, identified as $CD11b^{+}Ly6G^{-}Ly6C^{+}$ cells.

Interestingly, in p140Cap-TuBo tumours we found a strong and consistent decrease in the percentage of the MDSCs Granulocyte precursor infiltrate compared to Mock tumours (Fig. 11A). As expected, consistent with the fact that the G-CSF is a specific factor for the

polymorphonuclear precursors able to maximize Granulocyte recruitment, we were not able to detect any difference in the Monocyte precursors (Fig. 11A).

These data indicate that the p140Cap-expressing tumours, which secrete a lower levels of G-CSF, have lower recruitment of gMDSC compared to the Mock tumours.

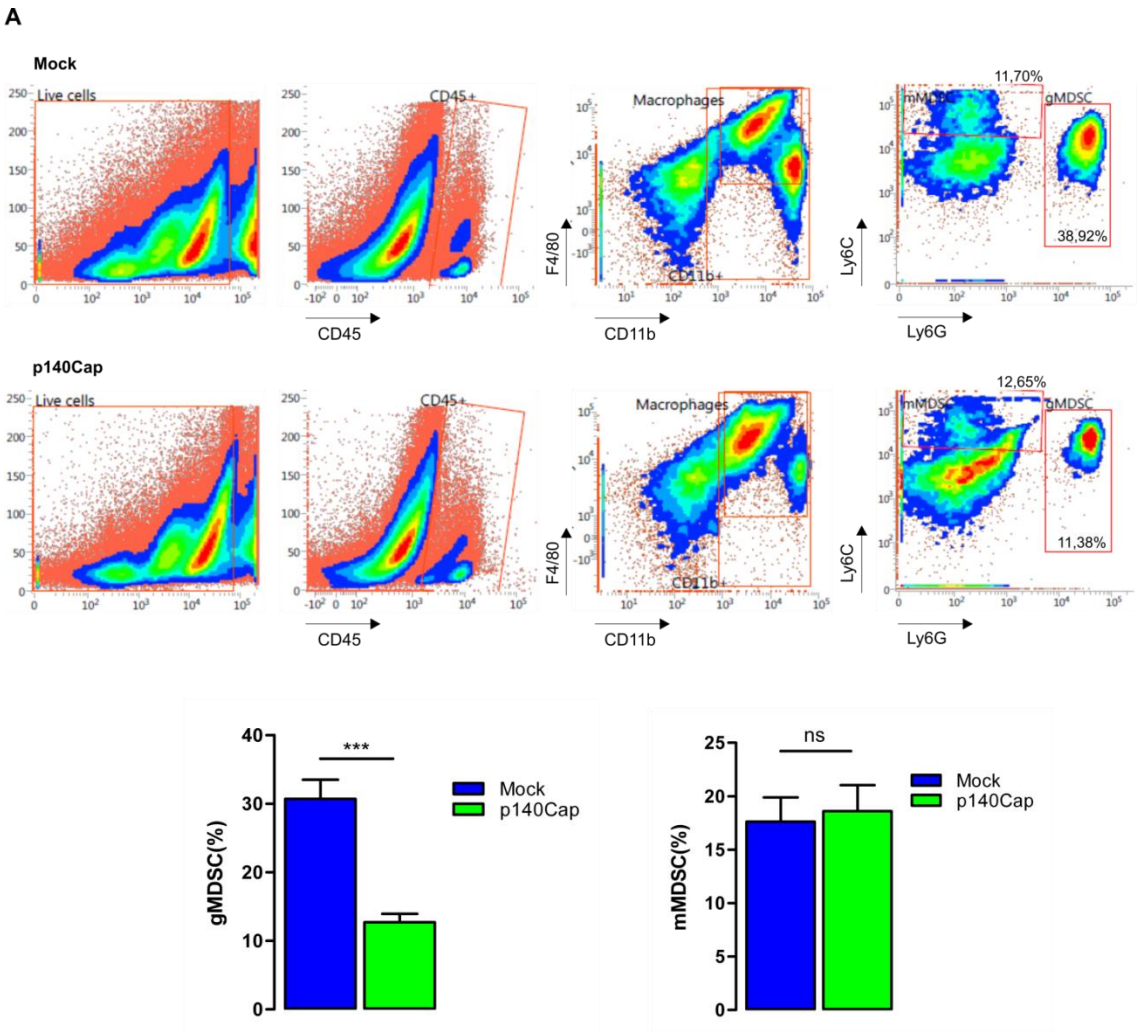

Figure 11. p140Cap reduces gMDSC tumour accumulation. (A) FACS analysis on Mock and p140Cap disaggregated tumours. The samples were stained by using PI, CD45, CD11b, F4/80, Ly6G and Ly6C conjugated antibodies. Live CD45^{+}cells were gated for CD11b and F4/80 and then the proportion of Ly6C and Ly6G cells was evaluated. The analysis was performed on ten independent tumours for each type. Statistical significative differences were evaluated using unpaired *t*-tests (***P<0.001). Error bar: s.e.m.

p140Cap-expressing tumours mobilize less gMDSCs from the bone marrow

It is widely reported that the G-CSF is not only a driver of cell proliferation into the bone marrow, but also an important mobilizing factor. In particular, the G-CSF released by the primary tumour is able to mobilize the gMDSC precursors directly from the bone marrow to the circulation, increasing their ability to infiltrate the tumour site[49,50].

Based on this evidence, we performed FACS analysis in several organs of tumour-bearing mice, to quantify the gMDSC precursor levels not only in the dissected tumours, but also in the blood, the spleen and the bone marrow. We found a statistically significant reduction in the percentage of gMDSCs in both the blood and the spleen of the p140Cap tumour-bearing mice, as well as we detected the presence of a less enlarged spleen, compared to the Mock tumour-bearing mice (Fig. 12A, B), suggesting that p140Cap tumour-bearing mice show a decreased level of systemic inflammation. Conversely, we were not able to detect any difference in the gMDSCs levels in the bone marrow of both p140Cap-TuBo or Mock-TuBo injected mice (Fig. 12C). These result indicate that p140Cap tumour-bearing mice show a significative difference in gMDSCs in the blood and in the spleen, while, in the bone marrow, the different mobilization/proliferation rate in Mock tumour-bearing mice versus p140Cap tumour-bearing mice, is somewhat compensated.

To better explain the difference observed in circulating gMDSC precursor cells in p140Cap tumour-bearing mice, we also quantified the levels of G-CSF in the serum of these mice. By performing an ELISA assay, we found a significantly lower concentration of G-CSF in the serum of the p140Cap tumour-bearing mice compared to Mock tumour-bearing mice (Fig. 12D).

These data demonstrate that p140Cap-expressing tumours, by secreting lower levels of G-CSF, are able to mobilize a reduced number of gMDSC precursors directly from the bone marrow.

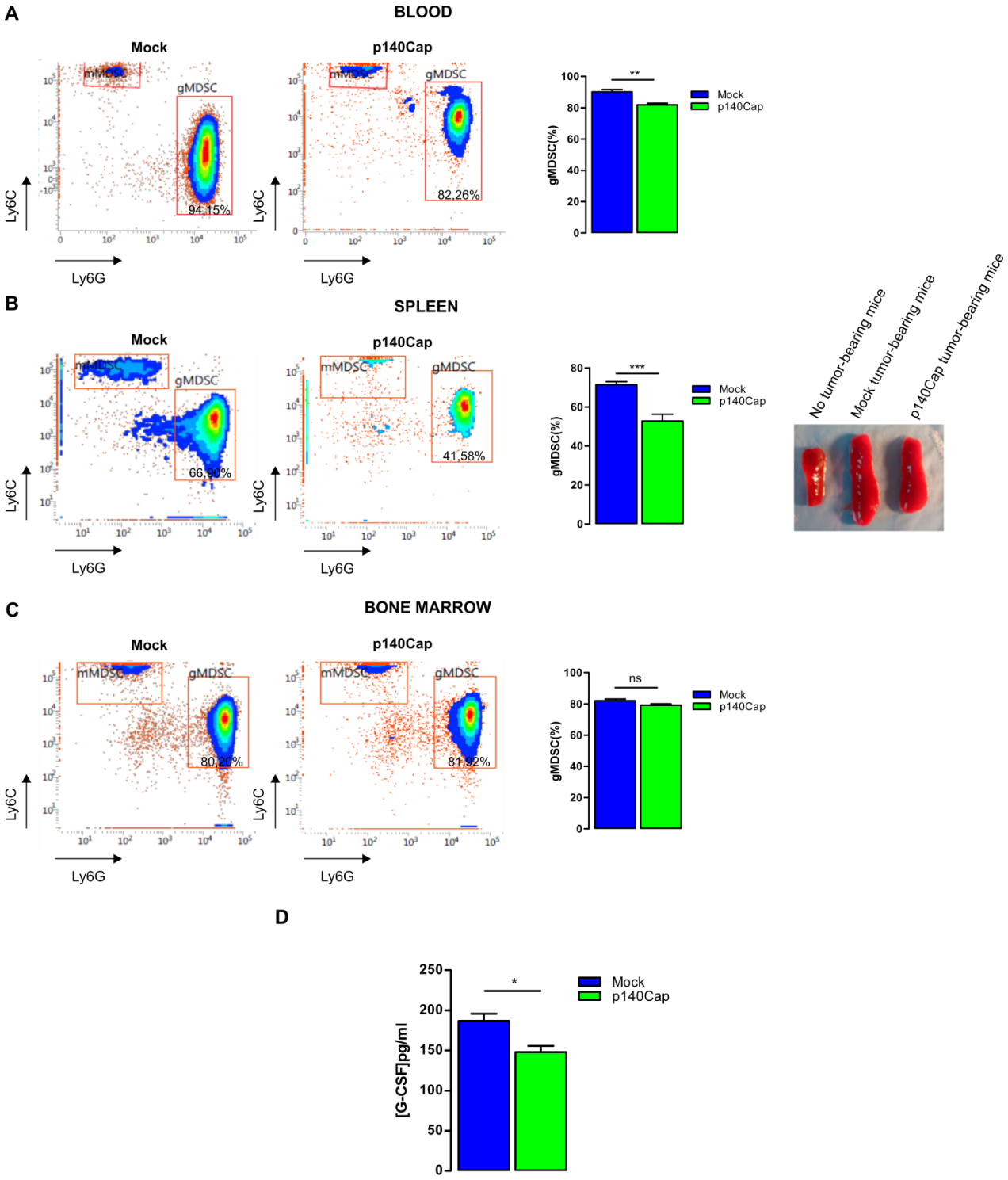

Figure 12. p140Cap mobilize less gMDSC from the bone marrow. (A, B, C) FACS analysis on blood **(A)**, spleen **(B)** and bone marrow **(C)** of p140Cap and Mock tumour-bearing mice. The samples were stained by using PI, CD45, CD11b, F4/80, Ly6G and Ly6C conjugated antibodies. Live $CD45^{+}$cells were gated for CD11band F4/80 and then the proportion of Ly6C and Ly6G cells was evaluated. The analysis was performed on ten independent tumours for each type. Statistical significative differences were evaluated using unpaired *t*-tests (**P<0.01; ***P<0.001). Error bar: s.e.m. **(D)** ELISA analysis on Mock and p140Cap tumour-bearing serum. The analysis was performed on five independent experiments on technical triplicates. Statistical significative differences were evaluated using unpaired *t*-tests (*P<0.05). Error bar: s.e.m.

p140Cap-expressing tumours display a poor immunosupressive microenvironment

As widely reported in the literature, the MDSCs are characterized by a strong immunosuppressive activity. In particular, inside the tumours, the IMC populations are able to produce high levels of reactive oxygen species, nitrogen species and anti-inflammatory cytokines, which in turn modulate the T-Lymphocytes and Natural Killer (NK) cell proliferation, recruit Regulatory T Lymphocytes (Treg) and Macrophages toward the M2-like state[51,52].

Based on the data above reported, since p140Cap-expressing tumours show a lower percentage of gMDSCs infiltrate, we further analyzed their immunosuppressor activity, by performing additional FACS analysis on disaggregated tumours of the same volume, for quantifying additional immune populations. The p140Cap tumours showed a significant increase in the percentage of M1 Macrophages, and a decreasing trend in M2 Macrophages compared to Mock tumours(Fig. 13A). M1 and M2 populations have been widely described to possess an anti- and a pro-tumour activity, respectively[53,54]. Moreover, we found a significant increase in $CD8^+$ T-Lymphocytes upon p140Cap expression, while no differences were detectable in the $CD4^+$ subpopulation (Fig. 13B). Finally, p140Cap expression also correlated with a statistically significant increase in the percentage of NK cells, as well as a significant reduction in Treg cells by IHC analysis, endowed with a relevant anti- and pro-tumour activity, respectively (Fig. 13C, D).

Overall, these data demonstrate that the p140Cap-expressing tumours show a differential composition in immune cell populations, suggestive of a poor immunosuppressive microenvironment.

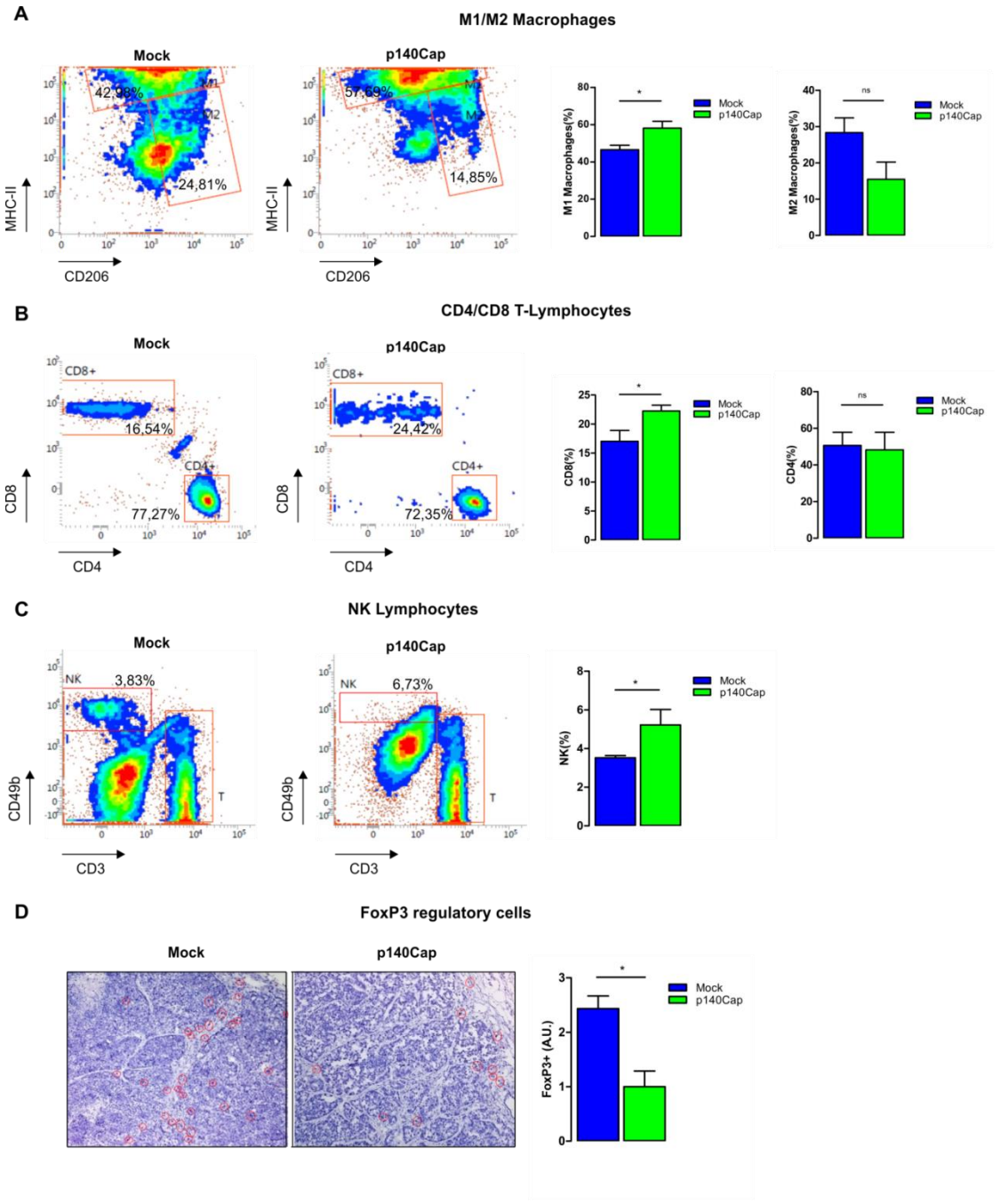

Figure 13. p140Cap-tumours have a poor immunosuppressive microenvironment. (A-B-C) FACS analysis on p140Cap and Mock tumours taken when tumours reached a 10mm diameter. The samples were stained by using PI, CD45, CD49b, CD3, CD8, CD206 and MHC-II conjugated antibodies. Live $CD45^{+}$cells, were evaluated for the proportion of MHC-II and CD206 for M1 and M2 macrophages, were gated for CD3 and evaluated for the proportion of CD4 and CD8 T-lymphocytes and for CD49b positivity for NK cells. The analysis was performed on ten independent tumours for each type. Statistical significative differences were evaluated using unpaired *t*-tests (*P<0.05). Error bar: s.e.m. **(D)** Paraffin-embedded sections from five Mock and five p140Cap tumours taken when tumours reached a 10mm diameter were analyzed for immunohistochemistry with antibodies to FoxP3. Representative images are shown. Scale bar, 20μm. Histograms on the right show the percentage of $FoxP3^{+}$ cells. Statistical significative differences were evaluated using unpaired *t*-tests (*P<0.05).Error bar: s.e.m.

p140Cap regulates breast CSC compartment

From the literature and from unpublished data of Prof.ssa Federica Cavallo's group (MBC, Torino), it has been already shown that the Tumour-Initiating Cell (TIC) compartment exhibits an enhanced G-CSF production[48]. To test the hypothesis whether p140Cap could affect the G-CSF expression levels by regulating the breast Cancer Stem Cell (CSC) compartment, we performed *in vivo* and *in vitro* analysis.

First, relevant data to support the hypothesis that p140Cap can affect the CSC compartment, come from the GSEA analysis on the RNAseq data from Mock TuBo and p140Cap TuBo cells. In particular, in p140Cap-expressing cells we found a significant anti-correlation with a self-renewal gene signature (Fig. 14A). This result was further confirmed by WB analysis on cell extracts with antibodies against the stem cell marker Oct-4. Oct-4 expression was significantly reduced in p140Cap-TuBo cells compared to Mock cells (Fig. 14B).

Moreover, we have recently demonstrated that p140Cap limits EMT in ERBB2-positive breast cancer cell lines, by down-regulating Snail, Slug, and N-Cadherin proteins, and by up-regulating E-Cadherin expression[25]. In the literature, a direct link between the EMT signature and the gain of epithelial stem-cell properties has also been reported[55]. Interestingly, also in our TuBo model, we found that the expression of some EMT markers, such as Snail, Twist, E-Cadherin and N-Cadherin, was significantly decreased in p140Cap-expressing cells compared to Mock TuBo cells, using qRT-PCR and Western Blot analysis (Fig. 14C, D).

To further investigate our hypothesis, we performed the classical mammosphere formation assay, by seeding single-cell suspension of TuBo cells in low adhesion conditions. Cells were derived from both 2D *in vitro* cultures or *in vivo* disaggregated tumour cells. After 5 days in culture, floating spherical mammospheres were analyzed. Interestingly, the expression of p140Cap significantly reduced both the ability of TuBo cells to initiate sphere formation and their growth, measured as mammosphere size (Fig. 15A, B). Indeed, a decreased percentage of spheres of large diameter was counted in p140Cap expressing cells compared to Mock TuBo cells.

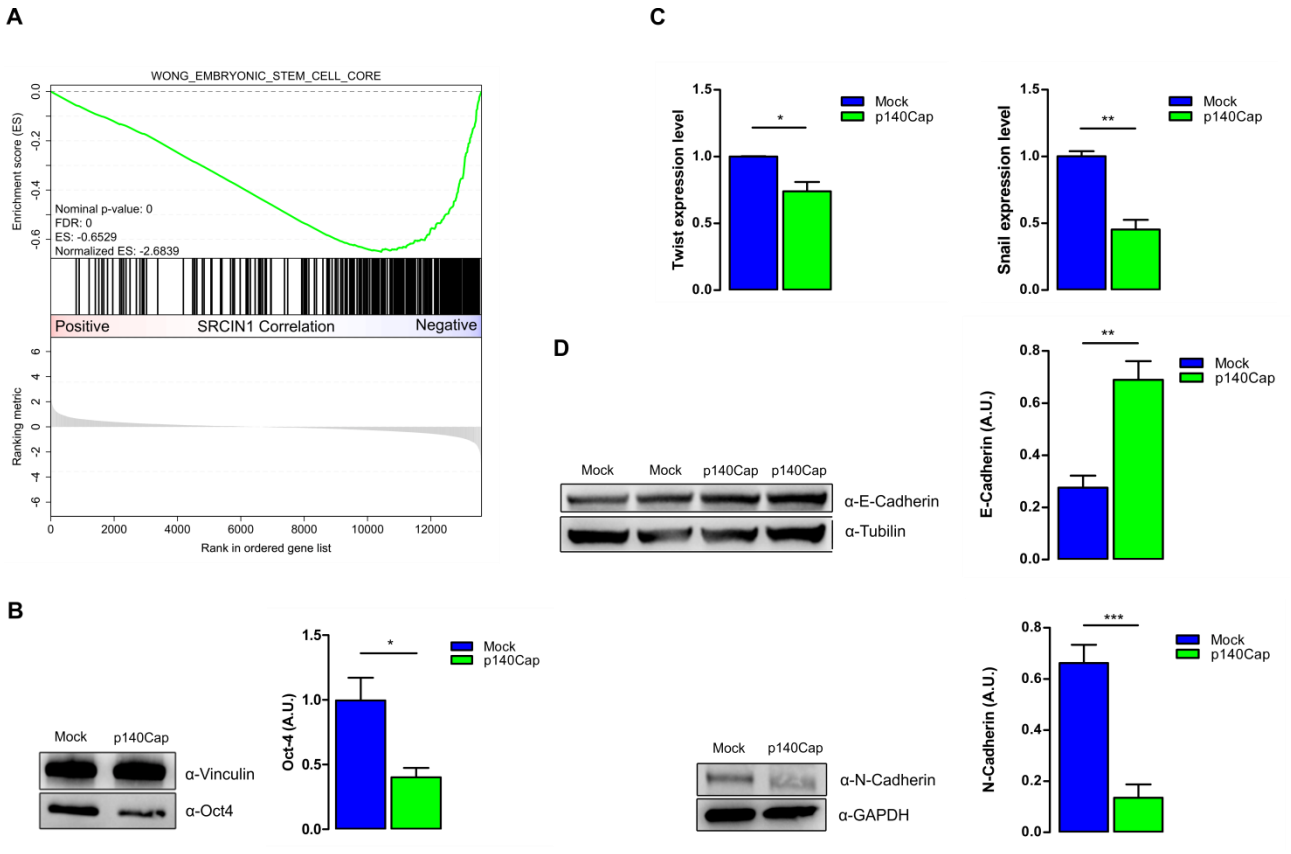

Figure 14. p140Cap limits self-renewal and EMT. (A) GSEA plot of WONG_EMBRYONIC_STEM_CELL_CORE gene set from MSigDB~5.0 from TuBo RNAseq data. The plot shows the distribution of genes in the set that are correlated or not with p140Cap expression. **(C)** RT-PCR was performed to quantify mRNA level expression of Snail and Twist in Mock and p140Cap TuBo cell lines. RNA was prepared from five biological replicates. RT–PCR was performed on technical triplicates. Results are expressed in fold change of Snail and Twist gene expression in p140Cap cells relative to Mock cells. Statistical significative differences were evaluated using unpaired *t*-tests (*P<0.05; **P<0.01). Error bar: s.e.m. **(B, D)** Western blot analysis of Oct-4, E-Cadherin and N-Cadherin protein expression in Mock and p140Cap cells. Protein extracts from Mock and p140Cap samples were run on 4–15% SDS–PAGE and stained with antibodies to Oct-4, N-Cadherin and E-Cadherin. Vinculin, Tubulin and GAPDH were used as internal standard for protein loading. Histograms show in a.u. the quantification of three independent experiments. Statistical significative differences were evaluated using unpaired *t*-tests (**P<0.01; ***P<0.001). Error bar: s.e.m

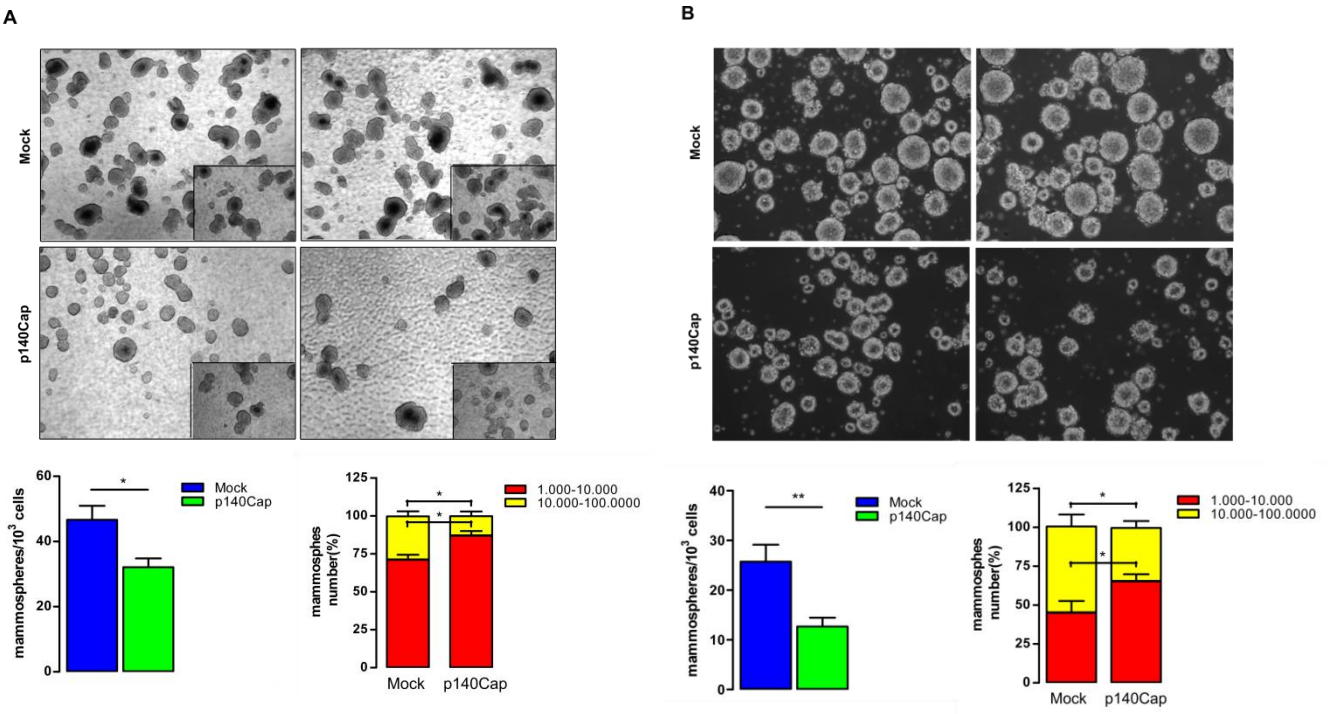

Figure 15. p140Cap regulates the tumour-inititing ability. (A, B) Mammosphere formation assay from 2D *in vitro* cultures **(A)** and from *in vivo* disaggregated tumours **(B)**. 6x10^4/ml single-cell suspension were seeded in mammosphere medium in ultra low-attachment plates and after 5 days culture were analyzed. Representative images of long-term P1 culture (5x and 10x magnification). The number of mammospheres was indicated as mammosphere number generated from every 10^3 single cells plated; for the size, two different range were identified: 1.000-10.000 and 10.000-100.000 inch^2. The analysis was performed on five independent experiments for each type. Statistical significative differences were evaluated using unpaired *t*-tests (*P<0.05;**P<0.01). Error bar: s.e.m.

To further investigating the tumour-initiating ability of p140Cap, we also performed a preliminary *in vivo* limiting dilution assay (LDA), considering LDA as the gold standard to calculate the cancer stem cell frequency. We injected 10^5, 10^4 and 2x10^3 dissociated Mock-TuBo and p140Cap-TuBo cells into syngeneic BALB/c mice. The first dilution is our internal positive control that always generate tumours in both Mock and p140Cap injected mice. Tumour formation was monitored for 5 weeks. Interestingly, we found a reduction of *in vivo* generated tumours in mice injected with both 10^4 and 2x10^3 p140Cap expressing cells (Fig. 16A). In particular, in p140Cap expressing cells, the lower dilution (2 x 10^3 cells) generated tumours only in 2 out of 5 injected mice, while the intermediary dilution (10^4 cells) only in 3 out of 5 injected mice.

Moreover, the mammosphere formation assay, performed on the tumours generated from the LDA assay, gave results similar to those shown in figure 15B, further sustaining the hypothesis of the CSC reduction (Fig. 16B). These data are still preliminary, and additional experiments are required for reaching the statistical significance. Overall, the LDA assay is consistent with our hypothesis that p140Cap-expressing cells are poorly enriched in TIC cells.

A

Dissociated TuBo cells	Number of Transplanted Cells		
	10^5	10^4	$2x10^3$
Mock	3/3	5/5	4/4
p140Cap	3/3	3/5	2/5

B

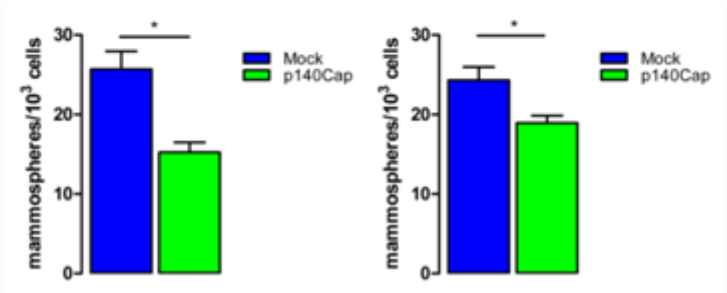

Figure 16. p140Cap expression down-regulates the CSC frequency. (A) LDA assay performed on dissociated TuBo Mock and p140Cap cells after 5 weeks post-injection. In the table are indicated the tumour incidence upon the number of mice after injection of different concentrations of cells. **(B)** Mammosphere formation assay. $6x10^4$ single-cell suspension from disaggregated tumours generated from 10^4 and $2x10^3$ cells injected mice, were seeded in mammosphere medium in ultra low-attachment plates and after 5 days culture were analyzed. The number of mammospheres was indicated as mammosphere number generated from every 10^3 single cells plated. The analysis was performed on three independent experiments for each type. Statistical significative differences were evaluated using unpaired *t*-tests (*P<0.05). Error bar: s.e.m.

p140Cap affects breast CSC proliferative compartment

We and other groups have previously demonstrated that p140Cap is a tumour suppressor protein, able to counteract different tumour features such as tumour growth[15,24,25]. As shown above, p140Cap may affect cell proliferation *in vitro* and *in vivo*, with a marked decrease of proliferative markers, such as PCNA on tumour sections (see figure 4). Based on these

observations, here we focused our attention on the ability of p140Cap to affect the proliferative CSC compartment.

To this end, we performed FACS analysis on disaggregated tumours, staining for both the stem cell antigen 1 (Sca1), a well characterized cancer stem cell marker in TuBo cell line[56], and the Ki67 proliferation marker. As shown in figure 17, we detected a significant reduction in $Sca1^+$ cells in p140Cap expressing tumours, compared to Mock tumours, indicating that tumours expressing p140Cap show a reduced number of cells expressing this cancer stem cell marker. This observation is consistent with the decrease in the CSCs compartment observed both in the mammosphere and in the LDA assays. Moreover, these data also show a significant decrease in $Ki67^+Sca1^+$ double positive cells in p140Cap tumours compared to Mock tumours, suggesting that the presence of p140Cap may specifically affect the proliferating stem cell compartment. Overall, these data show that p140Cap is involved in the regulation of the CSC compartment, likely reducing its proliferation rate.

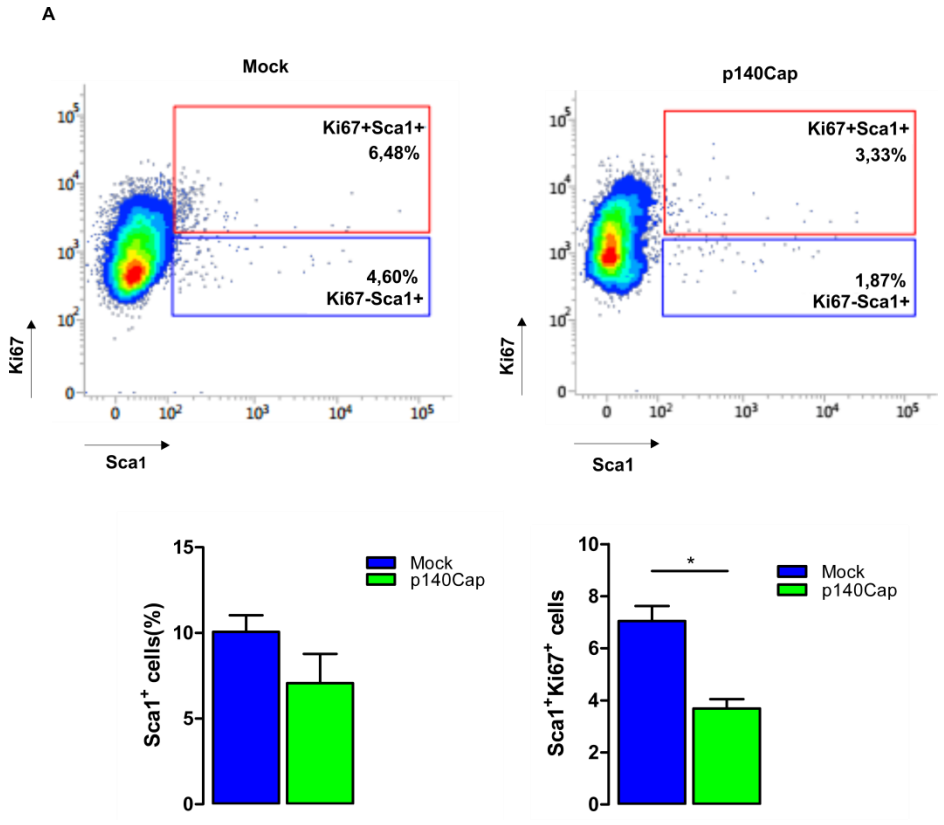

Figure 17. p140Cap affects CSC proliferative compartment. (A) FACS analysis on p140Cap and Mock tumours taken when tumours reached a 10mm diameter. The samples were stained by using, Sca1 and Ki67 conjugated antibodies. The analysis was performed on three independent tumours for each type. Statistical significative differences were evaluated using unpaired *t*-tests (*P<0.05). Error bar: s.e.m.

DISCUSSION

We herein show for the first time that the expression of the p140Cap adaptor protein is clinically relevant to the naturally occurring ERBB2-related breast cancer disease. Indeed, ERBB2 patients who display a positive p140Cap status have significantly higher survival rate, with lower probability of developing a distant recurrence[25].

To characterize the role of p140Cap in the NeuT preclinical model, we generated new Tg mice over-expressing p140Cap into the mammary gland under the MMTV promoter. MMTV-p140Cap Tg mice do not show any defects in the development or the differentiation of the mammary gland that could impair tumour growth. In the double Tg mice, expressing both NeuT and p140Cap, p140Cap expression reduces tumour burden, indicating that p140Cap is causative in limiting ERBB2 tumorigenic *in vivo* features. Indeed, p140Cap expression delays spontaneous tumour appearance and show decreased tumour masses, consistent with a decreased staining of the proliferative marker PCNA, with respect to NeuT mice. In addition, p140Cap expressing tumours show a different histology, reminiscent of that observed in the less aggressive human breast carcinoma[57,58].

The effect of p140Cap on EMT program is witnessed by the marked down-regulation of major EMT transcription factors, such as Snail, Slug and Zeb1[59], accompanied by a reversion of the so-called 'Cadherin switch' (that is, increase of the mesenchymal marker N-Cadherin and a concomitant decrease of the epithelial marker E-Cadherin), which is a canonical hallmark of EMT in cancer[13,59,60]. Indeed, p140Cap tumours display a homogeneous increased level of membrane E-Cadherin, compared to NeuT tumours. Overall, the results point to the ability of p140Cap to counteract the EMT invasive program of ERBB2 tumour cells.

Notably, by taking advantage of the TuBo murine breast cancer cell model, we found that p140Cap expression significantly limits the ability of ERBB2 transformed cells to give rise to metastasis, both in experimental and in spontaneous metastasis assays. Indeed, when comparing tumours of the same size, p140Cap tumours give rise to a significantly lower number of spontaneous lung metastasis compared to NeuT tumours, suggesting that p140Cap affects metastatic spread. However, when analyzing the metastatic lesions from p140Cap tumours, we observed a strong p140Cap expression only in smaller lung metastasis, rather than in larger ones, suggesting that p140Cap has also a strong effect on local metastatic growth. Therefore, from these data we can conclude that p140Cap significantly impairs metastasis acting both on tumour cell spreading and on metastatic growth.

The increasing evidence that the tumour microenvironment strongly contributes to cancer progression, through the interactions between tumour and stromal cells, lead us to investigate the possible link between p140Cap expression in epithelial breast cancer cells and the tumour microenvironment cells. Interestingly, we found in the large TCGA breast cancer data set, an inverse correlation between p140Cap expression and the immune infiltrate signature in GSEA, suggesting that p140Cap may alter the immune landscape of breast tumours. Moreover, RNAseq analysis revealed a significant reduction in the G-CSF expression, which was fully validated at the level of mRNA and protein by western blot analysis and ELISA, both in tumour cell supernatants and in organs from *in vivo* tumour-bearing mice. Indeed, p140Cap tumour-bearing mice display reduced levels of circulating G-CSF in sera compared to mice bearing Mock tumours.

G-CSF exert its action triggering proliferation and dissemination of a number of hematopoietic precursors. In cancer patients, G-CSF is able to mobilize immature myeloid cells directly from the bone marrow to secondary sites, such as the primary cancer, through blood vessels and spleen. Its reduced level in p140Cap tumour-bearing mice well correlates with a significant decrease in the number of granulocytes immature myeloid cells (gMDSCs) infiltrate in these tumours, as well as in blood and spleen of p140Cap tumour-bearing mice. A consistent feedback of the reduced levels of gMDSCs infiltrate in p140Cap tumours comes from the analysis of other immune cell populations with an increase in populations endowed of anti-tumour activities. Indeed, an increased level of M1 macrophages, $CD8^+$ and NK lymphocytes and a reduction of M2 macrophages and T-Regulatory cells was detected in p140Cap tumours. Overall, this analysis provides evidence that, in the preclinical NeuT model, the microenvironment of p140Cap-expressing tumours is characterized by poorly immunosuppressive cell populations.

Our data also show for the first time the existence of an anti-correlation between p140Cap and the Tumour-Initiating Cell compartment. In particular, we found that p140Cap may negatively modulate the proliferation rate of the breast CSC compartment, in terms of *in vitro* mammosphere formation and *in vivo* LDA assays in the TuBo model. Based on previous data showing that the Tumour-Initiating Cell compartment exhibits an enhanced G-CSF production[48], our major hypothesis is that the lower capability of p140Cap tumours to secrete G-CSF compared to Mock tumours depends on the decreased CSC compartment observed in p140Cap expressing tumours. Therefore, the tumour suppressive activity of p140Cap depends not only on its ability to limit tumour pathways involved in survival and proliferation of bulk tumour cells, as already reported[25], but also on its involvement in the specific regulation of the CSC compartment. CSCs have been identified in many types of cancers, including breast cancer[61,62,63]. Due to their role in driving

tumorigenesis, the identification of anti-CSC therapies holds great promise to improve targeted cancer treatment.

Overall, herein we identify that p140Cap may impair tumour features through a new mechanism, consisting in its ability to negatively regulate the CSC compartment, leading to a decrease in G-CSF cytokine secretion. The unbalanced production of G-CSF in turn affects the tumour immune microenvironment composition, specifically affecting the recruitment of pro-tumour MDSC immune infiltrate (Fig. 18). Ultimately, these events may profoundly impair tumour progression.

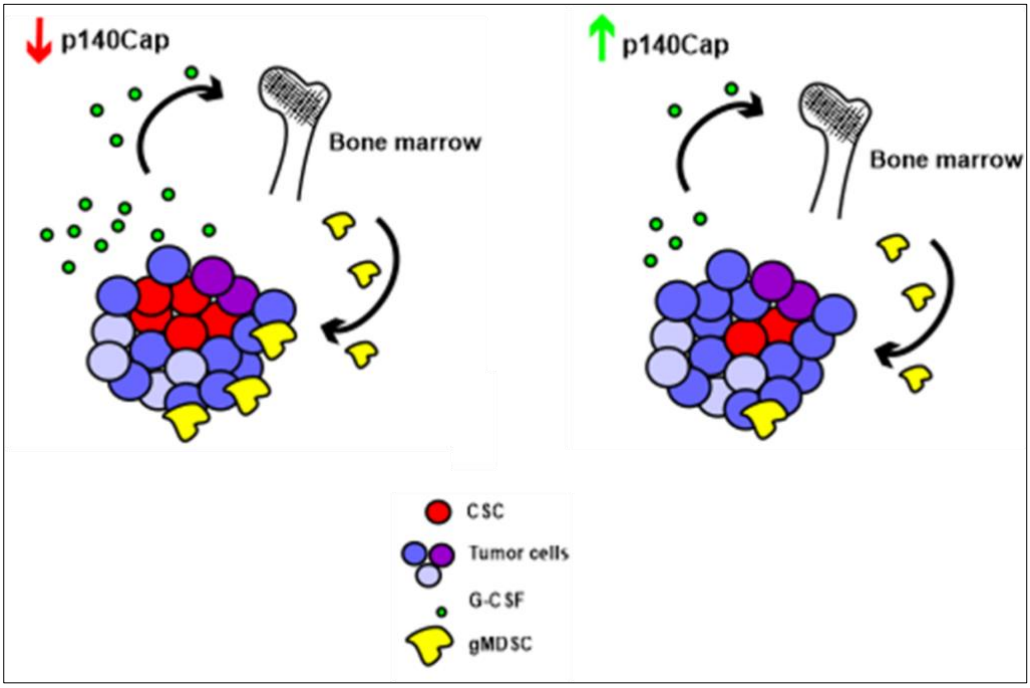

Figure 18. Working model. p140Cap, by regulating the CSC compartment, leads to a decrease in the G-CSF secretion that in turn results in a reduced mobilization of gMDSC from the bone marrow, resulting in a decrease of this specific IMCs population in tumours.

FUTURE PERSPECTIVES

To fully confirm that the poorly immunosuppressive microenvironment, described in our preclinical p140Cap tumours, is mainly dependent on a reduced CSC compartment, we will perform additional experiments, trying to affect the CSC compartment in Mock tumour-bearing mice, with anti-CSC therapy, able to mimic the protective effects of p140Cap in tumours.

Numerous therapies aiming to eradicate cancer stem cells have been developed during last year's. The most common approaches consist in targeting surface biomarkers or signaling pathways that regulate cancer stem cells self-renewal and differentiation. For example, drug-efflux pumps involved in apoptosis resistance, such as the ATP-binding cassette (ABC) transporter family or the xCT cystine/glutamate antiporter system[64], can be exploited. Moreover, microenvironmental signals that sustain CSCs growth can be affected by specific miRNA expression, inducing CSCs apoptosis and differentiation, with the specific aim of hampering CSCs regeneration and cancer relapse[65,66].

An additional relevant question to which we wish to answer in the next few months is how p140Cap regulates CSC proliferation. In this context, we will perform detailed confocal analysis of CSC symmetric versus asymmetric division, to quantify the orientation of the division axis. Moreover, we already know that p140Cap is able to bind β-Catenin (Figure 19A), and maybe to strengthen its localization at the cell membrane. This process would affect β-Catenin translocation into the nucleus, impairing transcription of genes involved in the self-renewal and proliferation signatures. To this end, relevant data come from the GSEA analysis on RNAseq data in TuBo cells, in which we found a significant anti-correlation between p140Cap expression and β-Catenin target gene signature (Figure 19B). Wnt signaling is one of the key cascades regulating development and stemness, and it has also been tightly associated with cancer[67]. Interestingly, by performing PHANTER[68] classification system analysis from these p140Cap anti-correlated genes, we found that in the cellular process category, the 63,6% of the genes are involved in the cell cycle, as shown in figure 19C. In particular, we found a significantly reduction in the β-Catenin target gene CCND2, that codifies for the cyclin D2. At this stage, it is temptative to speculate that an unbalance of cyclin D2 expression might be involved as a causative event to explain the different CSC proliferation rate in tumours expressing p140Cap. Therefore, we would like to focus further experiments on the existence of a p140Cap-β-Catenin-cyclin D2 axis, to gain insights of their involvement, if any, in the Tumour-Initiating Cell compartment in p140Cap tumours.

Finally, to further validating the new role of p140Cap in the regulation of the CSC compartment in breast cancer, we need to validate our observations on human breast cancer patients. This is an

essential goal to achieve together with the clinical units that already collaborated with us (see[25]), by analyzing on breast cancer patient cohorts the presence of specific immune cell populations in the tumour microenvironment, with conventional IHC or with advanced optical imaging.

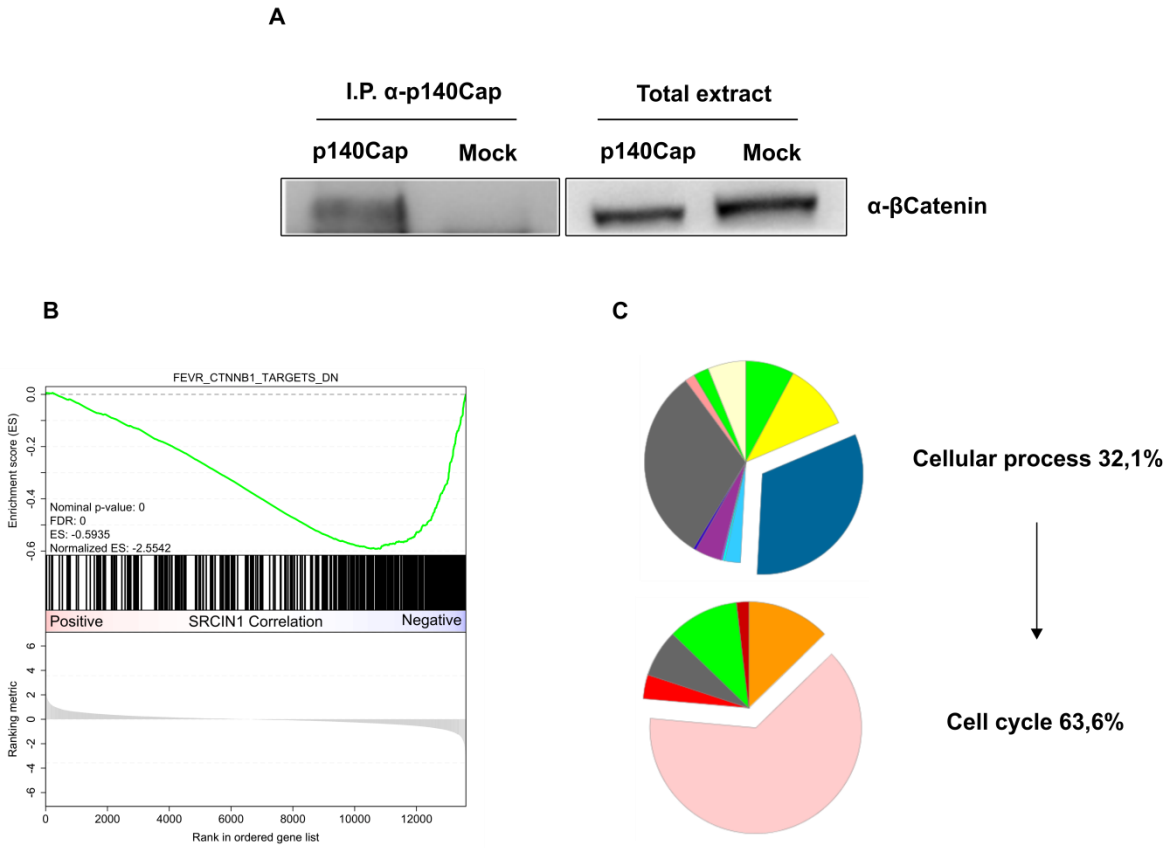

Figure 19. p140Cap and β-Catenin target genes. (A) Extracts from Mock and p140 expressing cancer cells, and p140Cap-expressing, or Mock TuBo cells were immunoprecipitated with antibodies to p140Cap. Cell extracts and immunoprecipates were run on 4-15% SDS–PAGE and blotted with antibodies to β-Catenin. **(B)** GSEA plot of FEVR_CTNNB1_TARGETS_DN gene set from MSigDB~5.0 from TuBo RNAseq data. The plot shows the distribution of genes in the set that are correlated or not with p140Cap expression. **(C)** Gene Ontology analysis on anti-correlated β-Catenin target genes by using PANTHER (Protein ANalysis THrough Evolutionary Relationships) Classification System~13.0. The 32,1% of the genes fall in cellular process category and in turn 63,3% of the latter are cell cycle genes.

MATERIAL AND METHODS

Antibodies, reagents, cell lines and mammosphere cultures

Mouse monoclonal antibodies to p140Cap were produced at the Antibody production facility of the Dept of Molecular Biotechnology and Health Sciences, University of Torino. A recombinant p140Cap protein, obtained in Escherichia coli by fusing the sequence corresponding to amino acids 800-1000 of mouse SRCIN1 gene to the Glutathione S-transferase (GST) was incubated with 4% paraformaldehyde in 1X phosphate buffered saline - pH 7.4 for 30 min, at a concentration of 750 micrograms/ml, dialyzed, and injected into p140Cap KO mice[21] for enhancing immunogenic activity. The resulting purified monoclonal antibodies were characterized by Western blotting and IHC.

For western blot analysis, the following antibodies were used: anti c-ErbB2/c-Neu (Ab-3) (Calbiochem, Merck KGaA, Darmstadt, Germany),anti-G-CSF(Cloud-Clone Corp., Katy, TX, USA), anti-β-catenin (BD Transduction Laboratories, Franklin Lakes, NY), anti-GAPDH, anti-Actin, anti-Tubulin (Santa Cruz Biotechnologies, Palo Alto, CA, USA). Secondary antibodies conjugated with peroxidase were purchased from GE Healthcare. Alexa Fluor Dye secondary antibodies were obtained from Invitrogen (Carlsbad, CA, USA).

For immunohistochemistry, slides were stained with the following primary antibodies: rabbit polyclonal anti-HER2 (Dako, Carpinteria, CA, USA), mouse monoclonal anti-PCNA (Dako, Carpinteria, CA, USA), rabbit polyclonal anti-Caspase3 (R&D System, Minneapolis, MN, USA**,** anti-p140Cap, followed by the appropriate secondary antibodies. Immunoreactive antigens were detected using streptavidin peroxidase (Thermo Scientific UK) and the DAB Chromogen System (Dako, Carpinteria, CA, USA) or alkaline phosphatase conjugated streptavidin (Thermo Scientific UK) and Vulcan fast red chromogen (Biocare Medical, Concord, CA, USA).

PVDF, and films were obtained from GE Healthcare (Buckinghamshire, UK). Culture media were from Invitrogen (Carlsbad, CA, USA). Fetal Bovine Serum (FBS) was from EuroClone (Pero, Milano, Italy).

TuBo cells were derived from a spontaneous breast tumour arisen in a female BALB/c-MMTV-NeuT mice 37 and cultured in DMEM 20% FBS.

For the mammosphere formation assay, TuBo cells were detached and plated in ultra-low-attachment plates (Corning) at 6×10^4 viable cells/ml in mammosphere medium, serum-free

DMEM-F12 medium (Invitrogen) supplemented with 20 ng/ml basic fibroblast growth factor (bFGF), 20 ng/ml epidermal growth factor (EGF), 5 μg/ml insulin, and 0.4% bovine serum albumin (BSA), all from Sigma-Aldrich. Non-adherent spherical clusters of cells, named P1, were collected after 5 d.

Human breast cancer immunohistochemical analysis

Immunohistochemical (IHC) analysis of p140Cap expression was performed on formalin-fixed paraffin-embedded tissue microarrays, prepared with tumour breast specimens, using a mouse monoclonal antibody anti-p140Cap, which was used at a dilution of 1:1000 following an antigen retrieval procedure in EDTA pH 8.0. Immunocomplexes were visualized by the EnVision™+ HRP Mouse (DAB+) kit, DAKO (K4007), and acquired with the AperioScanScope system (Leica Biosystems). Informed consent was obtained from all subjects. For the purpose of correlation with clinical and pathological parameters, tumours were classified based on the intensity of p140Cap staining as p140Cap-Low (IHC score <1) and p140Cap-High (IHC score ≥1).

aCGH and gene expression analyses

Normalized aCGH profiles from 200 ErbB2 breast cancers together with matching gene expression profiles from 50 cases were obtained from the data described in[8]. Correlation analyses between gene copy number, determined by aCGH, and mRNA expression for SCRIN1 were performed using the Pearson correlation as described in[8, 23].

FISH analysis of SRCIN1 gene status

A specific SRCIN1 locus probe was prepared from the BAC RP11-606B22 (17q12) clone, obtained from BAC PAC Resources Center (Children's Hospital, Oakland Research Institute, USA). The BAC was directly labeled with red Spectrum Aqua-dUTP (Abbott Molecular, Europe), using the BioPrime DNA Labeling System (Invitrogen Corporation, USA) according to manufacturer's instructions. An alpha satellite probe specific for chromosome 17 (CEP17) (Abbott Molecular) directly labeled with green fluorocrome, was used as a control probe.

To further analyze the position and strength of the signal, the presence/absence of background, cross-hybridization and, finally, the hybridization efficiency, the BAC clone was tested on metaphase and interphase healthy donor cells obtained using conventional cytogenetic methods. The PathVysion ERBB2 DNA probe kit was used (Abbott Molecular, Europe) for the ERBB2 locus. FISH with the two probes mix, SRCIN1/CEP17 and ERBB2/CEP17, was routinely

performed on formalin fixed paraffin embedded tissue. Red (SRCIN1) and green (CEP7) spots on significant selected areas were automatically acquired, using Metafer, by a Meta System scanning station (Carl Zeiss Meta Systems Gbmh), equipped with an Axio Imager epifluorescence microscope.

The first automatic lecture of the slides, made using the PathVysionV2 software, was performed on the acquired images with Isis software (Zeiss). The ASCO/CAP 2013 Guideline Recommendations for ERBB2 Testing in the Breast were used for the interpretation of both FISH probes: positive for amplification with ERBB2 - SRCIN1/CEP17 ratio >2.0 or with average ERBB2 - SRCIN1 copy number >6; negative for amplification with ERBB2 - SRCIN1/CEP17 ratio<2.0 or *ERBB2* - SRCIN1 copy<4. Gene loss was considered to occur when an average ERBB2 - SRCIN1 copy number <1.8 was found and gene gain when copy number was >3<6. Finally, when heterogeneity was present (such as the presence in the same sample of amplified and not amplified cells), we considered samples where the amplified cell population consisted of more than 10% tumour cells as being amplified.

Generation of the MMTV-p140Cap Transgenic Mice

Full-length mouse p140Cap cDNA was inserted into pspT2 MMTV-LTR plasmid and microinjected at 3.4 ng/ul in the pronucleus of fertilized eggs from FVB mice as previously described [24]. Transgene integration was tested via PCR analysis of genomic DNA, with the primers: 5'-TGGCCCTGCGAGGTCAGCAGGACA-3', 5'-ATCCTGCTGAAGC-CCAGGGGCAGC-3'. MMTV-NeuT FVB and MMTV-NeuT BALB/c mice have been previously described [25, 26, 27, 28]. p140Cap/NeuT double transgenic mice were generated by crossing MMTV-p140Cap with MMTV-NeuT mice. The mice that were positive for both transgenes were included in further analyses, while animals positive only for the NeuT transgene were used as controls. The size of the tumours was evaluated weekly using calipers in blind experiments. Procedures were conducted in conformity with national and international laws and policies as approved by the Faculty Ethical Committee.

Retrovirus production and cell infection

To over-express p140Cap into NeuT-TuBo cells**,** p140Cap cDNA was cloned into pBABE-puro. The retroviruses particles were produced by the calcium phosphate transfection of Platinum Retroviral Packaging Cell Lines (Cell BioLabs), in 10-cm dishes. 48 h after transfection, supernatant that contained the retrovirus particles was collected, filtered through a 45 micrometer

syringe filter and added directly to subconfluent cells. After 48 h, cells were washed and cultured with a selection medium containing puromycin (Sigma) at a final concentration of 1 microgram/ml. The efficiency of infection was controlled by Western blot analysis. Individual clones were isolated 20 days after the start of the selection. Four individual positive clones were pooled together to rule out clonal artifacts.

Immunohistochemistry analyses of NeuT tumours

Tumour samples were fixed in 10% neutral buffered formalin and embedded into paraffin or fixed in 4% PFA and frozen in a cryo-embedding medium (OCT, BioOptica); 5 µm slides were cut and stained with Hematoxylin (BioOptica) and Eosin (BioOptica) for histological examination.

The percentage of PCNA or Caspase3 positive cells was evaluated on digital images of 3 tumors per group (4-6 X 200 microscopic fields per sample); clear brown nuclei were regarded as positive cells and the percentage of labeling index (number of positive cells/total cells x100) was calculated for each field, by two pathologists, independently, and in a blind fashion.

Whole mount experiments

Whole mount preparation was performed as described in 26. The fourth abdominal mammary glands were analyzed from at least three mice for age group. Only whole mounts that contained the entire ductal network including the primary duct and were free of mounting artifacts such as tissue folds were used for subsequent image analysis. A digital photomicrograph was taken of each whole mount using a Leica MZ6stereo microscope fitted with a Nikon Coolpix color digital microscope camera. Within each age group, a consistent magnification was established that allowed the entire epithelial complex to be captured in a single image. For each age group, the photomicrographic settings remained constant. Four different measurements were obtained from each whole-mount image using Photoshop software. TEB count was performed only on 6 weeks of age glands. Ductal length (pixels) was measured by drawing and measuring a straight-line caliper from the most distal point of the ductal network to the nipple. Ductal network area tumours from NeuT mice and xenografts were routinely fixed in 10% formaldehyde buffer (pH 7.4) for 24 h, paraffin-embedded and processed for immunohistochemical analysis with standard procedures 64.

***In vivo* tumor growth, experimental and spontaneous metastasis assay in TuBo cells**

Six week old female BALB/c mice were purchased from Charles River Laboratories (Calco, Italy) and treated in accordance with the European Community guidelines. $1x10^5$Mock-TuBo or

p140Cap-TuBo cells were mixed with 100 microliters PBS and then injected into the left fat pad of female BALB/c mice. The size of the tumours was evaluated weekly using calipers in blind experiments.

For experimental lung metastasis assay, Mock-TuBo and p140Cap-TuBo cells were trypsinized, resuspended in PBS, and then $5x10^4$ cells(in 0.1 mL) were injected via the lateral tail vein of seven-weeks old female NSG mice. Mice were killed 25 days after injection and lungs were fixed in 10% neutral-buffered formalin (BioOptica, Milan, Italy) and paraffin embedded. To optimize the detection of microscopic metastasis and ensure systematic uniform and random sampling, lungs were cut transversally, to the trachea, into 2 mm thick parallel slabs with a random position of the first cut in first 2 mm of the lung, resulting in 5-8 slabs for lung. The slabs were then embedded cut surface down and sections were stained with Hematoxylin and Eosin (BioOptica, Milan, Italy).The metastatic lung tissue was evaluated with Adobe Photoshop by selecting metastasis with the lasso tool and reporting the number of pixels indicated in the histogram window as percentage of the total lung area.

For spontaneous lung metastasis assay, Mock and p140Cap-TuBo cells were trypsinized, resuspended in PBS, and then 10^5 cells (in 0.1 mL) were injected into the right fat pad of seven-weeks old female NSG mice. We monitored mammary tumour growth by regular measurements using a digital caliper. Tumours were surgically removed when reached a 10mm diameter. After 5 weeks, mice were sacrified and lungs were explanted and processed as previously described.

RNA extraction and RNAseq analysis

Total RNA were extracted using Trizol reagent (Invitrogen,Carlsbad, CA) according to the manufacturer's instructions RNA integrity measurements were performed using Fragment Analyzer™ (Advanced Analytical). All samples had RNA Quality Number (RQN) greater than 9.8. For RNA-seq library preparation, 2µg of total RNA were used as input for the TruSeq RNA Library Prep Kit v2 (Illumina), and libraries were prepared following manufacturer instructions. RNA extracted from 6 samples, 3 Mock-TuBo and 3 p140Cap-TuBo has been analyzed on Illumina HiScanSQ. To maintain a reasonable homogeneity between the samples Mock samples were reduced to 20 million reads, which was the average size of the p140 group. Raw reads were converted to FastQ, and examined using the FastQC tool. First mapping performed with STAR software. Reads were mapped on mouse mm10 using UCSC annotation and RSEM software. Mapped reads were used to detect differentially expressed genes between p140 and mock group, used as reference. Differential expression analysis was performed with DESeq2.

RT-PCR and qRT-PCR

For RT-PCR 1 µg of total RNA was used for cDNA synthesis with random hexamers. Real-time PCR was carried out using a 7300 Real Time PCR System (Applied Biosystems). Reactions were run in triplicate in three independent experiments. The geometric mean of housekeeping gene 18S was used as an internal control to normalize the variability in expression levels. Expression data were normalized to the geometric mean of housekeeping gene 18S to control the variability in expression levels and were analyzed using the $2^{-\Delta\Delta CT}$ method.

The following primers were used for Real Time-PCR:

	Forward(5'-3')	Reverse(5'-3')
G-CSF	GTTGTGTGCCACCTACAAGC	CCATCTGCTGCCAGATGGTGGT
SNAIL	GTCTGCACGACCTGTGGAA	CAGGAGAATGGCTTCTCACC
TWIST	AGCTACGCCTTCTCCGTCT	TCCTTCTCTGGAAACAATGACA

Cell lysis and immunoblotting

Cells were extracted using a RIPA buffer (see above). Cell lysates were centrifuged at 13,000g for 15 minutes and the supernatants were collected and assayed for protein concentration using the Bio-Rad protein assay method (Biorad, Hercules, CA, USA). Proteins were run on SDS-PAGE under reducing conditions, were transferred to PVDF membranes, incubated with specific antibodies and then detected with peroxidase-conjugated secondary antibodies and the chemiluminescent ECL reagent. When appropriate, the PVDF membranes were stripped according to manufacturers' recommendations and re-probed.

To assay p140Cap expression in MMTV-p140Cap transgenic mouse lines, mammary gland tissue protein extracts were prepared at three days lactation from different Tg female mice. To assay p140Cap expression in different tissues of the MMTV-p140Cap transgenic mice, protein extracts were prepared from distinct tissues collected from FVB WT or MMTV-p140Cap Tg female at 15 days of pregnancy. Protein extracts run on 6% SDS-PAGE were stained with antibodies to Myc, p140Cap, vinculin and actin for loading control.

***Ex vivo* experiments**

All tumours were explanted when reached 10mm diameter. For FACS analysis and mammosphere formation assay, tumours were mechanically and enzymatically disaggregated for 1 hour at 37°C

with collagenase (Sigma-Aldrich). Then tumours but also spleen and bone marrow were filtered in 40μm cell strainer (Corning), centrifuged and resuspended in PBS. Blood was collected inS-Monovette® (Sarstedt, Nümbrecht, Germany). Only for FACS analysis, the single cell suspension was subjected to red blood cell lysis.

ELISA

Supernatants of 6×10^4/ml TuBo cells, were harvested after 7 days of culture. For serum, blood was collected in EDTA tubes S-Monovette® (Sarstedt, Nümbrecht, Germany). To separate serum from blood cells, after coagulation, a 15 min centrifugation at 4,000 rpm, 4°C, was performed. Plasma and cell culture supernatants were stored at −80 °C before G-CSF analysis by Mini ABTS ELISA development kit (Peprotech) according to manufacturer's instructions.

Flow Cytometry Analysis

TuBo cells and tumours were collected, disaggregated using enzymatic and mechanical dissociation, and washed in PBS. Cell suspensions were either stained for membrane antigens or fixed and permeabilized with 2% PFA and 0,5% saponin-1% BSA and then stained for intracellular antigens. The following antibodies were used: Alexa Fluor 647–conjugated anti-stem cell antigen 1 (Sca-1), BrilliantViolet-Ki67 from Biolegend (London, UK), VioGreen-conjugated anti-CD45, FITC-conjugated anti-CD11b, VioBlue-conjugated anti-Ly6G, APC-Vio770-conjugated anti-Ly6C, PE-Vio770-conjugated anti-F4/80, PE-conjugated anti-CD206, APC-conjugated anti-MHC II, FITC-conjugated anti-CD3, APC-Vio770-conjugated anti-CD4, VioBlue-conjugated anti-CD8, PE-Vio770-conjugated anti-B220, PE-conjugated anti-CD49b from Miltenyi Biotec (Bergisch Gladbach, Germany).Samples were collected and analyzed using a BD FACSVerse™ Flow Cytometer Systems.

GSEA analysis

Gene Set Enrichment Analysis[69,70], was performed by running the GSEA Preranked tool from command line (gsea2-2.2.0.jar, with the following parameters: -mode Max_probe, -norm meandiv, -nperm 1000, -rnd_seed timestamp, -set_max 500 and -set_min 15). The list's ranking metric was calculated on the Spearman's Rho correlation coefficient between SRCIN1 expression levels and all the genes present in the analyzed cohort (for what concern TCGA BRCA, 20530 genes in 1095 primary tumour samples cohort. For what concerns TuBo cell lines, the ranking metrics was calculated on log2 fold change between TuBo over-expressing SRCIN1 and control vector. The gene sets used in the analysis (HALLMARK_INFLAMMATORY_RESPONSE,

WONG_EMBRYONIC_STEM_CELL_CORE, FEVR_CTNNB1_TARGETS_DN), were downloaded (on May 16, 2016) from the Broad Institute GSEA website (http://software.broadinstitute.org/gsea/index.jsp), MSigDB database v5.2.

Statistical analysis

Tissue microarray data analysis was performed using JMP 10.0 statistical software (SAS Institute, Inc). The association between p140Cap expression and clinico-pathological parameters was evaluated using the Pearson chi-square test. For univariate and multivariate analysis, Hazard Ratios (HR) and 95% Confidence Intervals were obtained from the Cox proportional regression method. Differences in the growth rate of mouse tumours were analyzed using the Student's *t*-test and Fisher's Exact Test. Results are expressed as means ± S.E.M. Two-way ANOVA followed by Bonferroni multiple comparison *post hoc* test was performed for tumour analysis.

BIBLIOGRAPHY

1. Siegel, R., Naishadham, D. & Jemal, A. Cancer Statistics , 2012. *CA Cancer J Clin* **62,** 10–29 (2012).
2. Cancer, T. & Atlas, G. Comprehensive molecular portraits of human breast tumours. *Nature* **490,** 61–70 (2012).
3. Slamon, D. J. *et al.* Human breast cancer: correlation of relapse and survival with amplification of the HER-2/neu oncogene. *Science (80-.).* **235,** 177–182 (1987).
4. Hynes, N. E. & MacDonald, G. ErbB receptors and signaling pathways in cancer. *Current Opinion in Cell Biology* **21,** 177–184 (2009).
5. Arteaga, C. L. & Engelman, J. A. ERBB receptors: From oncogene discovery to basic science to mechanism-based cancer therapeutics. *Cancer Cell* **25,** 282–303 (2014).
6. Staaf, J. *et al.* Identification of subtypes in human epidermal growth factor receptor 2-positive breast cancer reveals a gene signature prognostic of outcome. *J. Clin. Oncol.* **28,** 1813–1820 (2010).
7. Kauraniemi, P., Kuukasjärvi, T., Sauter, G. & Kallioniemi, A. Amplification of a 280-Kilobase Core Region at the ERBB2 Locus Leads to Activation of Two Hypothetical Proteins in Breast Cancer. *Am. J. Pathol.* **163,** 1979–1984 (2003).
8. Staaf, J. *et al.* High-resolution genomic and expression analyses of copy number alterations in HER2-amplified breast cancer. *Breast Cancer Res.* **12,** R25 (2010).
9. Slamon, D. J. & Press, M. F. Alterations in the TOP2A and HER2 genes: Association with adjuvant anthracycline sensitivity in human breast cancers. *Journal of the National Cancer Institute* **101,** 615–618 (2009).
10. Lamy, P.-J. *et al.* Quantification and clinical relevance of gene amplification at chromosome 17q12-q21 in human epidermal growth factor receptor 2-amplified breast cancers. *Breast Cancer Res.* **13,** R15 (2011).
11. Sahlberg, K. K. *et al.* The HER2 amplicon includes several genes required for the growth and survival of HER2 positive breast cancer cells. *Mol. Oncol.* **7,** 392–401 (2013).
12. Arteaga, C. L. *et al.* Treatment of HER2-positive breast cancer: current status and future perspectives. *Nat. Rev. Clin. Oncol.* **9,** 16–32 (2011).
13. Lamouille, S., Xu, J. & Derynck, R. Molecular mechanisms of epithelial-mesenchymal transition. *Nature Reviews Molecular Cell Biology* **15,** 178–196 (2014).

14. Di Stefano, P. *et al.* P130Cas-associated protein (p140Cap) as a new tyrosine-phosphorylated protein involved in cell spreading. *Mol. Biol. Cell* **15,** 787–800 (2004).

15. Di Stefano, P. *et al.* p140Cap protein suppresses tumour cell properties, regulating Csk and Src kinase activity. *EMBO J.* **26,** 2843–2855 (2007).

16. Damiano, L. *et al.* P140Cap suppresses the invasive properties of highly metastatic MTLn3-EGFR cells via impaired cortactin phosphorylation. *Oncogene* **31,** 624–633 (2012).

17. Cabodi, S., Del Pilar Camacho-Leal, M., Di Stefano, P. & Defilippi, P. Integrin signalling adaptors: Not only figurants in the cancer story. *Nature Reviews Cancer* **10,** 858–870 (2010).

18. Sharma, N. *et al.* Identification of two regions in the p140Cap adaptor protein that retain the ability to suppress tumor cell properties. *Am. J. Cancer Res.* **3,** 290–301 (2013).

19. Cao, M. *et al.* miR-150 promotes the proliferation and migration of lung cancer cells by targeting SRC kinase signalling inhibitor 1. *Eur. J. Cancer* **50,** 1013–24 (2014).

20. Chen, B. *et al.* MicroRNA-346 functions as an oncogene in cutaneous squamous cell carcinoma. *Tumor Biol.* **37,** 2765–2771 (2016).

21. Xu, X. *et al.* miR-374a promotes cell proliferation, migration and invasion by targeting SRCIN1 in gastric cancer. *FEBS Lett.* **589,** 407–413 (2015).

22. Ye, L., Wang, H. & Liu, B. miR-211 promotes non-small cell lung cancer proliferation by targeting SRCIN1. *Tumor Biol.* **37,** 1151–1157 (2016).

23. Wang, P. *et al.* SRCIN1 suppressed osteosarcoma cell proliferation and invasion. *PLoS One* **11,** (2016).

24. Damiano, L. *et al.* P140Cap dual regulation of E-cadherin/EGFR cross-talk and Ras signalling in tumour cell scatter and proliferation. *Oncogene* **29,** 3677–3690 (2010).

25. Grasso, S. *et al.* The scaffold protein p140Cap limits ERBB2-mediated breast cancer progression interfering with Rac GTPase-controlled circuitries. *Nat. Commun.* **8,** (2017).

26. Hudis, C. A. *et al.* Proposal for standardized definitions for efficacy end points in adjuvant breast cancer trials: The STEEP system. *J. Clin. Oncol.* **25,** 2127–2132 (2007).

27. Wolff, A. C. *et al.* Recommendations for Human Epidermal Growth Factor Receptor 2 Testing in Breast Cancer: American Society of Clinical Oncology/College of American Pathologists Clinical Practice Guideline Update. *Arch. Pathol. Lab. Med.* **138,** 241–256 (2014).

28. Jönsson, G. *et al.* Genomic subtypes of breast cancer identified by array-comparative genomic hybridization display distinct molecular and clinical characteristics. *Breast Cancer Res.* **12,** R42 (2010).

29. Muller, W. J., Sinn, E., Pattengale, P. K., Wallace, R. & Leder, P. Single-step induction of mammary adenocarcinoma in transgenic mice bearing the activated c-neu oncogene. *Cell* **54,** 105–115 (1988).

30. Boggio, K. *et al.* Interleukin 12-mediated prevention of spontaneous mammary adenocarcinomas in two lines of Her-2/neu transgenic mice. *J. Exp. Med.* **188,** 589–596 (1998).

31. Galiè, M. *et al.* In Vivo Mapping of Spontaneous Mammary Tumors in Transgenic Mice Using MRI and Ultrasonography. *J. Magn. Reson. Imaging* **19,** 570–579 (2004).

32. Rovero, S. *et al.* DNA Vaccination Against Rat Her-2/Neu p185 More Effectively Inhibits Carcinogenesis Than Transplantable Carcinomas in Transgenic BALB/c Mice. *J. Immunol.* **165,** 5133–5142 (2000).

33. Salvatore, V. *et al.* The tumor microenvironment promotes cancer progression and cell migration. *Oncotarget* **8,** 9608–9616 (2017).

34. Nienhuis, H. H. *et al.* Targeting breast cancer through its microenvironment: Current status of preclinical and clinical research in finding relevant targets. *Pharmacology and Therapeutics* **147,** 63–79 (2015).

35. Conti, L. *et al.* Microenvironment, oncoantigens, and antitumor vaccination: Lessons learned from BALB-neuT mice. *BioMed Research International* **2014,** (2014).

36. Semenza, G. L. Hypoxia-inducible factors: coupling glucose metabolism and redox regulation with induction of the breast cancer stem cell phenotype. *EMBO J.* **36,** 252–259 (2017).

37. Albini, A. & Sporn, M. B. The tumour microenvironment as a target for chemoprevention. *Nature Reviews Cancer* **7,** 139–147 (2007).

38. Gajewski, T. F., Schreiber, H. & Fu, Y.-X. Innate and adaptive immune cells in the tumor microenvironment. *Nat. Immunol.* **14,** 1014–1022 (2013).

39. Ben-Baruch, A. Host microenvironment in breast cancer development: Inflammatory cells, cytokines and chemokines in breast cancer progression: reciprocal tumor–microenvironment interactions. *Breast Cancer Res.* **5,** 31 (2002).

40. Nagarsheth, N., Wicha, M. S. & Zou, W. Chemokines in the cancer microenvironment and their relevance in cancer immunotherapy. *Nature Reviews Immunology* **17,** 559–572 (2017).

41. Joyce, J. A. & Pollard, J. W. Microenvironmental regulation of metastasis. *Nature Reviews Cancer* **9,** 239–252 (2009).

42. Criscitiello, C., Esposito, A. & Curigliano, G. Tumor-stroma crosstalk: targeting stroma in breast cancer. *Curr. Opin. Oncol.* **26,** 551–5 (2014).

43. Roberts, A. W. G-CSF: A key regulator of neutrophil production, but that's not all! *Growth Factors* **23,** 33–41 (2005).

44. Panopoulos, A. D. & Watowich, S. S. Granulocyte colony-stimulating factor: Molecular mechanisms of action during steady state and 'emergency' hematopoiesis. *Cytokine* **42,** 277–288 (2008).

45. Mueller, M. M. & Fusenig, N. E. Friends or foes - Bipolar effects of the tumour stroma in cancer. *Nature Reviews Cancer* **4,** 839–849 (2004).

46. Mroczko, B. & Szmitkowski, M. Hematopoietic cytokines as tumor markers. *Clinical Chemistry and Laboratory Medicine* **42,** 1347–1354 (2004).

47. Bronte, V. *et al.* Recommendations for myeloid-derived suppressor cell nomenclature and characterization standards. *Nature Communications* **7,** (2016).

48. Welte, T. *et al.* Oncogenic mTOR signalling recruits myeloid-derived suppressor cells to promote tumour initiation. *Nat. Cell Biol.* **18,** 632–644 (2016).

49. Shojaei, F. *et al.* G-CSF-initiated myeloid cell mobilization and angiogenesis mediate tumor refractoriness to anti-VEGF therapy in mouse models. *Proc. Natl. Acad. Sci.* **106,** 6742–6747 (2009).

50. Kowanetz, M. *et al.* Granulocyte-colony stimulating factor promotes lung metastasis through mobilization of Ly6G+Ly6C+ granulocytes. *Proc Natl Acad Sci U S A* **107,** 21248–21255 (2010).

51. Gabrilovich, D. I. & Nagaraj, S. Myeloid-derived suppressor cells as regulators of the immune system. *Nature Reviews Immunology* **9,** 162–174 (2009).

52. Umansky, V., Blattner, C., Gebhardt, C. & Utikal, J. The Role of Myeloid-Derived Suppressor Cells (MDSC) in Cancer Progression. *Vaccines* **4,** 36 (2016).

53. Liu, Y. & Cao, X. The origin and function of tumor-associated macrophages. *Cell. Mol. Immunol.* **12,** 1–4 (2015).

54. Mantovani, A., Marchesi, F., Malesci, A., Laghi, L. & Allavena, P. Tumour-associated macrophages as treatment targets in oncology. *Nature Reviews Clinical Oncology* **14,** 399–416 (2017).

55. Mani, S. A. *et al.* The Epithelial-Mesenchymal Transition Generates Cells with Properties of Stem Cells. *Cell* **133,** 704–715 (2008).

56. Grange, C., Lanzardo, S., Cavallo, F., Camussi, G. & Bussolati, B. Sca-1 identifies the tumor-initiating cells in mammary tumors of BALB-neuT transgenic mice. *Neoplasia* **10,** 1433–1443 (2008).

57. Lopez-Garcia, M. A., Geyer, F. C., Lacroix-Triki, M., Marchió, C. & Reis-Filho, J. S. Breast cancer precursors revisited: Molecular features and progression pathways. *Histopathology* **57,** 171–192 (2010).

58. Zhang, W. *et al.* Invasive cribriform carcinoma in a chinese population: Comparison with low-grade invasive ductal carcinoma-not otherwise specified. *Int. J. Clin. Exp. Pathol.* **6,** 445–457 (2013).

59. Bill, R. & Christofori, G. The relevance of EMT in breast cancer metastasis: Correlation or causality? *FEBS Lett.* **589,** 1577–1587 (2015).

60. Hanahan, D. & Weinberg, R. A. Review Hallmarks of Cancer : The Next Generation. *Cell* **144,** 646–674 (2011).

61. Al-Hajj, M., Wicha, M. S., Benito-Hernandez, A., Morrison, S. J. & Clarke, M. F. Prospective identification of tumorigenic breast cancer cells. *Proc. Natl. Acad. Sci.* **100,** 3983–3988 (2003).

62. Li, C. *et al.* Identification of pancreatic cancer stem cells. *Cancer Res.* **67,** 1030–1037 (2007).

63. Singh, S. K. *et al.* Identification of a cancer stem cell in human brain tumors. *Cancer Res.* **63,** 5821–5828 (2003).

64. Lanzardo, S. *et al.* Immunotargeting of antigen xCT attenuates stem-like cell behavior and metastatic progression in breast cancer. *Cancer Res.* **76,** 62–72 (2016).

65. Dragu, D. L., Necula, L. G., Bleotu, C., Diaconu, C. C. & Chivu-Economescu, M. Therapies targeting cancer stem cells: Current trends and future challenges. *World J. Stem Cells* **7,** 1185–201 (2015).

66. Ramos, E. K., Hoffmann, A. D., Gerson, S. L. & Liu, H. New Opportunities and Challenges to Defeat Cancer Stem Cells. *Trends in Cancer* (2017). doi:10.1016/j.trecan.2017.08.007

67. Zhan, T., Rindtorff, N. & Boutros, M. Wnt signaling in cancer. *Oncogene* **36,** 1461–1473 (2017).

68. Mi, H. *et al.* PANTHER version 11: Expanded annotation data from Gene Ontology and Reactome pathways, and data analysis tool enhancements. *Nucleic Acids Res.* **45,** D183–D189 (2017).

69. Subramanian, A. *et al.* Gene set enrichment analysis: A knowledge-based approach for interpreting genome-wide expression profiles. *Proc. Natl. Acad. Sci.* **102,** 15545–15550 (2005).

70. Mootha, V. K. *et al.* PGC-1α-responsive genes involved in oxidative phosphorylation are coordinately downregulated in human diabetes. *Nat. Genet.* **34,** 267–273 (2003).

nature COMMUNICATIONS

ARTICLE

Received 5 May 2016 | Accepted 27 Jan 2017 | Published 16 Mar 2017

DOI: 10.1038/ncomms14797 OPEN

The scaffold protein p140Cap limits ERBB2-mediated breast cancer progression interfering with Rac GTPase-controlled circuitries

Silvia Grasso[1], Jennifer Chapelle[1], Vincenzo Salemme[1], Simona Aramu[1], Isabella Russo[1], Nicoletta Vitale[1], Ludovica Verdun di Cantogno[2], Katiuscia Dallaglio[3], Isabella Castellano[2], Augusto Amici[4], Giorgia Centonze[1], Nanaocha Sharma[1], Serena Lunardi[1], Sara Cabodi[1], Federica Cavallo[1], Alessia Lamolinara[5], Lorenzo Stramucci[5], Enrico Moiso[1], Paolo Provero[1], Adriana Albini[6], Anna Sapino[2], Johan Staaf[7], Pier Paolo Di Fiore[8,9,10], Giovanni Bertalot[8], Salvatore Pece[8,10], Daniela Tosoni[8], Stefano Confalonieri[8,9], Manuela Iezzi[5], Paola Di Stefano[1], Emilia Turco[1,*] & Paola Defilippi[1,*]

The docking protein p140Cap negatively regulates tumour cell features. Its relevance on breast cancer patient survival, as well as its ability to counteract relevant cancer signalling pathways, are not fully understood. Here we report that in patients with *ERBB2*-amplified breast cancer, a p140Cap-positive status associates with a significantly lower probability of developing a distant event, and a clear difference in survival. p140Cap dampens ERBB2-positive tumour cell progression, impairing tumour onset and growth in the NeuT mouse model, and counteracting epithelial mesenchymal transition, resulting in decreased metastasis formation. One major mechanism is the ability of p140Cap to interfere with *ERBB2*-dependent activation of Rac GTPase-controlled circuitries. Our findings point to a specific role of p140Cap in curbing the aggressiveness of *ERBB2*-amplified breast cancers and suggest that, due to its ability to impinge on specific molecular pathways, p140Cap may represent a predictive biomarker of response to targeted anti-ERBB2 therapies.

[1] Department of Molecular Biotechnology and Health Sciences, University of Torino, 10126 Torino, Italy. [2] Department of Medical Sciences, University of Torino, 10126 Torino, Italy. [3] Research Infrastructure, IRCCS Arcispedale Santa Maria Nuova, 42100 Reggio Emilia, Italy. [4] Department of Bioscience and Veterinary Medicine, University of Camerino, 62032 Camerino, Italy. [5] Department of Medicine and Aging Science, Center of Excellence on Aging and Translational Medicine (CeSi-Met), G. D'Annunzio University, Chieti-Pescara, 66100 Chieti, Italy. [6] Scientific and Technology Pole, IRCCS MultiMedica, 20100 Milan, Italy. [7] Division of Oncology and Pathology, Department of Clinical Sciences, Lund University, Lund 22100, Sweden. [8] Molecular Medicine Program, European Institute of Oncology, 20100 Milan, Italy. [9] IFOM, The FIRC Institute for Molecular Oncology Foundation, 20100 Milan, Italy. [10] Department of Oncology and Hemato-oncology, University of Milan, 20100 Milan, Italy. * These authors contributed equally to this work. Correspondence and requests for materials should be addressed to P.D. (email: paola.defilippi@unito.it).

Breast cancer is one of the most common cancers with greater than 1,300,000 cases and 450,000 deaths each year worldwide[1,2]. Clinically, breast cancer is classified into three basic therapeutic groups: the oestrogen receptor (ER)-positive group, the ERBB2 (also called HER2)-positive group, and the triple-negative breast cancers (TNBCs, also called basal-like), lacking expression of ER, progesterone receptor (PR) and ERBB2 (ref. 2).

The ERBB2 oncogene (the human V-Erb-B2 Avian Erythroblastic Leukemia Viral Oncogene Homolog 2) is a tyrosine kinase receptor, which belongs to the ERBB family. *ERBB2* gene amplification and receptor over-expression are causally linked to oncogenesis in ~20% of breast cancers and define a molecular breast cancer subtype characterized by an adverse clinical outcome[3–5]. *ERBB2* amplified tumours are a biologically non-homogeneous subgroup of breast cancers[6]. Indeed, although the *ERBB2* gene is located in the most highly rearranged segment in chromosome 17 (17q12-q21)[7], the amplification of the surrounding genomic region is a highly variable process that leads to a complex pattern of amplicons. The genes included in the amplicons may significantly contribute to ERBB2 tumour progression and treatment efficacy[7–11].

ERBB2 tyrosine kinase activation at the plasma membrane triggers key signalling pathways that direct general tumorigenicity, including escape from apoptosis, increased cell proliferation and migration, and epithelial to mesenchymal transition (EMT)[12–15].

We have previously described the p140Cap adaptor protein as a molecule that interferes with adhesion properties and growth factor-dependent signalling, thus affecting tumour features in breast cancer cells[16–19]. Recent reports have underlined that p140Cap regulates proliferation and migration in colon, lung, gastric, cutaneous squamous carcinoma and osteosarcoma cancer cells[19–24]. Indeed, in a cohort of breast cancer patients, p140Cap expression was linked to a less aggressive breast cancer disease[25], leading to the hypothesis that in these tumours p140Cap may counteract tumour fitness. However, it was not possible to assess the relevance of p140Cap expression for patient survival in that cohort[25], thus leaving open the question of the relevance of p140Cap to breast cancer prognosis.

In this work, we set out to tackle the relevance of p140Cap in human breast cancer by analysing a large consecutive cohort of patients with invasive breast cancer and we demonstrated a strong association between p140Cap and improved survival of ERBB2 patients. We also found that the p140Cap coding gene, *SRCIN1*, located on Chromosome 17, one million base pair centromeric from the *ERBB2* gene, is amplified together with *ERBB2*, in >60% of ERBB2 patients. We took advantage of the NeuT mouse model of mammary breast cancer, and of human ERBB2 breast cancer cells, to address the role of p140Cap protein in the ERBB2-related breast cancer disease. Altogether, our results argue for a key role of p140Cap in curbing the aggressiveness of the ERBB2 tumours, counteracting in vivo tumour growth, epithelial mesenchymal transition and metastatic lesions.

Results

Decreased metastatic risk in ERBB2 tumours expressing p140Cap. In a previous study, we showed that p140Cap expression was linked to a less aggressive breast cancer disease[25]. However, the lack of complete clinical follow-up for the cohort used in that study did not allow to assess the prognostic relevance of p140Cap expression in breast cancer. Here, we analysed p140Cap expression, by immunohistochemistry (IHC), on a consecutive cohort of 622 invasive breast cancers available in a tissue microarray (Supplementary Table 1). Data for p140Cap expression were available for 515 out of 622 samples (Fig. 1a; Supplementary Table 2). Positive p140Cap status (IHC score ≥ 1) was associated with good prognosis markers, such as negative lymph node status ($P = 0.014$, where $P =$ Pearson χ^2-test), ER and progesterone receptor (PgR)-positive status ($P = 0.0002$ and $P = 0.0049$, respectively), small tumour size (pT1 versus pT2–pT4, $P < 0.0001$), low grade ($P < 0.0001$), low proliferative status (Ki67, $P = 0.0013$), and ERBB2-positive status ($P = 0.0344$). Positive p140Cap status was also associated to breast cancer molecular subtypes, being expressed in >85% of Luminal A tumours, 77% of Luminal B, and only 56% of triple-negative tumours (Supplementary Table 2).

In univariate analysis, a positive p140Cap status was associated with a lower risk of developing distant metastases, and of death from breast cancer in the entire breast cancer cohort (Fig. 1b). However, a more in-depth analysis revealed that the prognostic effect of p140Cap in the consecutive cohort of breast cancer patients was to be ascribed to its performance in the subgroup of *ERBB2*-amplified breast cancers (Fig. 1c), in which a high p140Cap status predicts a significantly lower probability of developing a distant event (left panel), and a clear difference in survival (right panel). By contrast, no significative differences could be observed in patients not harbouring *ERBB2* amplification (Fig. 1d). The prognostic power of p140Cap was lost in a multivariate analysis, indicating that p140Cap is not an independent prognostic marker in breast cancer (Supplementary Fig. 2A; Supplementary Table 2). However, in the *ERBB2*-amplified subgroup, the lymph node status was the sole independent predictive marker, in multivariate analysis. When this group of tumours was subjected to a bivariate analysis, with nodal status and p140Cap expression, the two variables were found to be independent of each other in their association with prognostic outcome (Supplementary Fig. 2B).

In conclusion, p140Cap expression associates with reduced risk of metastasis (and death from cancer), in the *ERBB2*-amplified subgroup of breast cancer patients, arguing for a possible role of p140Cap in counteracting the migratory and/or metastatic ability of *ERBB2*-amplified tumour cells.

SRCIN1 is co-amplified with ERBB2 in ERBB2 amplified patients. p140Cap is encoded by the *SRCIN1* gene, located at Chromosome 17q12, one million base pair centromeric to the *ERBB2* gene. Several genes included in the amplicons have been reported to play a role in ERBB2 tumour progression[7–11]. However, the co-amplification of *SRCIN1* gene in the context of the ERBB2-related disease has not yet been deeply investigated.

To assess how frequently *SRCIN1* gene may be included in the *ERBB2* amplicon, BAC array Comparative Genomic Hybridization (aCGH) was performed. The analysis of 200 *ERBB2*-amplified tumours from a large Swedish Cohort[8], showed that the *SRCIN1* gene is altered in 70% of cases, with 123 cases (61.5% of the total) showing a copy number (CN) gain for *SRCIN1* (Fig. 2a). Kaplan–Meier analysis of these tumours showed that *SRCIN1* amplification correlates with significantly improved survival (Supplementary Fig. 3). Moreover, mRNA expression and *SRCIN1* gene CN from 50 of the 200 *ERBB2* amplified tumours were significantly correlated, giving a Pearson correlation of 0.77 (Fig. 2b).

Further, we analysed by FISH a consecutive series of 77 breast cancer patients at diagnosis with a mix of probes for *SRCIN1* and the centromeric region (CEP17) of chromosome 17. While in 43 ERBB2-negative breast cancers SRCIN1 CN was never altered, in ERBB2-amplified tumours[26], 56% of the specimens were

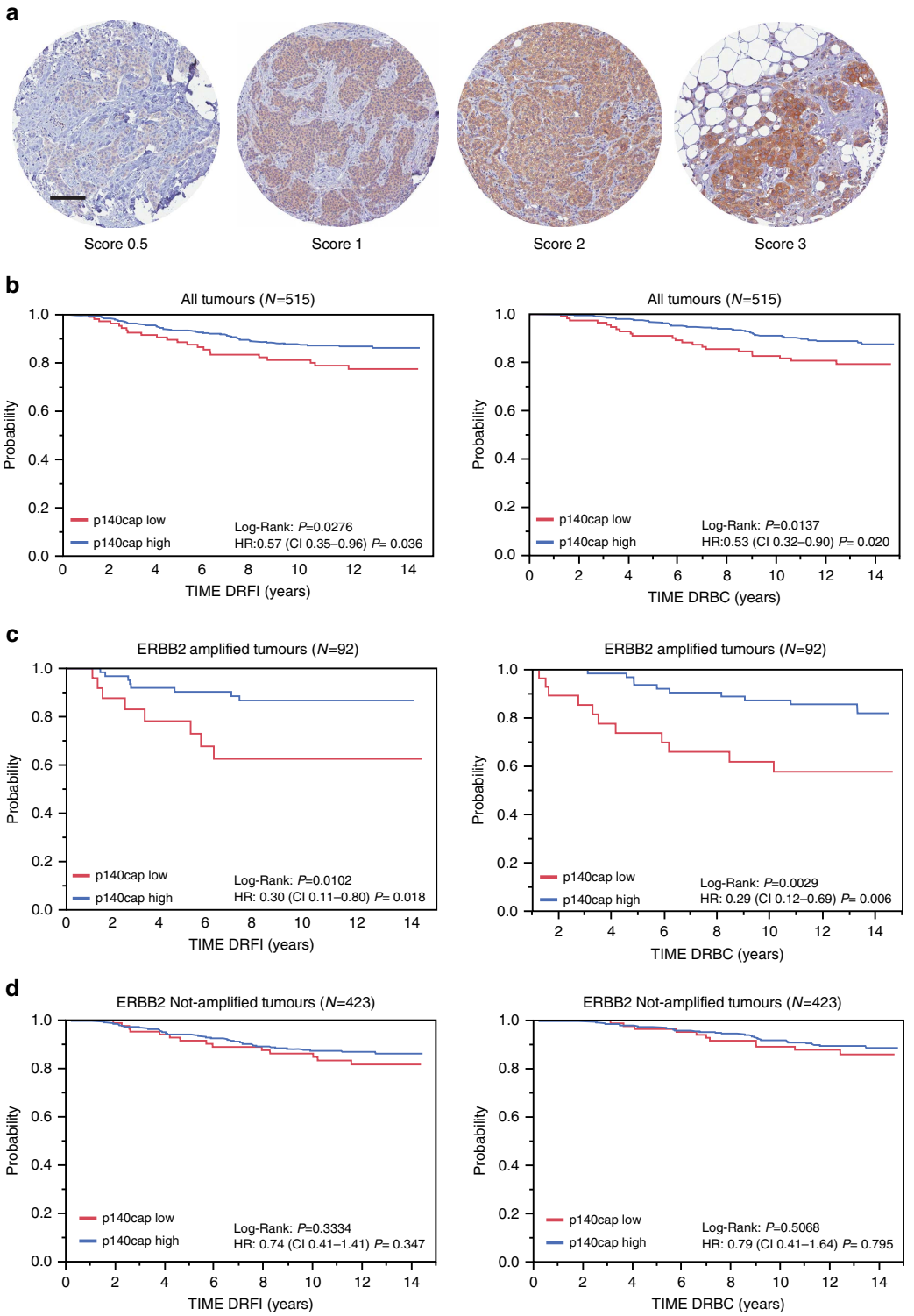

Figure 1 | Prognostic relevance of p140Cap expression in breast tumours. (**a**) p140Cap expression was measured by IHC on tissue microarray (TMA) samples. For the purpose of correlation with clinical and pathological parameters, tumours were classified based on the intensity of p140Cap staining as 0.5–3: p140Cap-Low (IHC score <1) and p140Cap-High (IHC score ≥ 1). Images are representative of p140Cap expression scoring according to intensity staining in TMA. In tumour tissues, the IHC signals were associated with the tumour cell component and not with the adjacent or infiltrating stroma. TMA data analysis was performed using JMP 10.0 statistical software (SAS Institute, Inc). Scale bar, 100 μm. (**b**) p140Cap expression in the whole cohort: Distant Recurrence Free Interval (DRFI)[65] (left panel: hazard ratio: 0.57, $P=0.036$); and Death Related to Breast Cancer (DRBC; right panel: hazard ratio: 0.53, $P=0.020$). (**c**) p140Cap expression in ERBB2-positive patients: DRFI (left panel: hazard ratio: 0.30, $P=0.018$); and DRBC (right panel: hazard ratio: 0.29, $P=0.006$). (**d**) p140Cap expression in ERBB2-negative patients: DRFI (left panel: hazard ratio: 0.74, $P=0.347$); and DRBC (right panel: hazard ratio: 0.41, $P=0.795$). $P=$ Pearson χ^2-test.

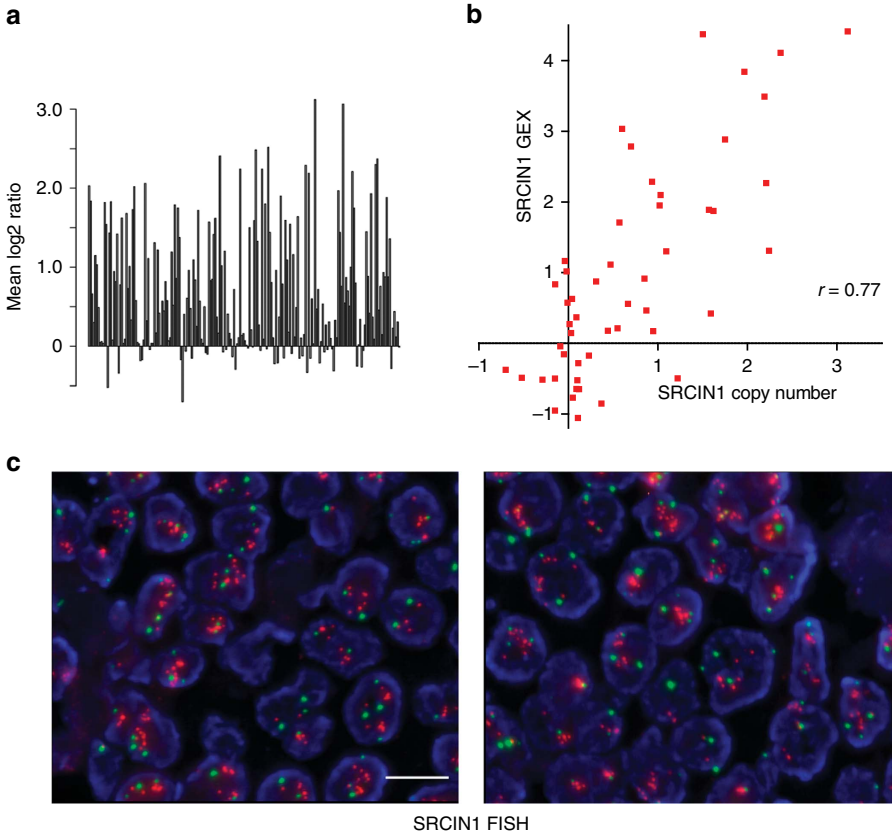

Figure 2 | *SRCIN1* gene alterations in human ERBB2 breast cancer samples. (**a**) *SRCIN1* gene copy number across 200 *ERBB2*-amplified breast cancer samples analysed by aCGH. *Y* axis corresponds to log2 transformed copy number, where values >0 correspond to increased copy numbers, and values <0 to copy-number loss. Bars represent individual samples. (**b**) Correlation of *SRCIN1* gene expression (GEX; *y* axis) and *SRCIN1* gene copy number (*x* axis) for 50 ERBB2 amplified cases from ref. 6. To assess whether this increase in *SRCIN1* gene copy number results in increased mRNA expression, gene expression data were compared with aCGH log2ratios using the Pearson correlation as described in ref. 61. Pearson's coefficient of correlation is 0.77. (**c**) p140Cap FISH of breast cancer tissues. Representative images of two cases of *ERBB2* amplified tissues, labelled with a mix of two probes *SRCIN1*/CEP1; Red (*SRCIN1*) and green (CEP17) spots were automatically acquired at 40X, using Metafer, by a MetaSystem scanning station. left panel: 95% *SRCIN1* amplification; average *SRCIN1*/nuclei = 11.7; right panel: 90% *SRCIN1* amplification; average *SRCIN1*/nuclei = 13,4. Scale bar, 10 μm.

amplified for SRCIN1 (Fig. 2c). These data indicate that alterations at the level of the *SRCIN1* locus are strictly linked to chromosomal rearrangements that result in *ERBB2* amplification. Altogether, these results show that the *SRCIN1* gene is frequently, but not obligatorily, co-amplified with *ERBB2* in breast cancers, arguing for a potential role of *SRCIN1* as a determinant of the clinical heterogeneity of ERBB2 tumours. These observations also provided us with the testable hypothesis that the presence of *SRCIN1* may attenuate the intrinsic biological aggressiveness of breast tumours with *ERBB2* alterations.

p140Cap limits tumorigenicity of NeuT-driven breast tumours. To test the above hypothesis, we generated a transgenic (Tg) mouse model in which p140Cap expression is driven under the control of the MMTV promoter (MMTV-p140Cap; Fig. 3a), to cross them with a well-characterized model of ERBB2-dependent breast carcinogenesis, the Tg MMTV-NeuT mouse model[27,28]. We selected two MMTV-p140Cap lines with a strong p140Cap expression in the mammary gland (see Supplementary Fig. 4 for detailed characterization of the Tg mice) that were crossed with both FVB-MMTV-NeuT[29] and BALB/c-MMTV-NeuT[27,28] mice, which display different tumour onset times, to generate p140-NeuT mice. p140Cap expression in tumours derived from these mice was confirmed by Western blot analysis (Fig. 3b). When compared to either FVB-NeuT or BALB/c-NeuT mice, the corresponding p140-NeuT mice showed a significant delay in the appearance of the first tumour (Fig. 3c, Fisher's exact test, Two sided, $P=0.0022$; $P=0.0056$) associated with a significant decrease in the total tumour burden (Fig. 3d, unpaired *t*-test: $P<0.001$, $P<0.05$). Histological analyses showed morphological differences in the appearance of the two types of tumours (Fig. 3e). NeuT tumours were composed of large solid nodules, separated by delicate bundles of stromal tissue, with necrosis often evident in the centre of the largest nodules (Fig. 3e, panels a,b). Tumours developed in p140-NeuT mice consisted of smaller nodules and sheets of cells separated by more abundant stroma, with cancer cells extending into the stroma in nest-like formations showing distinctive holes between the cancer cells (Fig. 3e, panels c,d). Both tumour types were strongly positive for NeuT ((Fig. 3e, panels e–h) and for cytokeratins CK8/18 (see Supplementary Fig. 5A). A larger percentage of NeuT tumour cells were positive for the proliferation marker PCNA (Fig. 3e, panels i,j), compared to p140-NeuT tumour cells (Fig. 3e, panels k,l). PCNA quantification is shown on the right of Fig. 3e ($32\pm1,560$ versus $18,65\pm2,141$). Angiogenic infiltration, as assessed by CD31 marker staining, was also decreased in p140 tumours ($9,648\pm351.5$ versus $5,344\pm232.8$; Supplementary Fig. 5B). Not significant differences were detectable in activated Caspase3 staining, in which only a few cells were positive in both tumour types ($7,694\pm2,257$ versus $7,381\pm2,408$;

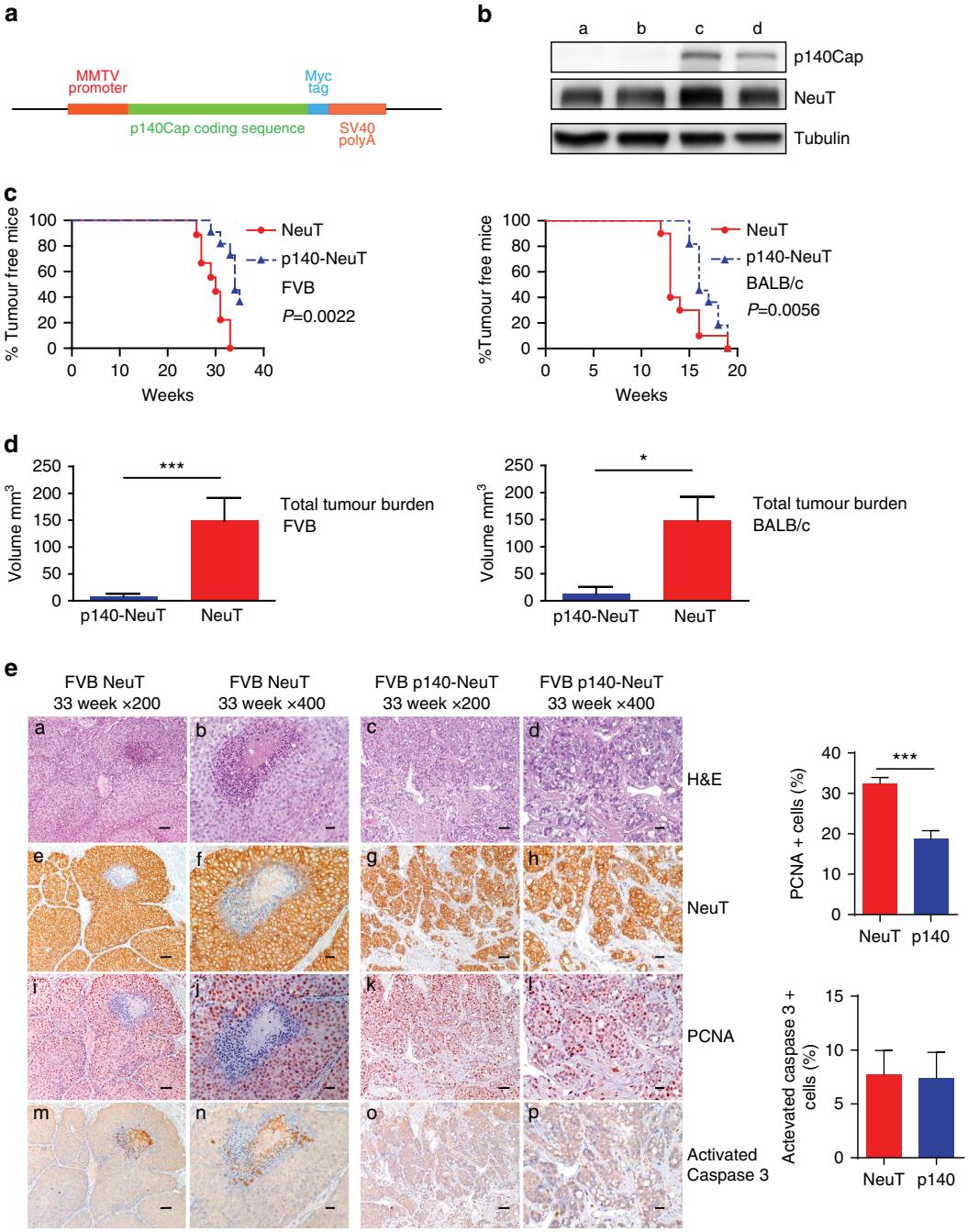

Figure 3 | p140Cap expression is causative in limiting tumour growth in NeuT mice. (**a**) Expression cassette used for the generation of MMTV-p140Cap transgenic mice. The Myc epitope is inserted at the carboxyterminal region of the protein. (**b**) Extracts of tumours derived from NeuT mice (a,b) or p140-NeuT mice (c,d) were run on 6% SDS-PAGE and stained with antibodies to p140Cap, ERBB2 and tubulin for loading control. (**c**) Percentage of tumour free mice in NeuT (red line) and p140-NeuT (blue-dashed line) transgenic animals in both FVB (left) or BALB/c background (right). Twelve mice were analysed for each group. Fisher's exact test, Two sided, $P=0{,}0022$; $P=0{,}0056$. Error bar: s.e.m. (**d**) Total tumour burden in NeuT (red) and p140-NeuT (blue) mice in both the FVB (left) or BALB/c backgrounds (right) was measured. Ten mice were analysed in each group. Unpaired *t* test: ($^{*}P<0.05$; $^{***}P<0.001$). Error bar: s.e.m. (**e**) Paraffin-embedded sections from three NeuT and three p140-NeuT tumours taken from mice at 33 weeks of age were analysed for hematoxylin–eosin (H&E) (a–d) and for immunohistochemistry with antibodies to NeuT (e–h), PCNA (i–l) and activated Caspase3 (m–p). Representative images are shown. Scale bar, 50 μm (first and third columns); 20μm (second and fourth columns). Histograms on the right show the percentage of PCNA+ (upper panel) and Activated Caspase3+ (lower panel) cells. Statistical significative differences were evaluated using unpaired *t*-tests ($^{***}P<0.001$).

Fig. 3e, panels m–p). Activated Caspase3 quantification is shown on the right of Fig. 3e. Altogether, these results show that p140Cap expression attenuates the phenotype of NeuT tumours *in vivo*, resulting in the development of smaller and lower grade mammary carcinomas.

p140Cap reverts the NeuT effects on mammary morphogenesis. It is well known that activation of the ERBB2 oncogene is sufficient to disrupt the morphogenetic program that drives the formation of the mammary gland acini *in vitro*[30,31]. Indeed, normal mammary epithelial cells embedded into three-

dimensional (3D) Matrigel-Collagen cultures give rise to hollow glandular-like acini displaying features of luminal differentiation[32–34]. In contrast, ERBB2 transformed cells escape apoptosis responsible for the cavitation process and originate aberrant filled-type structures, a phenotype linked to the cellular transformation with loss of apical–basal polarity[30,31]. On the basis of our evidence that p140Cap is able to curb NeuT-driven tumorigenesis *in vivo*, we set out to evaluate whether p140Cap also counteracts the disruption of the mammary morphogenetic program caused by ERBB2. To this aim, we established primary

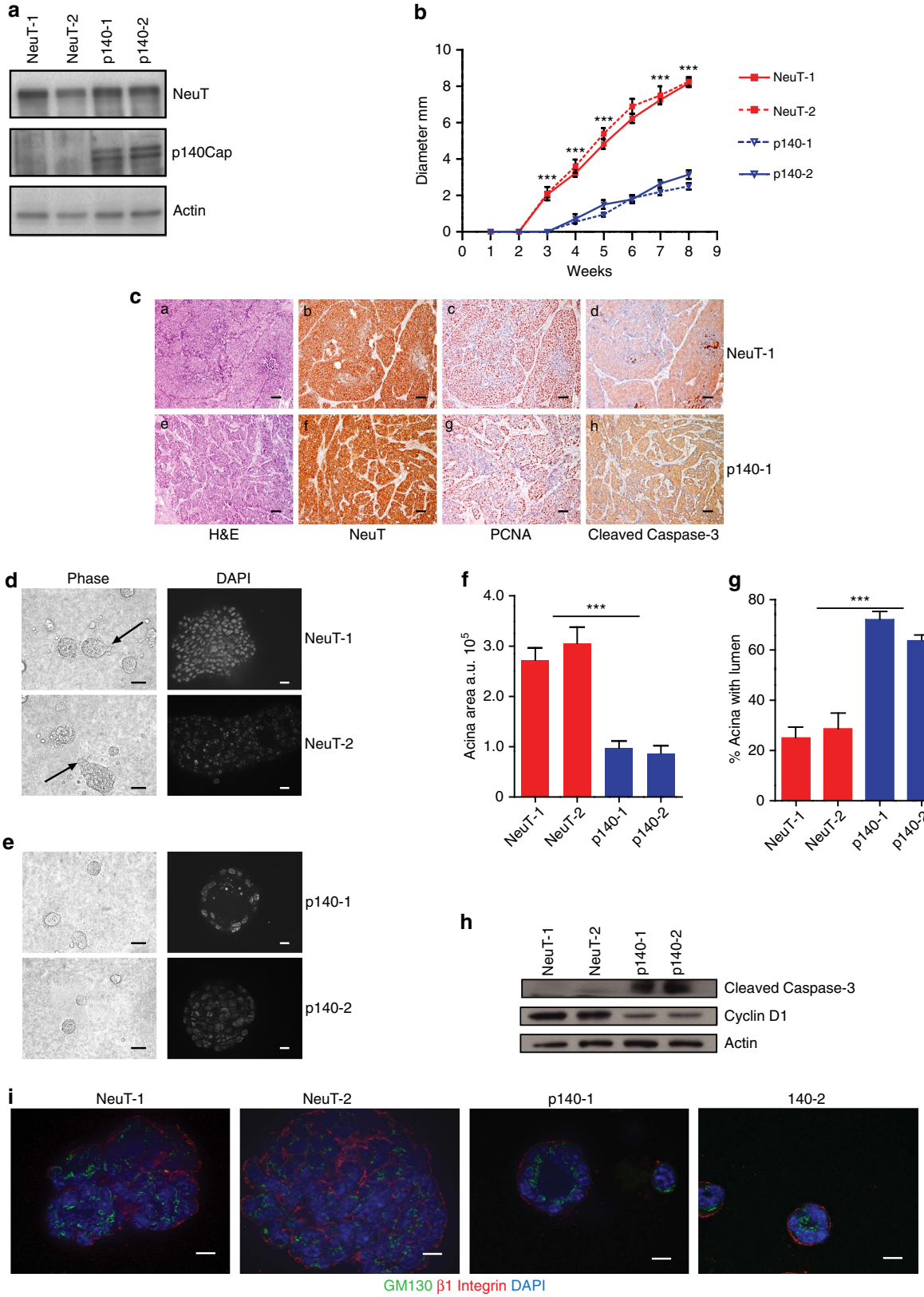

epithelial cancer cells from NeuT and p140-NeuT tumours in the BALB/c background. Two populations for each genotype, which expressed comparable levels of NeuT (NeuT-1 and NeuT-2) or p140Cap (p140-1 and p140-2; Fig. 4a), were chosen for further experiments. The cell lines, even if in standard culture condition did not show difference in proliferation (Supplementary Fig. 6A), displayed a distinct behaviour in apoptosis assays. Indeed, p140Cap primary tumour cells showed increased percentage of cells expressing the apoptosis marker Annexin 5 and increased expression of cleaved Caspase 3, when subjected to apoptotic stimuli, such as starvation or matrix cell detachment in culture conditions (Supplementary Fig. 6B). Moreover, they retained in transplantation assays the characteristics of the parental tumours, as evidenced by reduced tumour burden (Fig. 4b) and a more differentiated appearance of tumours (Fig. 4c), comparing p140 to NeuT cells.

When these cells were plated in 3D Matrigel-Collagen cultures for 15 days, NeuT-1 and NeuT-2 cells yield large multi acinar, apolar structures of irregular shape (Fig. 4d) that sometimes displayed protrusions (see arrows), suggestive of invasive features. These structures frequently did not show a lumen. In contrast, p140-1 and p140-2 cells formed smaller acinar-like structures with regular borders, without protrusions, which frequently displayed a lumen (Fig. 4e). Figure 4f,g show a quantification of these two phenotypes. Biochemically, these events were measured via the decreased expression of the proliferation marker Cyclin D1 (Fig. 4h), which is consistent with the decreased PCNA levels detected in p140-NeuT tumours *in vivo*. Moreover, p140Cap expression resulted in a substantial increase in the levels of activated Caspase3 in 3D cultures (Fig. 4h). Overall, in 3D conditions, p140Cap restores the dynamic equilibrium between cell proliferation and cell death which is typical of normal mammary epithelial cells during tissue morphogenesis[35].

The observed morphological features were mirrored by restoration of apical–basal polarity. Polarity properties were dissected in cells grown in 3D Matrigel-Collagen cultures for 15 days, via staining with the apical Golgi marker GM130 and the basal marker beta1 integrin[30]. The structures formed by the NeuT cells showed loss of Golgi marker GM130 orientation towards the lumen, and beta1 integrin mis-localization (Fig. 4h). In contrast, in p140 cells, GM130 always localized in the inner part of the acini, oriented towards the lumen, while beta1 integrin was clearly restricted in the outer part of the acini, to define the basal compartment (Fig. 4i). Thus, at least under the conditions of *in vitro* assays, the mitigating effect of p140Cap on ERBB2 tumour growth could be correlated with the re-enactment by p140Cap of the differentiation program disrupted by ERBB2.

p140Cap limits EMT in the NeuT cells. EMT is integral to several steps of the metastatic process[15,36]. In keeping with this, we found that the presence of p140Cap was associated with a marked down-regulation of an EMT transcription program, as witnessed by the significantly reduced expression of mRNA transcripts for the EMT transcription factors Snail, Slug and Zeb1 (Fig. 5a), and for the mesenchymal cell-cell adhesion protein N-cadherin in p140 cells compared to NeuT cells. Consistent with these findings, p140 tumour cells also displayed up-regulation of the mRNA levels for the epithelial E-cadherin mRNA (Fig. 5b). The overall inhibitory effect of p140Cap on EMT was further confirmed by western blot analysis that showed, in p140 versus NeuT cells, reduced expression levels of Snail and N-cadherin proteins combined with increased levels of E-cadherin (Fig. 5c). Immunofluorescence staining of E-cadherin on tumour sections (Fig. 5d), confirmed the increased expression of E-cadherin at the cell membrane in p140 tumours compared to NeuT tumours. Altogether, the sum of these data argues that p140Cap may effectively decrease pathways related to the progression of ERBB2 tumours, contributing to increased patient survival.

p140Cap limits metastasis in NeuT expressing cells. On the basis of the association between p140Cap status and reduced risk of distant metastasis in ERBB2 breast cancer patients, and on the down-regulation of the EMT transcription program, we addressed the putative protective role of p140Cap against the metastatic risk. In a spontaneous metastasis assay from primary tumours, we did not detect lung metastasis from neither NeuT or p140 xenotransplants. To address this point, we moved to the NeuT-TUBO cells, an additional transplantable primary NeuT cell model derived from a tumour arisen in BALB/c-MMTV-NeuT mice[37]. Upon infection with empty or p140Cap retroviruses, we generated NeuT-TUBO (as mock cells), and p140-TUBO cells (Supplementary Fig. 7A). We showed that p140Cap expression significantly limited tumour cell growth upon transplantation (Supplementary Fig. 7B). In the experimental metastasis assays upon tail vein injection, NeuT-TUBO cells gave rise, after 25 days, to numerous large lung metastases substituting $\sim$80% of lung tissue area. At the same time point, p140-TUBO cells were grown to occupy only $\sim$54% of lung tissue area (Fig. 6a). Since this assay is only a proxy to measure the metastatic potential of cells, we moved to the spontaneous metastasis assay from primary tumours, comparing metastasis formation from tumours of the same size. As shown in Fig. 6b, tumours originated from p140-TUBO cells gave rise to a significantly reduced number of lung metastases over tumours grown from NeuT-TUBO cells.

Figure 4 | Primary p140 cancer cells restore mammary epithelial acina morphogenesis in 3D Matrigel-Collagen cultures. (**a**) Protein extracts from two independent primary cancer cells for each genotype (NeuT-1, NeuT-2, p140-1 and p140-2) were run on 6% SDS–PAGE and stained with antibodies to NeuT, p140Cap and actin for loading control. (**b**) 10^6 cells as in **a** were injected in the left and right fat pads of nude mice. Tumour diameters were measured every week for 8 weeks. Two independent experiments were performed using five mice per group. Differences in tumour diameter were evaluated using two-way analysis of variance (ANOVA) followed by Bonferroni multiple comparison *post hoc* tests (***$P<0.001$). (**c**) Paraffin-embedded sections were prepared at the end of the experiments from tumours derived from mice as in **b**. Sections were analysed for Hematoxylin–Eosin (a,e), and for immunohistochemistry with antibodies to NeuT (b,f), PCNA (c,g) and activated Caspase3 (d,h). Representative images are shown. Scale bar, 50 μm. (**d**,**e**) Primary cancer cells for each genotype (NeuT-1, NeuT-2, p140-1, and p140-2) were plated in Matrigel/Collagen I 1:1 and left to grow for 15 days. Day 15 acina are shown as phase images in the left panels, or as Dapi nuclei staining (bright grey) in right panels. Arrows indicate the presence of invasive protrusions. Representative images from three independent experiments are shown. Scale bar, 50 μm. (**f**) The histogram represents the area of the acina quantified by the computer-generated software Zeiss Axiovision 4.5 and shown in arbitrary units (a.u.). (**g**) The histogram represents the percentage of acina structures with an internal lumen. The lumen has been manually quantified. In **f** and **g**, statistical significative differences were evaluated using unpaired *t* tests. Error bar: s.e.m. (***$P<0.001$). (**h**) Primary cancer cells as in d were plated in Matrigel/Collagen I 1:1 and left to grow for 12 days. Protein extracts were run on 4–12% SDS–PAGE and stained with antibodies to Cleaved Caspase 3, Cyclin D1 and Actin for loading control. (**i**) Primary cancer cells as in **d** were analysed as day 15 acinar structures by immunostaining for a *cis*-Golgi matrix protein, GM130 (green), and a basal marker protein, beta1 integrin (red). Nuclei were co stained with DAPI (blue). Representative images are shown. Scale bar, 50 μm.

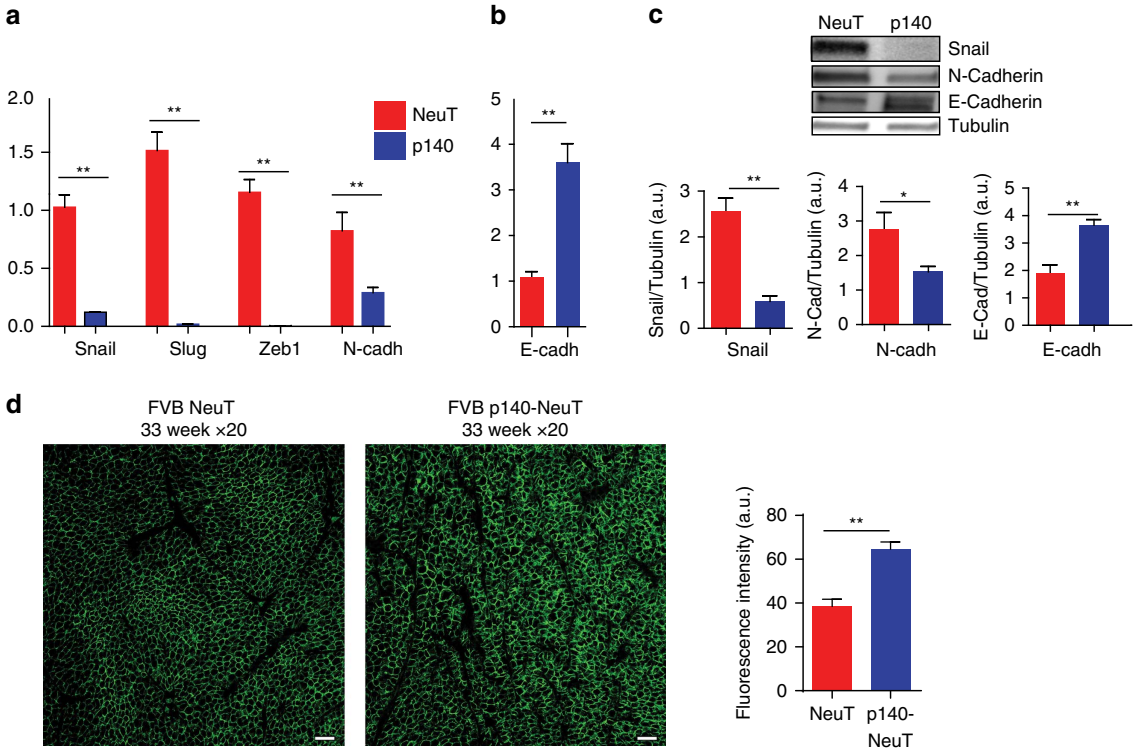

Figure 5 | Primary p140 cancer cells show impaired progression features. (**a**,**b**) RT-PCR was performed to quantify mRNA expression of EMT markers in NeuT and p140 cancer cell RNA. RNA was prepared from three biological replicates. RT-PCR was performed on triplicates. CNRQ (calibrated normalized relative quantity) is shown in arbitrary units (a.u.). Error bar: s.e.m. (**c**) Protein extracts from NeuT and p140 cells were run on 4–15% SDS-PAGE and stained with antibodies to Snail, N-cadherin and E-cadherin. Tubulin was used as an internal standard for protein loading. Histograms show in a.u. the quantification of three independent experiments. Statistical significative differences were evaluated using unpaired *t* tests (*$P<0.05$; **$P<0.01$; ***$P<0.001$). Error bar: s.e.m. (**d**) Paraffin-embedded sections from three NeuT and three p140-NeuT tumours taken from mice at 33 weeks of age were analysed for immunofluorescence with antibodies to E-Cadherin (green). Representative images are shown. Scale bar, 50 μm. Image acquisition was performed using Zeiss LSM 510 META confocal microscope. The E-cadherin mean fluorescence intensity was evaluated on the digital images of three tumours per group (4 × 200 microscopic fields per sample) with ImageJ, using the Mean Gray Value.

Moreover, the immunohistochemical staining with anti NeuT/ERBB2 and anti p140Cap antibodies of lungs with p140-TUBO metastases showed that while all the metastases were positive for the NeuT protein, p140Cap strong expression was conserved only in small metastases (Fig. 6c). Interestingly, larger metastases expressed only low levels of p140Cap and, accordingly, showed a less nodular histological structure similar to those developed from NeuT-TUBO tumours (Fig. 6d, compare upper and lower panels). Overall, these data indicate that p140Cap counteracts metastasis formation.

p140Cap attenuates ERBB2-driven Rac-dependent circuitries. The sum of results from (i) the analysis of the clinical cohort (reduction of metastatic risk in ERBB2 tumours), (ii) the experiments performed *in vivo* (reduced tumour masses, reduced 'metastatic' ability and decreased expression of EMT markers in the animal model) and (iii) *in vitro* (reduced protrusive ability of acini and restoration of polarity in the 3D-morphogenetic assays), points to a counteraction of p140Cap on ERBB2-dependent tumour progression. All these data show that p140Cap dampens tumour features, affecting tumour growth, sensitivity to apoptosis and metastatic properties of ERBB2-positive cancer cells. In search of a molecular mechanism, we decided to exploit SKBR3 breast cancer cells as a model of *ERBB2* gene amplification relevant to human breast cancer. In these cells, we both overexpressed and silenced p140Cap, without altering ERBB2 expression (Supplementary Fig. 8A,B), and tested the effects of these perturbations first on migratory abilities. In a transwell assay, migration was significantly decreased in p140Cap-overexpressing cells (oe p140; Fig. 7a) and increased in p140Cap-silenced cells (si p140; Fig. 7c). Increased migration of p140Cap-silenced cells was also observed in MDA-MB-453 breast cancer cells, another model of ERBB2 gene amplification relevant to human breast cancer (Fig. 7e; Supplementary Fig. 8C). Consistently, the migration of murine p140 cells lines, derived from transgenic mice, was profoundly inhibited, when compared to NeuT lines (Fig. 7g).

Furthermore, we examined whether p140Cap can control potential downstream signalling mechanisms. We have already shown that p140Cap can control Src activation[16,19]. Interestingly, both in NeuT and in SKBR3 cells, p140Cap expression did not affect the activation of the Src kinase and the phosphorylation of its effectors, p130Cas and paxillin, compared to MDA-MB-231 (ref. 19; Supplementary Fig. 9), suggesting that in ERBB2 transformed cells, p140Cap acts on additional pathways for the control of cell migration.

Several Rho GTPases are frequently altered in tumours and metastases and this often correlates with poor prognosis[38,39]. In particular, Rac is an essential effector pathway for ERBB2-mediated breast cancer progression to metastasis[40–43]. In SKBR3 cells, inhibition of ERBB2 activation by Lapatinib treatment significantly impaired both ERBB2 phosphorylation on Tyr 1,248 and Rac activation (Supplementary Fig. 10), confirming that

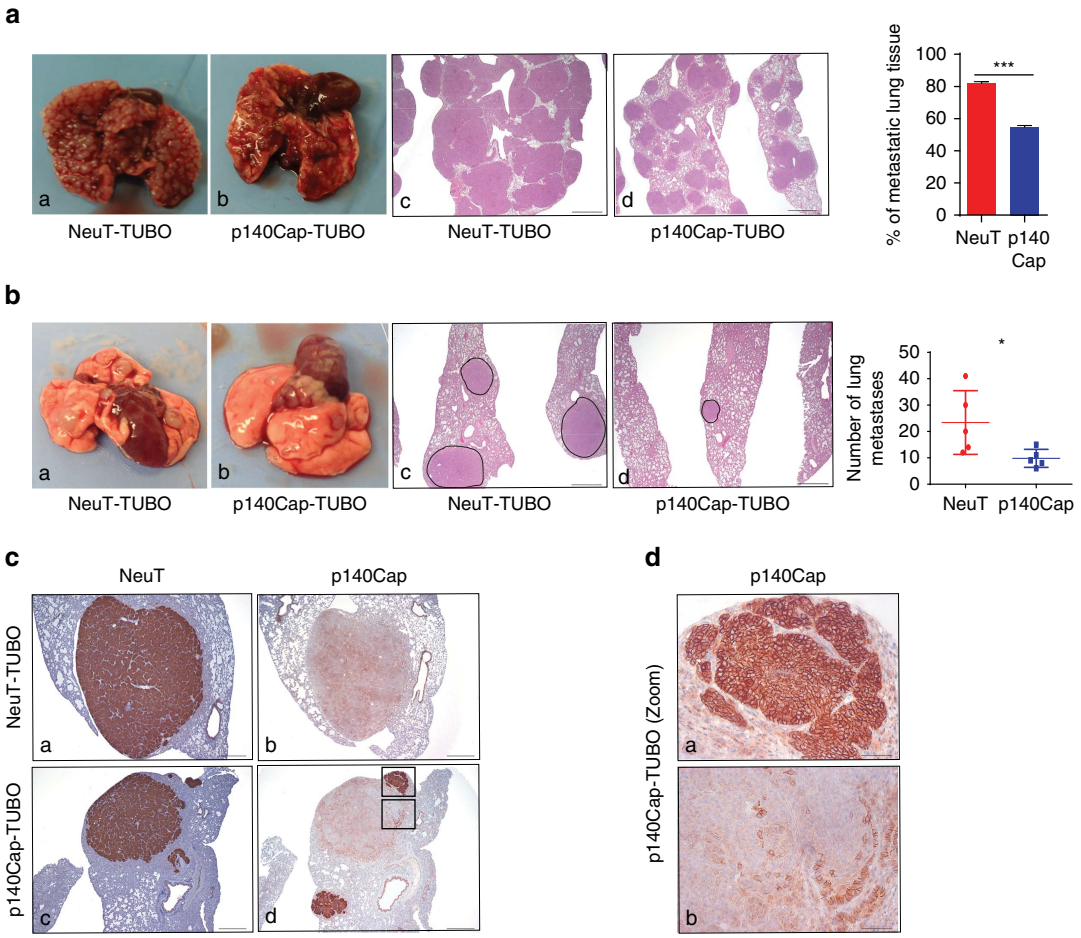

Figure 6 | p140Cap impairs spontaneous metastasis. (**a**,**b**) Representative gross observation (a,b), hematoxylin and eosin sections (c,d) and quantitative analysis in the experimental lung metastasis assay (**a**) and in the spontaneous lung metastasis assay (**b**). In **a**, 5×10^4 cells were injected into the tail vein of NSG mice. After 4 weeks, the lungs were explanted and analysed. Two independent experiments were performed using five mice per group. The histogram shows the percentage of metastatic lung tissue on total lung area. Statistical significance was evaluated with unpaired *t*-test (***$P<0.001$). Error bar: s.e.m. In **b**, 10^5 cells were injected in the right fat pads of NSG mice. Tumour volumes were measured every week; tumours were surgically removed when they reached a 10 mm diameter. After 5 weeks, mice were killed and lungs were explanted. The histogram shows the number of lung metastasis. Statistical significance was evaluated with unpaired *t*-test (*$P<0.1$). Error bar: s.e.m. Scale bar (a,b): 800 μm. (**c**) NeuT (a,c) and p140Cap expression (b,d) in spontaneous lung metastasis of mice injected with NeuT-TUBO cells (a,b) and mice injected with p140-TUBO cells (c,d). Scale bar, 400 μm. (**d**) High-magnification fields of rectangular areas in **c**, (panel **d**). Scale bar, 50 μm.

Rac is a downstream effector of ERBB2 also in our experimental system[44]. In the same cells, consistent with defective migration, Rac activity was significantly decreased upon p140Cap over-expression (Fig. 7b) or enhanced upon p140Cap silencing (Fig. 7d,f). These data mirrored those obtained in NeuT tumour-derived cells (Fig. 7h; Supplementary Fig. 11A), indicating that p140Cap affects Rac activity in both human and mouse ERBB2 transformed cells.

Treatment of NeuT cells with the Rac inhibitor NSC23766 (ref. 45) phenocopied the effects of p140Cap expression on the 3D morphogenetic program of NeuT cells, yielding acinar structures that were significantly smaller in size compared to those observed in the NeuT cells, and that frequently displayed a polarized phenotype (Fig. 7i). Finally, expression of a constitutively active mutant of Rac (RacV12) into p140 cells (Supplementary Fig. 12), caused a significant increase in the size of acini, accompanied by an almost complete loss in polarity and an enhancement in invasive protrusions (Fig. 7j). This latter set of data shows that Rac is epistatic to p140Cap, a scenario compatible with the possibility that p140Cap is an upstream regulator of Rac.

p140Cap limits Rac GEF Tiam1 activation in cancer cells. To probe into the hypothesis that p140Cap may act upstream of Rac, we focused on the Rac specific activator, the Guanine Exchange Factor (GEF) Tiam1, also in light of the fact that the Rac inhibitor NSC23766, which phenocopies p140Cap expression in NeuT cells (Fig. 7i), is a selective inhibitor of the interaction between Tiam1 and Rac[45]. In both p140 and NeuT expressing cells (Fig. 8a; Supplementary Fig. 11B) and in human p140Cap overexpressing SKBR3 cells (Fig. 8b), we found that p140Cap and Tiam1 co-immunoprecipitated, arguing for their physical interaction *in vivo*. We then investigated whether p140Cap could affect Tiam1 activity in both cell systems. This was established by *in vitro* pull-down experiments using as bait GST-RacG15A, a nucleotide-free Rac mutant that selectively interacts with active Tiam1 (ref. 46). Indeed, in p140 cells, we observed a marked decrease in the recovery of activated Tiam1 by GST-RacG15A, in comparison to NeuT expressing cells (Fig. 8c; Supplementary Fig. 11C). These data were mirrored by those obtained in SKBR3 cells, in which Tiam1 activity was significantly decreased upon p140Cap over-expression (Fig. 8d) or enhanced upon p140Cap silencing (Fig. 8e). Increased Tiam1 activity was also observed in

p140Cap-silenced MDA-MB-453 cells (Fig. 8f). Overall, these data indicate that Tiam1 activity is dependent on p140Cap in these cells.

Taken together, these data show that p140Cap interferes with the Rac circuitries that control *ERBB2* tumour progression, by binding to Tiam1, leading to both Tiam1 and Rac inactivation.

Discussion

We herein show for the first time that the expression of the p140Cap adaptor protein is clinically relevant to the naturally occurring ERBB2-related breast cancer disease. Indeed, ERBB2 patients who display a positive p140Cap status have significantly higher survival rate, with lower probability of

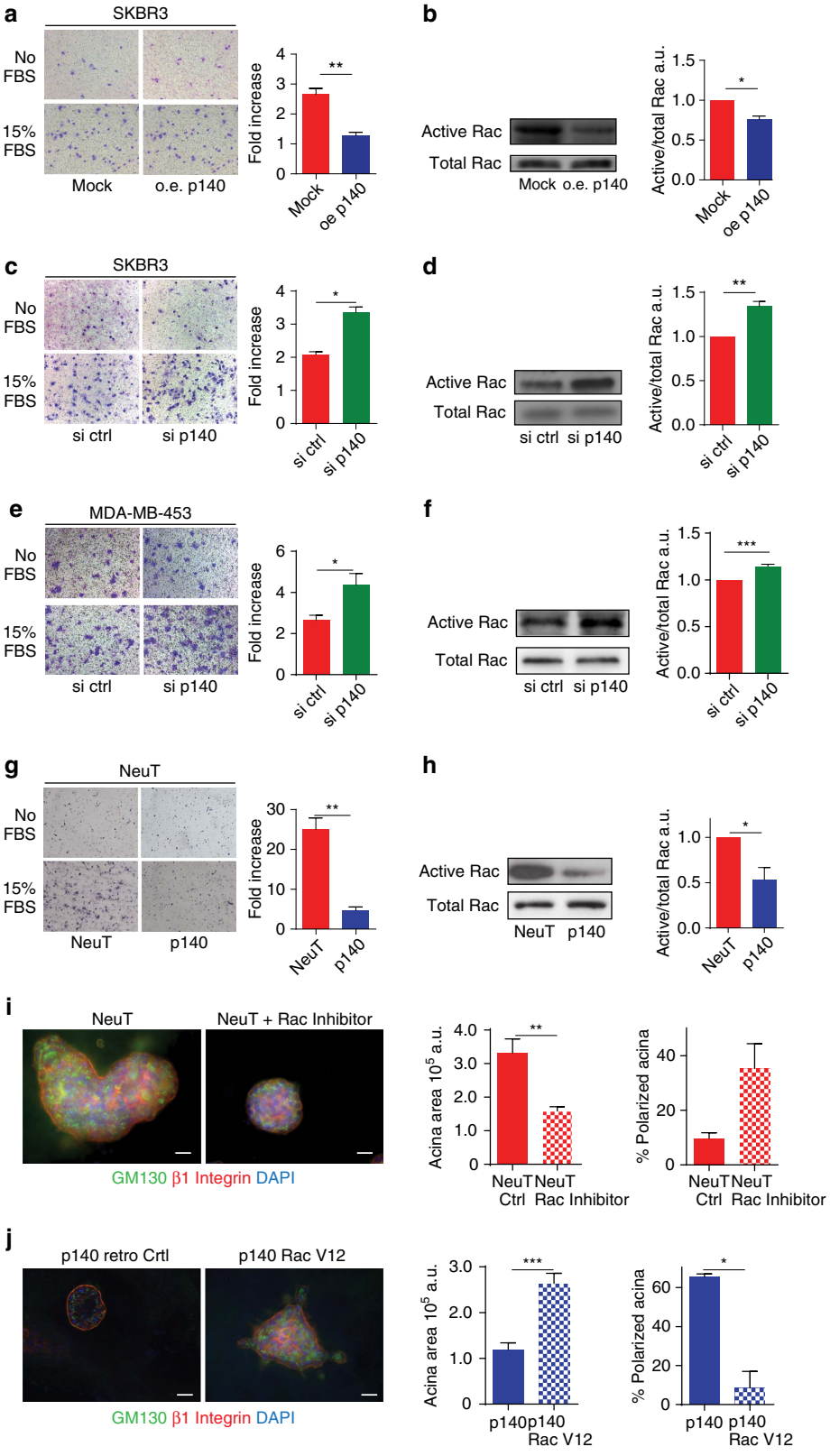

developing a distant recurrence. The clinical evidence that p140Cap correlates with a favourable outcome in ERBB2 breast cancer patients suggest that p140Cap is able to curb the intrinsic biological aggressiveness of ERBB2 tumour (Fig. 8g). Indeed, p140Cap confers to ERBB2 transformed cells limited in vivo tumour growth ability and spontaneous lung metastasis formation. This less aggressive phenotype is likely linked to reduced cell proliferation, assessed by a decreased staining of the proliferative marker PCNA in tumours, increased sensitivity to apoptosis, and strong inhibition in the EMT program observed in p140Cap expressing tumour cells.

To characterize the role of p140Cap in the NeuT preclinical model, we generated new Tg mice over-expressing p140Cap into the mammary gland under the MMTV promoter. MMTV-p140Cap Tg mice do not show any defects in the development or the differentiation of the mammary gland that could impair tumour growth (Supplementary Fig. 4). In the double Tg mice, expressing both NeuT and p140Cap, p140Cap expression reduces tumour burden, indicating that p140Cap is causative in limiting ERBB2 tumorigenic features *in vivo*. Indeed, p140Cap expression delays spontaneous tumour appearance and show decreased tumour masses, consistent with a decreased staining of the proliferative marker PCNA, with respect to NeuT mice. In addition, p140Cap expressing tumours show a different histology, reminiscent of that observed in the less aggressive human breast carcinoma[47,48]. When explanted, p140Cap Tg tumours do not display significant differences in apoptotic markers versus NeuT tumours. However, it is highly conceivable that the difference in total tumour burden reflects not only impaired tumour cell growth, but also the occurrence of local apoptotic events with remodelling of tumour structures, during tumour development. The *in vivo* analysis and the 3D Matrigel-Collagen cultures from primary cancer cells, suggest that p140Cap may limit the aggressiveness of ERBB2 tumours, both increasing tumour differentiation, restoring 'normal' mammary epithelial tissue morphogenesis[49,50] and differentially affecting the local tumour microenvironment[51]. In particular, upon apoptic stimuli and in 3D Matrigel-Collagen cultures, we observed that p140Cap cells have increased sensitivity to apoptosis. In the 3D conditions, p140Cap expression confers the ability to activate the apoptotic program and to give rise to internal lumen, typical of normal mammary epithelial cells during tissue morphogenesis[35].

The effect on EMT program is witnessed by the marked down-regulation of major EMT transcription factors, such as Snail, Slug and Zeb1 (ref. 36), accompanied by a reversion of the so-called 'cadherin switch' (that is, increase of the mesenchymal marker N-cadherin and a concomitant decrease of the epithelial marker E-cadherin), which is a canonical hallmark of EMT in cancer[15,36,52]. Indeed, p140 tumours display a homogeneous increased level of membrane E-cadherin, compared to NeuT tumours. Overall, the results point to the ability of p140Cap to counteract the EMT invasive program of ERBB2 tumour cells.

Notably, p140Cap expression significantly limits the ability of ERBB2 transformed cells to give rise to metastasis, both in experimental and in spontaneous metastasis assays. Indeed, when comparing tumours of the same size, p140Cap tumours give rise to a significantly lower number of spontaneous lung metastasis compared to NeuT tumours, suggesting that p140Cap affects metastatic spread. However, when analysing the metastatic lesions from p140Cap tumours, we observed a strong p140Cap expression only in smaller lung metastasis, rather than in larger ones, suggesting that p140Cap has also a strong effect on local metastatic growth. Therefore, from these data we can conclude that p140Cap significantly impairs metastasis acting both on tumour cell spreading and on metastatic growth, due to its ability to down-regulate tumour cell growth and to enhance apoptotic events.

Rac GTPase is a well-known mediator of human ERBB2 breast cancer progression[40–43], affecting signalling pathways impinging on tumour cell proliferation, apoptosis and acinar structure[53], as well as metastasis dissemination[54]. Here we show that p140Cap strongly impairs Rac activation in both human and mouse ERBB2 transformed cells. Indeed, in 3D Matrigel-Collagen morphogenetic assay, the Rac inhibitor NSC23766 (ref. 45) consistently decreased the area of the NeuT organotypic structures and restored cell polarity disrupted by the oncogene, thus recapitulating the effect of p140Cap expression. Of note, expression of a constitutively active form of Rac in p140Cap cells was able to rescue the aggressive ERBB2 phenotype, increasing acinar area and decreasing the percentage of polarized structures. These results further point to the mechanistic relevance of p140Cap/Rac counteraction as an essential step for limiting ERBB2 tumour progression. In the presence of p140Cap, only a constitutive alteration of Rac activation can reinstate the aggressive ERBB2 phenotype, suggesting that p140Cap may limit ERBB2 oncogenic features until at least significant Rac disregulation occurs.

Rac specific GEFs, like Dock, Tiam1 and PRex1, have also been shown to play a relevant role in breast cancers[42,54–56]. In particular, Tiam1 activation has been recently linked to the ERBB2 oncogene[57], where Tiam1-mediated Rac activation leads to uncontrolled actin dynamics that may compromise E-cadherin junctions, promoting metastasis[57–59]. Here working out the mechanisms underlying the observed decrease in Rac activation when p140Cap is expressed, we found a significant

Figure 7 | p140Cap negatively controls ERBB2-driven migratory ability and Rac GTPase activity. (**a**,**c**,**e**,**g**) Representative images of Transwell migration assays. 10^5 cells were left to migrate for 24 h in the presence or the absence of 15% FBS, fixed, stained and counted. Histograms represent on the *y* axes the fold increase (ratio between the number of cells migrated in the presence and in the absence of FBS), from three independent experiments, performed in triplicate. Error bar: s.e.m. (**a**) p140Cap over-expressing (oe p140) or mock SKBR3 (mock) cells. (**c**) SKBR3 cells transiently transfected with ON-TARGET plus human *SRCIN1* small-interfering RNA (si p140) or ON-TARGET plus non-targeting siRNA (Dharmacon RNAi; si ctrl). This patented approach strongly prevents off-target effects. (**e**) MDA-MB-453 cells transiently transfected with ON-TARGET plus small-interfering RNA as in **c**. (**g**) Primary NeuT and p140 cancer cells. (**b**,**d**,**f**,**h**) Active Rac pull-down from cells like in (**a**,**c**,**e**,**g**). Eluted material (upper panels) and cell extracts (lower panels) run on 12% SDS–PAGE revealed with anti Rac antibodies. Histograms show the ratio between active and total Rac protein levels in arbitrary units (a.u.) from five independent experiments. Statistical significative differences were evaluated using unpaired *t* tests (*$P<0.05$; **$P<0.01$). Error bar: s.e.m. (**i**) Primary NeuT cells were grown in Matrigel/CollagenI 1:1 for 1 week, before seven days treatment with 80μM Rac1 inhibitor NSC23766 and acini immunostained for GM130 (green), beta1 integrin (red) and DAPI for nuclei. Scale bar, 50 μm. Histograms represent quantification of acina area (left) and polarity (right) from three independent experiments. Differences in acina area were evaluated using a Mann–Whitney non parametric *t*-test (***$P<0.001$). Error bar: s.e.m. (**j**) p140 primary cancer cells were infected with retroviral particles that express Rac1-V12 or empty vector (retro Ctrl). Cells were plated in Matrigel/Collagen I 1:1 and day 15 acinar structures were immunostained as in **i**. Scale bar, 50 μm. Quantification of acini area in a.u., percentage of polarized acina and percentage of acina with protrusions are reported. The values from two independent experiments are reported. Differences were evaluated using a Mann–Whitney non parametric *t*-test (***$P<0.0001$; *$P<0.05$). Error bar: s.e.m.

decrease in the activation of Tiam1 in p140Cap tumour cells. The observation that p140Cap associates in a molecular complex with Tiam1, suggests that this interaction reduces the activity of Tiam1 as a Rac GEF and that this could represent one major upstream event in negatively regulating Rac downstream pathways.

Data on the regulation of expression of p140Cap gene are currently limited. We show here that the p140Cap coding gene, *SRCIN1*, at chr17; 17q12-q2, is co-amplified in the *ERBB2* amplicon in almost 60% of ERBB2 amplified patients. *SRCIN1* amplification is caused by its proximity to the *ERBB2* gene, and correlates with p140Cap mRNA levels and with patient

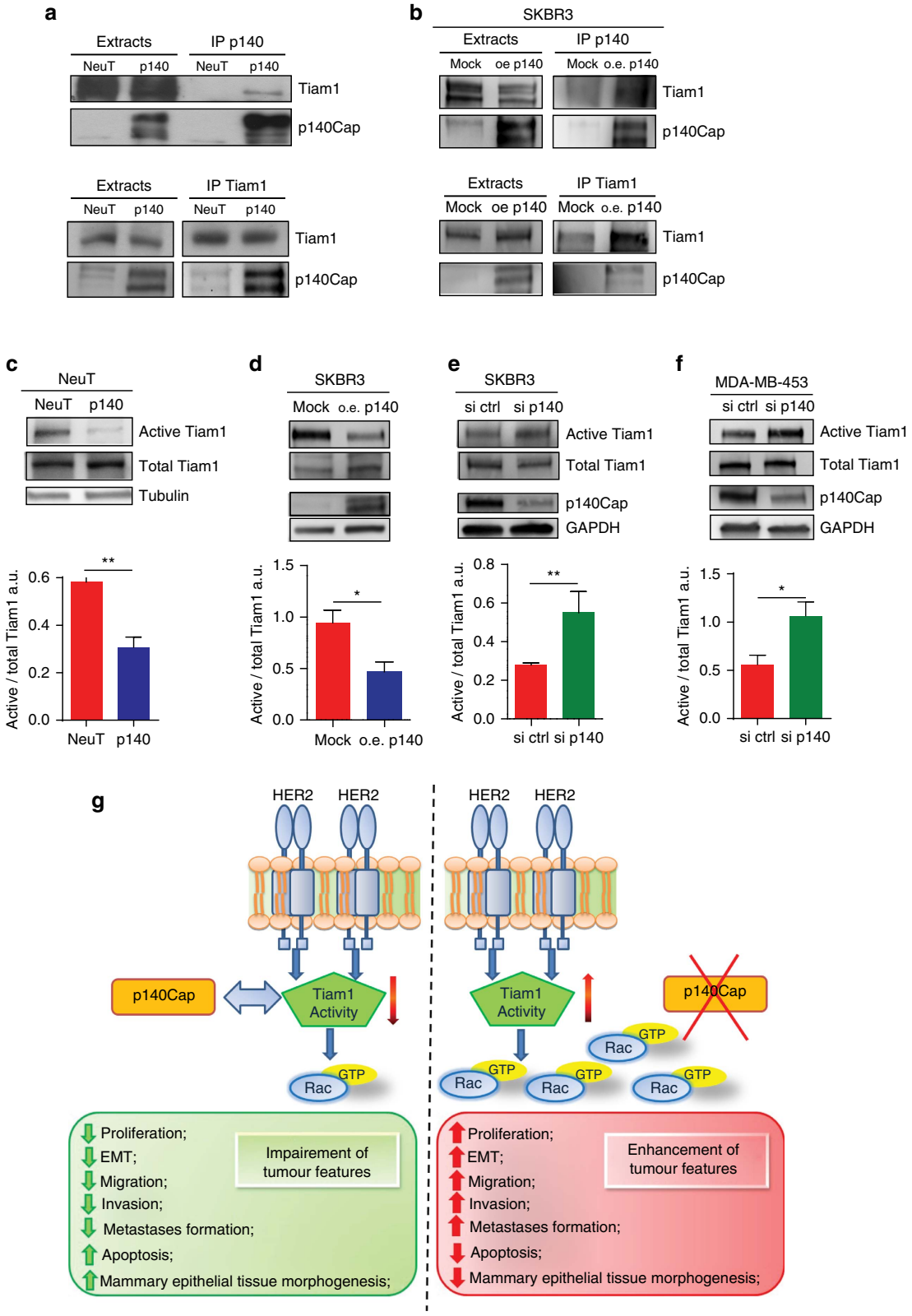

outcome. Interestingly, the aCGH data draw attention to a percentage of patients in which the *SRCIN1* gene is deleted (around 4–5% of the ERBB2 patients). These data highlight that in ERBB2 tumours, amplification of the *ERBB2* locus may lead to *SRCIN1* amplification or loss, thus contributing to the biological heterogeneity of this breast cancer subgroup[7–11]. However, besides amplification, additional mechanisms can account for alteration of p140Cap protein expression. Presently, data on the epigenetic regulation of p140Cap expression are not available. miR-150, miR-211, miR374a and miR346 have very recently been described as direct regulators of the p140Cap protein in lung, gastric and cutaneous squamous carcinoma cells[20–23], providing the first clues which link miRNAs to epithelial cancer cell features via the inhibition of p140Cap expression. Data on the ability of SRCIN1 to inhibit the osteosarcoma tumour cells proliferation have also been very recently reported[24].

In conclusion, our data are consistent with p140Cap exerting a suppressive function on ERBB2 oncogenic features and with it having a regulatory impact on molecular pathways that ERBB2 exploits for tumour progression (Fig. 8g). Moreover, p140Cap expression is advantageous for patient survival, strongly suggesting that p140Cap is still causal in limiting ERBB2 tumour aggressiveness within the complexity of the *ERBB2* amplicon. Indeed, our data provide the first evidence, to our knowledge, that a gene in the *ERBB2* amplicon may counteract ERBB2 oncogenic properties in breast cancer. Altogether, these data highlight the potential clinical impact of p140Cap expression and of p140Cap-regulated pathways in human ERBB2 breast tumours as new therapeutic targets.

Methods

Antibodies and cell lines. Mouse monoclonal antibodies to p140Cap were produced at the Antibody production facility of the Dept of Molecular Biotechnology and Health Sciences, University of Torino. A recombinant p140Cap protein, obtained in Escherichia coli by fusing the sequence corresponding to amino acids 800–1,000 of mouse *SRCIN1* gene to the Glutathione *S*-transferase (GST) was incubated with 4% paraformaldehyde in 1 × PBS—pH 7.4 for 30 min, at a concentration of 750 μg ml^{-1}, dialysed, and injected into p140Cap KO mice[60] for enhancing immunogenic activity. The resulting purified monoclonal antibodies were characterized by western blotting and IHC as shown in Supplementary Fig. 1. For western blot analysis, the following antibodies were used: anti Snail (#3895, 1:1,000), anti Caspase-3 (9,665, 1: 1,000), anti phospho Paxillin (Tyr118; #2541, 1:1,000), anti Paxillin (#2542, 1:1,000), anti phospho p130Cas (Tyr410; #4011. 1:1,000) and anti phospho-Src (Tyr416; #2101, 1:1,000; Cell Signaling, Beverly, MA), anti N-cadherin (ab10203, 1:1,000) and anti GFP (ab13970, 1:500; Abcam, Cambridge, UK), anti c-ErbB2/c-Neu (Ab-3, OPL15, 1:1,000; Calbiochem, Merck KGaA, Darmstadt, Germany), anti Rac1 (#05–389 clone 23A8, 1:2,000), anti GAPDH (MAB374, 1:8,000) and anti p1248Y ERBB2 (#06–229, 1:1,000; Millipore, Billerica, MA, USA), anti beta1 Integrin CD29-PE (12-0299-41, 1:200; eBioscience, San Diego, CA, USA), anti GM130 (6,10,823, 1:300), anti p130Cas (6,10,272, 1:2,500) and E-Cadherin (6,10,182, 1:2,500; BD Transduction Laboratories, Franklin Lakes, NY), anti Tiam1 (C-16, 1:1,000), anti Actin (I-19, 1:1,000), anti Src (B-12, 1:1,000), and anti Cyclin D1 (H-295, 1:1,000; Santa Cruz Biotechnologies, Palo Alto, CA, USA), and anti Tubulin (T5168, 1:8,000; Sigma-Aldrich Co, Italy). Secondary antibodies conjugated with peroxidase were purchased from GE Healthcare. Alexa Fluor Dye secondary antibodies were obtained from Invitrogen (Carlsbad, CA, USA). For immunohistochemistry, slides were stained with the following primary antibodies: rabbit polyclonal anti-HER2 (A0485, 1:700, Dako, Carpinteria, CA, USA), mouse monoclonal anti-PCNA (M0879, 1:800, Dako, Carpinteria, CA, USA), rabbit polyclonal anti-Caspase3 (af835, 1:350, R&D System, Minneapolis,MN, USA), rat monoclonal anti-CD31 (5,50,274, 1:40, BD Pharmingen, San Jose, CA, USA) mixed with rat monoclonal anti-CD105 (5,50,546, 1:40, BD Pharmingen, San Jose, CA, USA), rabbit polyclonal anti-Keratin 5 (PRB-160 P, 1:2,000, Covance, USA), guinea pig polyclonal anti-Keratins 8/18 (GP11, 1:750, PROGEN Biotechnik GmbH, Heidelberg, Germany) and mouse monoclonal antibody anti-p140Cap (1:500, see above) followed by the appropriate secondary antibodies. Immunoreactive antigens were detected using streptavidin peroxidase (Thermo Scientific UK) and the DAB Chromogen System (Dako, Carpinteria, CA, USA) or alkaline phosphatase conjugated streptavidin (Thermo Scientific UK) and Vulcan fast red chromogen (Biocare Medical, Concord, CA, USA). For immunofluorescence, slides were stained with the mouse anti-human E-cadherin antibody (M3612, 1:50, Dako, Carpinteria, CA, USA) followed by secondary antibody conjugated with Alexa 488 (A11029, 1:200, Invitrogen, Life Technologies, Monza, Italy). Lapatinib was bought from Selleckchem (Munich, Germany). Rac inhibitor (NSC23766) was bought from Calbiochem (Merck KGaA, Darmstadt, Germany. Glutathione-Sepharose, Protein G-Sepharose, PVDF, and films were obtained from GE Healthcare (Buckinghamshire, UK). Culture media were from Invitrogen (Carlsbad, CA, USA). Fetal Calf serum (FCS) was from EuroClone (Pero, Milano, Italy). SKBR3, MDA-MB-453 and MDA-MB-231 cells were obtained from ATCC (LGC Standards S.r.l.—Italy Office, Italy). SKBR3 cells were cultured in McCoy's 5a medium, supplemented with 15% FCS. MDA-MB-453 cells were cultured in DMEM 10% FCS. MDA-MB-231 cells were cultured in DMEM 10% FCS. NeuT-TUBO cells were derived from a spontaneous breast tumour arisen in a female BALB/c-MMTV-NeuT mice[37] and cultured in DMEM 20% FCS.

Human breast cancer immunohistochemical analysis. IHC analysis of p140Cap expression was performed on formalin-fixed paraffin-embedded tissue microarrays, prepared with tumour breast specimens, using a mouse monoclonal antibody anti-p140Cap (Supplementary Fig. 1), which was used at a dilution of 1:1,000 following an antigen retrieval procedure in EDTA pH 8.0. Immunocomplexes were visualized by the EnVision + HRP Mouse (DAB +) kit, DAKO (K4007), and acquired with the Aperio ScanScope system (Leica Biosystems). Informed consent was obtained from all subjects. For the purpose of correlation with clinical and pathological parameters, tumours were classified based on the intensity of p140Cap staining as p140Cap-Low (IHC score <1) and p140Cap-High (IHC score ≥ 1).

aCGH and gene expression analyses. Normalized aCGH profiles from 200 ErbB2 breast cancers together with matching gene expression profiles from 50 cases were obtained from the data described in ref. 8. Correlation analyses between gene CN, determined by aCGH, and mRNA expression for *SCRIN1* were performed using the Pearson correlation as described in refs 8,61.

FISH analysis of *SRCIN1* gene status. A specific SRCIN1 locus probe was prepared from the BAC RP11-606B22 (17q12) clone, obtained from BAC PAC Resources Center (Children's Hospital, Oakland Research Institute, USA). The BAC was directly labelled with red SpectrumAqua-dUTP (Abbott Molecular, Europe), using the BioPrime DNA Labeling System (Invitrogen Corporation, USA) according to manufacturer's instructions. An alpha satellite probe specific for chromosome 17 (CEP17; Abbott Molecular) directly labelled with green fluorochrome, was used as a control probe. To further analyse the position and strength of the signal, the presence/absence of background, cross-hybridization and, finally, the hybridization efficiency, the BAC clone was tested on metaphase and interphase healthy donor cells obtained using conventional cytogenetic

Figure 8 | p140Cap expression negatively regulates Tiam1 activity. (**a**,**b**) Extracts from NeuT and p140 expressing cancer cells, and p140 overexpressing (o.e.), or mock (mock) SKBR3 cells were immunoprecipitated with antibodies to p140Cap (upper panels) or Tiam1 (lower panels). Cell extracts and immunoprecipates were run on 6% SDS–PAGE and blotted with antibodies to p140Cap and Tiam1. Representative images from five independent experiments are shown. (**c**–**f**) The level of active Tiam1 was determined using the active Rac-GEF assay kit in NeuT, p140 primary cancer cells, p140 o.e. or mock (mock) SKBR3 cells, and p140 silenced SKBR3 (si p140) and MDA-MB-453 (si p140) cells. Equal amount of extracts were incubated for 1 h at 4 °C with Rac G15A agarose beads. Active Tiam1 and total Tiam1 levels were determined using an anti-Tiam1 antibody for western blot detection, from eluted material and input fractions, respectively. Antibodies to tubulin and GAPDH were used as loading controls. The histogram represents the quantification of active Tiam1 in three independent experiments, normalizing active Tiam1 levels to the corresponding total Tiam1 levels in arbitrary units (A.U.). In **c**–**f**, statistical significative differences were evaluated using unpaired *t*-tests (*$P<0.05$; **$P<0.01$). Error bar: s.e.m. (**g**) p140Cap exhibits a suppressive function on ERBB2 tumour features. In ERBB2 cancer cells, when p140Cap is expressed, proliferation, EMT, migration and metastasis formation are impaired and cancer cells enhance apoptosis and restore the proper mammary epithelial tissue morphogenesis disrupted by the ERBB2 oncogene. Moreover, the Tiam1/Rac signalling pathway is strongly decreased, through the ability of p140Cap to associating with Tiam1 and to downregulating its activity. On the contrary, when p140Cap is undetectable, Tiam1/Rac signalling pathway is active, and cancer cells exhibit an aggressive phenotype. The molecular mechanisms here reported link p140Cap expression with decreased metastatic risk in ERBB2 patients.

methods. The PathVysion *ERBB2* DNA probe kit was used (Abbott Molecular, Europe) for the *ERBB2* locus. FISH with the two probes mix, *SRCIN1*/CEP17 and *ERBB2*/CEP17, was routinely performed on formalin-fixed paraffin-embedded tissue. Red (*SRCIN1*) and green (CEP7) spots on significant selected areas were automatically acquired, using Metafer, by a MetaSystem scanning station (Carl Zeiss MetaSystems Gbmh), equipped with an AxioImager epifluorescence microscope. The first automatic lecture of the slides, made using the PathVysionV2 software, was performed on the acquired images with Isis software (Zeiss). The ASCO/CAP 2013 Guideline Recommendations for *ERBB2* Testing in the Breast were used for the interpretation of both FISH probes: positive for amplification with *ERBB2*—*SRCIN1*/CEP17 ratio >2.0 or with average *ERBB2*—*SRCIN1* CN >6; negative for amplification with *ERBB2*—*SRCIN1*/CEP17 ratio <2.0 or *ERBB2*—*SRCIN1* copy <4. Gene loss was considered to occur when an average *ERBB2*—*SRCIN1* CN <1.8 was found and gene gain when CN was $>3<6$. Finally, when heterogeneity was present (such as the presence in the same sample of amplified and not amplified cells), we considered samples where the amplified cell population consisted of $>10\%$ tumour cells as being amplified.

Generation of the MMTV-p140Cap transgenic mice. Full-length mouse p140Cap cDNA was inserted into pspT2 MMTV-LTR plasmid and microinjected at 3.4 ng/microliter in the pronucleus of fertilized eggs from FVB/NJ mice (Charles River, Calco, Italy) according to standard protocols[62]. Transgene integration was tested via PCR analysis of genomic DNA, with the primers: 5′-TGGCCCTGCGAGGTCAGCAGGACA-3′, 5′-ATCCTGCTGAAGC-CCAG GGGCAGC-3′. Heterozigous mice carrying the mutated rat HER-2/neu oncogene driven by the MMTV-LTR promoter (MMTV-NeuT mice), either on FVB/NJ (FVB-MMTV-NeuT) or BALB/c (BALB/c-MMTV-NeuT) background, are well-characterized transgenic models of spontaneous NeuT mammary adenocarcinoma[27–29,63]. p140Cap/Neu-T double transgenic mice were generated by crossing MMTV-p140Cap transgenic female (FVB background) with either FVB-MMTV-NeuT or BALB/c-MMTV-NeuT. The progeny was screened for both the transgene by PCR. The mice that were positive for both transgenes were included in further analyses, while animals positive only for the NeuT transgene were used as controls ($n=12$ for each group). The size of the tumours was evaluated weekly using calipers in blind experiments. The project had been approved by the Internal Bioethical Committee of the Department of Molecular Biotechnology and Health Sciences of the University of Torino. The handling of mice in our animal house meets the requirements of Italian law (authorization D.M. no. 279/95B 27/11/1995 and Ministry of Health 49/2014-PR to PD) and follows the dispositions of 'D.L. no. 116, 27/1/1992 in relation to animal use and protection in scientific research'.

Immunohistochemistry and immunofluorescence analyses of NeuT tumours. Tumour samples were fixed in 10% neutral buffered formalin and embedded into paraffin or fixed in 4% PFA and frozen in a cryo-embedding medium (OCT, BioOptica); 5 µm slides were cut and stained with Hematoxylin (BioOptica) and Eosin (BioOptica) for histological examination. The percentage of PCNA or Caspase3-positive cells was evaluated on digital images of 3 tumours per group ($4–6\times200$ microscopic fields per sample); clear brown nuclei were regarded as positive cells and the percentage of labelling index (number of positive cells/total cells $\times100$) was calculated for each field, by two pathologists, independently, and in a blind fashion. The vascularization was analysed evaluating CD31-105+ endothelial cells on digital images of 3 tumours per group (6×200 microscopic fields per sample) with Adobe Photoshop by selecting red stained vessels with the Magic Wand Tool and reporting the number of pixels indicated in the histogram window. For both experimental and spontaneous lung metastasis assay, lungs were fixed in 10% neutral buffered formalin and paraffin-embedded. To optimize the detection of microscopic metastases and ensure systematic uniform and random sampling, lungs were cut transversally, to the trachea, into 2 mm thick parallel slabs with a random position of the first cut in first 2 mm of the lung, resulting in 5–8 slabs for lung. The slabs were then embedded cut surface down and sections were stained with Hematoxylin and Eosin (BioOptica, Milan, Italy). The metastatic lung tissue was evaluated with Adobe Photoshop by selecting metastases with the lasso tool and reporting the number of pixels indicated in the histogram window as percentage of the total lung area. For immunofluorescence, slides were stained with the mouse anti-human E-cadherin antibody followed by secondary antibody conjugated with Alexa 488. Image acquisition was performed using Zeiss LSM 510 META confocal microscope. The E-cadherin mean fluorescence intensity was evaluated on the digital images of three tumours per group (4×200 microscopic fields per sample) with ImageJ, using the Mean Grey Value: for RGB images, the mean was calculated by converting each pixel to grayscale using the formula grey $=0.30$red $+0.59$green $+0.11$blue if 'Unweighted RGB to Grayscale Conversion' was checked in Edit > Options > Conversions. Whole-mount preparation were performed as described in ref. 60. The fourth abdominal mammary glands were analysed from at least three mice for age group. Only whole mounts that contained the entire ductal network including the primary duct and were free of mounting artifacts such as tissue folds were used for subsequent image analysis. A digital photomicrograph was taken of each whole-mount using a Leica MZ6 stereo microscope fitted with a Nikon Coolpix colour digital microscope camera. Within each age group, a consistent magnification was established that allowed the entire epithelial complex to be captured in a single image. For each age group, the photomicrographic settings remained constant. Four different measurements were obtained from each whole-mount image using Photoshop software. TEB count was performed only on 6 weeks of age glands. Ductal length (pixels) was measured by drawing and measuring a straight line caliper from the most distal point of the ductal network to the nipple. Ductal network area tumours from NeuT mice and xenografts were routinely fixed in 10% formaldehyde buffer (pH 7.4) for 24 h, paraffin-embedded and processed for immunohistochemical analysis with standard procedures[64].

Isolation of primary cancer epithelial cells from mammary gland tumours. Cells from tumours were isolated as described in refs 29,62. Briefly, tumours were surgically excised from 17-week-old BALB/c Neu-T and p140-NeuT mice and finely chopped. Tumour cell aggregates were then incubated in trypsin (0.25% in EDTA) for 2 h at 37 °C, washed in DMEM, centrifuged at low speed and then plated in 20% FBS/DMEM. After the sprouting of cells from tissue fragments, the cultures were periodically and briefly washed (1–3 min) with trypsin-EDTA to detach contaminating fibroblasts without damage to epithelial areas. Two months after plating, established epithelial cell populations were selected by several subculturing steps.

Three-dimensional cultures of primary cancer cells. For 3D-Matrigel cultures, eight-well Chamber slides (Corning) and Growth-factor-reduced Matrigel (BD Transduction Laboratories) were used. Three-dimensional culture assays were performed in agreement with protocols reported in: http://muthuswamy-lab.cshl.edu/protocols. Briefly, NeuT, p140-NeuT primary cancer cells or NeuT and p140-NeuT stable infected cells were embedded as single cells in Matrigel/Collagen I 1:1 and left to grow for 15 days. When indicated, the Rac inhibitor (NSC23766) was added to culture medium for the last 7 days. After 15 days, acini were subjected to immunostaining as described in http://muthuswamylab.cshl.edu/protocols/IF protocol.pdf. Images were taken using a Zeiss microscopy (Oberkochen, Germany) equipped with an Apotome module at $\times40$ magnitude. For immunoblotting analysis, NeuT or p140 cells were released from Matrigel-Collagen gels using BD cell recovery solution (BD Biosciences) and protein were extracted with RIPA buffer (50 mM Tris (pH7.5), 150 mM NaCl, 1% Triton X100, 1% Na Deoxycolate, 0.1% SDS and protease inhibitors). Cell lysates were centrifuged at 13,000 *g* for 15 min and the supernatants were collected and assayed for protein concentration using the Bio-Rad protein assay method (Biorad, Hercules, CA, USA). Proteins were run on SDS–PAGE under reducing conditions.

Retrovirus production and cell infection. To over-express p140Cap into SKBR3, NeuT-TUBO and MDA-MB-231 cells, p140Cap cDNA was cloned into pBabe-puro. The plasmid that encodes GFP-Rac1V12 was purchased from Addgene (Cambridge, MA, USA). The retroviruses particles were produced by the calcium phosphate transfection of Platinum Retroviral Packaging Cell Lines (Cell BioLabs), in 10 cm dishes. 48 h after transfection, supernatant that contained the retrovirus particles was collected, filtered through a 45 µm syringe filter and added directly to subconfluent cells. After 48 h, cells were washed and cultured with a selection medium containing puromycin (Sigma) at a final concentration of $1\,\mu g\,ml^{-1}$. The efficiency of infection was controlled by western blot analysis. For SKBR3, NeuT-TUBO and MDA-MB-231 cells, individual clones were isolated 20 days after the start of the selection. Four individual positive clones were pooled together to rule out clonal artifacts.

***In vivo* tumour growth and experimental and spontaneous metastasis assay in NeuT cells.** Five-week-old female CD-1 Nude Mouse were purchased from Charles River Laboratories (Calco, Italy) and treated in accordance with the European Community guidelines. 1×10^6 NeuT or p140 cells were mixed with 150 µl DMEM and then injected subcutaneously into the left and right inguinal region of female nude mice. The size of the tumours was evaluated weekly using calipers in blind experiments. For experimental lung metastasis assay, NeuT-TUBO and p140-TUBO cells were trypsinized, resuspended in PBS, and then 5×10^4 cells (in 0.1 ml) were injected via the lateral tail vein of 7-week-old female NSG mice (NOD.Cg-Prkdcscid Il2rgtm1Wjl/SzJ) from Charles River Laboratories (Calco, Italy; $n=5$ for group for each experiment). Mice were killed 25 days after injection and lungs were fixed in 10% neutral buffered formalin (BioOptica) and paraffin-embedded. To optimize the detection of microscopic metastases and ensure systematic uniform and random sampling, lungs were cut transversally, to the trachea, into 2 mm thick parallel slabs with a random position of the first cut in first 2 mm of the lung, resulting in 5–8 slabs for lung. The slabs were then embedded cut surface down and sections were stained with Hematoxylin and Eosin (BioOptica).The metastatic lung tissue was evaluated with Adobe Photoshop by selecting metastases with the lasso tool and reporting the number of pixels indicated in the histogram window as percentage of the total lung area. For spontaneous lung metastasis assay, NeuT-TUBO and p140-TUBO cells were trypsinized, resuspended in PBS, and then 10^5 cells (in 0.1 ml) were injected into the right fat pad of 7-week-old female NSG mice ($n=5$ for group for each experiment). We monitored mammary tumour growth by regular measurements using a digital caliper. Tumours were surgically removed when reached

a 10 mm diameter. After 5 weeks, mice were killed and lungs were explanted and processed as previously described.

Analysis of EMT markers by qRT–PCR. Total RNA was extracted using the RNeasy Mini kit (Qiagen, CA) with DNase I treatment and quality controlled by electrophoresis on 0.8% agarose gel. RT–PCR was performed on 0.5–1 μg total RNA with the SuperScript ViloTM cDNA Synthesis kit from Invitrogen. Gene expression was assessed by quantitative real-time PCR with the GeneAmp 7,500 system and Taqman chemistry (Applied Biosystems, CA). Each sample was tested in triplicate. The Δ-Ct method was used to calculate relative fold-changes normalized against three different housekeeping genes. Taqman Gene Expression Assay IDs (Applied Biosystems, CA) were: Mm00441533-g1 (Snail, snail1, NM_011427.2), Mm00441531-m1 (Slug, snail2, NM_011415.2), Mm00486906-m1 (E-cadh, cdh1, NM_009864.2), Mm00483213-m1 (N-cadh, cdh2, NM_007664.4), Mm00495564-m1 (zeb1, NM_011546.2), Mm99999915-g1 (GAPDH), Mm01197698-m1 (Gusb, NM_010368.1), Mm00607939-s1 (Actb, NM_007393.3).

Immunoprecipitation and immunoblotting. Cells were extracted using a RIPA buffer (see above). Cell lysates were centrifuged at 13,000 g for 15 min and the supernatants were collected and assayed for protein concentration using the Bio-Rad protein assay method (Biorad, Hercules, CA, USA). Proteins were run on SDS–PAGE under reducing conditions. For co-immunoprecipitation experiments, 1 mg of proteins was immunoprecipitated with antibodies to p140Cap for 2 h at 4 °C in the presence of 50 μl protein G-Sepharose beads. Following SDS–PAGE, proteins were transferred to PVDF membranes, incubated with specific antibodies and then detected with peroxidase-conjugated secondary antibodies and the chemiluminescent ECL reagent. When appropriate, the PVDF membranes were stripped according to manufacturers' recommendations and re-probed.

Transient silencing of p140Cap in SKBR3 and MDA-MB-453. Transient transfections of ON-TARGET plus human SRCIN1 small-interfering RNA (siRNA) or ON-TARGET plus non-targeting siRNA (Dharmacon RNAi, GE Healtcare, Buckinghamshire, UK) were performed with Lipofectamine 2,000 (Invitrogen, USA) according to manufacturer's protocol. This patented approach is the best strategy to prevent off-target effects caused by both the sense and antisense strands while maintaining high silencing potency. Briefly, cells were plated on six-well plate and transfected at 80% confluency. Either 5 μl of 20 microMolar p140Cap siRNA or non-targeting siRNA were added to each well, and cells were incubated for 48 h at 37 °C in a humidified CO_2 incubator. Transfected cells were used for different assay.

Proliferation and apoptosis assays. To assess the NeuT and p140 cell proliferation rate, 15×10^4 cells were seeded per well in a 24-well plate and counted at the indicated times. Quantification of Neu-T TUBO cell growth was done by MTT assay. For apoptosis assays, NeuT and p140 cells were serum-starved for 12 h or detached and kept in suspension for 12 h. Apoptosis was assayed by annexin V staining (BD Biosciences, San José, CA, USA) or by immunoblotting with anti caspase-3 antibody (Cell Signaling).

Transwell migration assay. For the migration assay, Transwell chambers (Corning, Corning, NY, USA) were coated with 10 μg ml^{-1} type I collagen (Corning). Cells were detached using 5 mM EDTA and suspended in serum-free medium. The cells were seeded on top of the 8.0 μm pore size at a density of 1×10^5 cells per well in 100 microliters of serum-free medium 0.1% BSA. As chemoattractant, 700 μl of medium containing 15% FBS was placed in the lower chamber. After 24 h, the cells on the top surface of the filter were removed with a cotton swab, and the migrating cells on the lower surface of the membrane filter were fixed and stained with Diff-Quick kit (Medion Diagnostics International Inc, Miami. USA), and counted using a light microscope × 10 magnification.

Rac GTPases *in vitro* activity assay. Cells were washed twice on ice with PBS and then lysed in a MLB buffer (25 mM EDTA, 150 mM NaCl, 2% glycerol, 1% NP40, 1 mM EDTA, 10 mM MgCl2, 10 μg ml^{-1} each of leupeptin, pepstatin and aprotinin). For pull-down experiments glutathione-coupled Sepharose 4B beads bound to recombinant GST-PAK CRIB domain fusion proteins were incubated with cell extracts at 4 °C for 30 min, eluted in Laemmli buffer and analysed for the presence of Rac1 by western blot.

Tiam1 activity assay. Assays were performed using the active Rac-GEF assay kit (Cell Biolabs, San Diego, USA) according to the manufacturer's instructions. Briefly, cells were washed twice with ice-cold PBS and lysed in ice-cold 1 × Assay/Lysis Buffer (1 mM PMSF, 10 μg ml^{-1} leupeptin and 10 μg ml^{-1} aprotinin). Extracts were incubated with 40 μl of resuspend Rac1 G15A agarose bead slurry and incubate for 1 h at 4 °C. Beads were washed three times with the 1 × Assay/Lysis Buffer, resuspended in 40 μl of 2 × reducing SDS–PAGE sample buffer and boiled for 5 min. Pull-down supernatant were subjected to SDS–PAGE electrophoresis and western blotting with anti-Tiam1 antibody.

Statistical analysis. Tissue microarray data analysis was performed using JMP 10.0 statistical software (SAS Institute, Inc). The association between p140Cap expression and clinico-pathological parameters was evaluated using the Pearson chi-square test. For univariate and multivariate analysis, hazard ratios and 95% confidence intervals were obtained from the Cox proportional regression method. Differences in the growth rate of mouse tumours were analysed with Fisher's Exact Test, or two-way ANOVA followed by Bonferroni multiple comparison *post hoc* test. Differences in acina area were evaluated using a Mann–Whitney non parametric *t*-test. For quantification, statistical significative differences were evaluated using unpaired *t*-tests. Error bar: s.e.m. using the Student's *t*-test.

Data availability. All other remaining data are available within the Article and Supplementary Files, or available from the authors upon request.

References

1. Siegel, R. *et al.* Cancer treatment and survivorship statistics, 2012. *CA Cancer J. Clin.* **62,** 220–241 (2012).
2. Cancer Genome Atlas N. Comprehensive molecular portraits of human breast tumours. *Nature* **490,** 61–70 (2012).
3. Slamon, D. J. *et al.* Human breast cancer: correlation of relapse and survival with amplification of the HER-2/neu oncogene. *Science* **235,** 177–182 (1987).
4. Hynes, N. E. & MacDonald, G. ErbB receptors and signaling pathways in cancer. *Curr. Opin. Cell Biol.* **21,** 177–184 (2009).
5. Arteaga, C. L. & Engelman, J. A. ERBB receptors: from oncogene discovery to basic science to mechanism-based cancer therapeutics. *Cancer Cell* **25,** 282–303 (2014).
6. Staaf, J. *et al.* Identification of subtypes in human epidermal growth factor receptor 2--positive breast cancer reveals a gene signature prognostic of outcome. *J. Clin. Oncol.* **28,** 1813–1820 (2010).
7. Kauraniemi, P., Kuukasjarvi, T., Sauter, G. & Kallioniemi, A. Amplification of a 280-kilobase core region at the ERBB2 locus leads to activation of two hypothetical proteins in breast cancer. *Am. J. Pathol.* **163,** 1979–1984 (2003).
8. Staaf, J. *et al.* High-resolution genomic and expression analyses of copy number alterations in HER2-amplified breast cancer. *Breast Cancer Res.* **12,** R25 (2010).
9. Slamon, D. J. & Press, M. F. Alterations in the TOP2A and HER2 genes: association with adjuvant anthracycline sensitivity in human breast cancers. *J. Natl Cancer Inst.* **101,** 615–618 (2009).
10. Lamy, P. J. *et al.* Quantification and clinical relevance of gene amplification at chromosome 17q12-q21 in human epidermal growth factor receptor 2-amplified breast cancers. *Breast Cancer Res.* **13,** R15 (2011).
11. Sahlberg, K. K. *et al.* The HER2 amplicon includes several genes required for the growth and survival of HER2 positive breast cancer cells. *Mol. Oncol.* **7,** 392–401 (2013).
12. Arteaga, C. L. *et al.* Treatment of HER2-positive breast cancer: current status and future perspectives. *Nat. Rev. Clin. Oncol.* **9,** 16–32 (2012).
13. Citri, A. & Yarden, Y. EGF-ERBB signalling: towards the systems level. *Nat. Rev. Mol. Cell Biol.* **7,** 505–516 (2006).
14. Moody, S. E. *et al.* The transcriptional repressor Snail promotes mammary tumor recurrence. *Cancer Cell* **8,** 197–209 (2005).
15. Lamouille, S., Xu, J. & Derynck, R. Molecular mechanisms of epithelial-mesenchymal transition. *Nat. Rev. Mol. Cell Biol.* **15,** 178–196 (2014).
16. Di Stefano, P. *et al.* p140Cap protein suppresses tumour cell properties, regulating Csk and Src kinase activity. *EMBO J.* **26,** 2843–2855 (2007).
17. Damiano, L. *et al.* p140Cap suppresses the invasive properties of highly metastatic MTLn3-EGFR cells via impaired cortactin phosphorylation. *Oncogene* **31,** 624–633 (2012).
18. Cabodi, S., del Pilar Camacho-Leal, M., Di Stefano, P. & Defilippi, P. Integrin signalling adaptors: not only figurants in the cancer story. *Nat. Rev. Cancer* **10,** 858–870 (2010).
19. Sharma, N. *et al.* Identification of two regions in the p140Cap adaptor protein that retain the ability to suppress tumor cell properties. *Am. J. Cancer Res.* **3,** 290–301 (2013).
20. Cao, M. *et al.* miR-150 promotes the proliferation and migration of lung cancer cells by targeting SRC kinase signalling inhibitor 1. *Eur. J. Cancer* **50,** 1013–1024 (2014).
21. Chen, B. *et al.* MicroRNA-346 functions as an oncogene in cutaneous squamous cell carcinoma. *Tumour Biol.* **37,** 2765–2771 (2015).
22. Xu, X. *et al.* miR-374a promotes cell proliferation, migration and invasion by targeting SRCIN1 in gastric cancer. *FEBS Lett.* **589,** 407–413 (2015).
23. Ye, L., Wang, H. & Liu, B. miR-211 promotes non-small cell lung cancer proliferation by targeting SRCIN1. *Tumor Biol.* **37,** 1151–1157 (2015).
24. Wang, P. *et al.* SRCIN1 suppressed osteosarcoma cell proliferation and invasion. *PLoS ONE* **11,** e0155518 (2016).

25. Damiano, L. *et al.* p140Cap dual regulation of E-cadherin/EGFR cross-talk and Ras signalling in tumour cell scatter and proliferation. *Oncogene* **29,** 3677–3690 (2010).
26. Wolff, A. C. *et al.* Recommendations for human epidermal growth factor receptor 2 testing in breast cancer: American Society of Clinical Oncology/ College of American Pathologists clinical practice guideline update. *Arch. Pathol. Lab. Med.* **138,** 241–256 (2014).
27. Muller, W. J., Sinn, E., Pattengale, P. K., Wallace, R. & Leder, P. Single-step induction of mammary adenocarcinoma in transgenic mice bearing the activated c-neu oncogene. *Cell* **54,** 105–115 (1988).
28. Boggio, K. *et al.* Interleukin 12-mediated prevention of spontaneous mammary adenocarcinomas in two lines of Her-2/neu transgenic mice. *J. Exp. Med.* **188,** 589–596 (1998).
29. Galie, M. *et al.* In vivo mapping of spontaneous mammary tumors in transgenic mice using MRI and ultrasonography. *J. Magn. Resonan. Imaging* **19,** 570–579 (2004).
30. Muthuswamy, S. K., Li, D., Lelievre, S., Bissell, M. J. & Brugge, J. S. ErbB2, but not ErbB1, reinitiates proliferation and induces luminal repopulation in epithelial acini. *Nat. Cell Biol.* **3,** 785–792 (2001).
31. Liu, H., Radisky, D. C., Wang, F. & Bissell, M. J. Polarity and proliferation are controlled by distinct signaling pathways downstream of PI3-kinase in breast epithelial tumor cells. *J. Cell Biol.* **164,** 603–612 (2004).
32. Inman, J. L. & Bissell, M. J. Apical polarity in three-dimensional culture systems: where to now? *J. Biol.* **9,** 2 (2010).
33. Han, J. *et al.* Molecular predictors of 3D morphogenesis by breast cancer cell lines in 3D culture. *PLoS Comput. Biol.* **6,** e1000684 (2010).
34. Weigelt, B., Ghajar, C. M. & Bissell, M. J. The need for complex 3D culture models to unravel novel pathways and identify accurate biomarkers in breast cancer. *Adv. Drug Deliv. Rev.* **69-70,** 42–51 (2014).
35. Mailleux, A. A. *et al.* BIM regulates apoptosis during mammary ductal morphogenesis, and its absence reveals alternative cell death mechanisms. *Dev. Cell* **12,** 221–234 (2007).
36. Bill, R. & Christofori, G. The relevance of EMT in breast cancer metastasis: Correlation or causality? *FEBS Lett.* **589,** 1577–1587 (2015).
37. Rovero, S. *et al.* DNA vaccination against rat her-2/Neu p185 more effectively inhibits carcinogenesis than transplantable carcinomas in transgenic BALB/c mice. *J. Immunol.* **165,** 5133–5142 (2000).
38. Hua, K. T. *et al.* N-alpha-acetyltransferase 10 protein suppresses cancer cell metastasis by binding PIX proteins and inhibiting Cdc42/Rac1 activity. *Cancer Cell* **19,** 218–231 (2011).
39. Vega, F. M. & Ridley, A. J. Rho GTPases in cancer cell biology. *FEBS Lett.* **582,** 2093–2101 (2008).
40. Goka, E. T. & Lippman, M. E. Loss of the E3 ubiquitin ligase HACE1 results in enhanced Rac1 signaling contributing to breast cancer progression. *Oncogene* **34,** 5395–5405 (2015).
41. Guo, W. *et al.* Beta 4 integrin amplifies ErbB2 signaling to promote mammary tumorigenesis. *Cell* **126,** 489–502 (2006).
42. Laurin, M. *et al.* Rac-specific guanine nucleotide exchange factor DOCK1 is a critical regulator of HER2-mediated breast cancer metastasis. *Proc. Natl Acad. Sci. USA* **110,** 7434–7439 (2013).
43. Strumane, K., Rygiel, T. & van der Valk, M. Collard JG. Tiam1-deficiency impairs mammary tumor formation in MMTV-c-neu but not in MMTV-c-myc mice. *J. Cancer Res. Clin. Oncol.* **135,** 69–80 (2009).
44. Zhao, Y., Wang, Z., Jiang, Y. & Yang, C. Inactivation of Rac1 reduces Trastuzumab resistance in PTEN deficient and insulin-like growth factor I receptor overexpressing human breast cancer SKBR3 cells. *Cancer Lett.* **313,** 54–63 (2011).
45. Gao, Y., Dickerson, J. B., Guo, F., Zheng, J. & Zheng, Y. Rational design and characterization of a Rac GTPase-specific small molecule inhibitor. *Proc. Natl Acad. Sci. USA* **101,** 7618–7623 (2004).
46. Garcia-Mata, R. *et al.* Analysis of activated GAPs and GEFs in cell lysates. *Methods Enzymol.* **406,** 425–437 (2006).
47. Lopez-Garcia, M. A., Geyer, F. C., Lacroix-Triki, M., Marchio, C. & Reis-Filho, J. S. Breast cancer precursors revisited: molecular features and progression pathways. *Histopathology* **57,** 171–192 (2010).
48. Zhang, W. *et al.* Invasive cribriform carcinoma in a Chinese population: comparison with low-grade invasive ductal carcinoma-not otherwise specified. *Int. J. Clin. Exp. Pathol.* **6,** 445–457 (2013).
49. Aranda, V., Nolan, M. E. & Muthuswamy, S. K. Par complex in cancer: a regulator of normal cell polarity joins the dark side. *Oncogene* **27,** 6878–6887 (2008).
50. Muthuswamy, S. K. & Xue, B. Cell polarity as a regulator of cancer cell behavior plasticity. *Annu. Rev. Cell Dev. Biol.* **28,** 599–625 (2012).
51. Brizzi, M. F., Tarone, G. & Defilippi, P. Extracellular matrix, integrins, and growth factors as tailors of the stem cell niche. *Curr. Opin. Cell Biol.* **24,** 645–651 (2012).
52. Hanahan, D. & Weinberg, R. A. Hallmarks of cancer: the next generation. *Cell* **144,** 646–674 (2011).
53. Arias-Romero, L. E. *et al.* A Rac-Pak signaling pathway is essential for ErbB2-mediated transformation of human breast epithelial cancer cells. *Oncogene* **29,** 5839–5849 (2010).
54. Wertheimer, E. *et al.* Rac signaling in breast cancer: a tale of GEFs and GAPs. *Cell Signal* **24,** 353–362 (2012).
55. Ebi, H. *et al.* PI3K regulates MEK/ERK signaling in breast cancer via the Rac-GEF, P-Rex1. *Proc. Natl Acad. Sci. USA* **110,** 21124–21129 (2013).
56. Sosa, M. S. *et al.* Identification of the Rac-GEF P-Rex1 as an essential mediator of ErbB signaling in breast cancer. *Mol. Cell* **40,** 877–892 (2010).
57. Xue, B., Krishnamurthy, K., Allred, D. C. & Muthuswamy, S. K. Loss of Par3 promotes breast cancer metastasis by compromising cell-cell cohesion. *Nat. Cell Biol.* **15,** 189–200 (2013).
58. Boissier, P. & Huynh-Do, U. The guanine nucleotide exchange factor Tiam1: a Janus-faced molecule in cellular signaling. *Cell Signal.* **26,** 483–491 (2014).
59. Chen, X. & Macara, I. G. Par-3 controls tight junction assembly through the Rac exchange factor Tiam1. *Nat. Cell Biol.* **7,** 262–269 (2005).
60. Repetto, D. *et al.* p140Cap regulates memory and synaptic plasticity through Src-mediated and citron-N-mediated actin reorganization. *J. Neurosci.* **34,** 1542–1553 (2014).
61. Jonsson, G. *et al.* Genomic subtypes of breast cancer identified by array-comparative genomic hybridization display distinct molecular and clinical characteristics. *Breast Cancer Res.* **12,** R42 (2010).
62. Cabodi, S. *et al.* p130Cas as a new regulator of mammary epithelial cell proliferation, survival, and HER2-neu oncogene-dependent breast tumorigenesis. *Cancer Res.* **66,** 4672–4680 (2006).
63. Lucchini, F. *et al.* Early and multifocal tumors in breast, salivary, harderian and epididymal tissues developed in MMTY-Neu transgenic mice. *Cancer Lett.* **64,** 203–209 (1992).
64. Cabodi, S. *et al.* p130Cas is an essential transducer element in ErbB2 transformation. *FASEB J.* **24,** 3796–3808 (2010).
65. Hudis, C. A. *et al.* Proposal for standardized definitions for efficacy end points in adjuvant breast cancer trials: the STEEP system. *J. Clin. Oncol.* **25,** 2127–2132 (2007).

Acknowledgements

We thank: M.F. Brizzi, and D. Noonan for critical reading of the manuscript and insightful discussion; C. Luise, G. Jodice, D. Ricca, M. Coazzoli and the Molecular Pathology of the Molecular Medicine Program at IEO for technical support. This work was supported by the Associazione Italiana Ricerca Cancro (AIRC; IG-15,399 to PD; IG-11,346 to S.C.); Ministero Università Ricerca (MIUR; PRIN 2015 to P.D. and to P.P.D.F.); Regione Piemonte (Project Acronym: Oncoprot: Onco-proteins, Druidi: Drug Innovation and Discovery to P.D.); Compagnia San Paolo, Torino; Progetto d'Ateneo, Università di Torino 2011 to P.D. and E.T.

Author contributions

S.G., J.C., V.S., S.A., S.C., D.T., G.C. performed cell biology experiments; S.G., S.L., I.R., N.S., A.A., F.C., M.I., L.S., V.S., N.V. and A.L. generated and characterized the animal models; J.S., L.V.C., I.C., A.S., K.D.; A.A. G.B., S.P., S.C., P.P.D.F., E.M. and P.P. conceived and generated the data on human cohorts; P.D.S., E.T. and P.D. conceived the study; S.G., S.P., P.P.D.F, E.T. and P.D. wrote the paper with input from all authors.

Additional information

Supplementary Information accompanies this paper at http://www.nature.com/naturecommunications

Competing interests: The authors declare no competing financial interests.

Reprints and permission information is available online at http://npg.nature.com/reprintsandpermissions/

How to cite this article: Grasso, S. *et al.* The scaffold protein p140Cap limits ERBB2-mediated breast cancer progression interfering with Rac GTPase-controlled circuitries. *Nat. Commun.* **8,** 14797 doi: 10.1038/ncomms14797 (2017).

Publisher's note: Springer Nature remains neutral with regard to jurisdictional claims in published maps and institutional affiliations.